Correlation of Aortic Wall Shear Stress with MMP-9 Levels in Human Abdominal Aortic Aneurysms.

By

Anne Athena Ducas

A Thesis submitted to the Faculty of Graduate Studies of

The University of Manitoba

in partial fulfilment of the requirements of the degree of

MASTER OF SCIENCE

Department of Surgery
University of Manitoba
Winnipeg

Abstract

Currently, there is no truly reliable way to evaluate the susceptibility of particular abdominal aortic aneurysms (AAA) to rupture. In order to elucidate the pathogenesis of AAA, a correlation of aortic blood flow with intraluminal thrombus (ILT) and aortic wall composition might vastly improve understanding the development, growth and rupture of AAA.

We numerically simulated aortic blood flow in non-ruptured AAA, from this; high and low wall shear stress (WSS) were identified as well as thickness of ILT. Multiple sites of tissue of electively repaired AAA was harvested to analyze inflammatory cells, collagen, elastin content and MMP-9 levels.

We showed that there is significant variability of MMP-9 content throughout AAA, and that areas of thick ILT had higher levels of MMP-9 and were associated with lower velocity and recirculation. This variability in proteolytic enzymes in AAA has never been shown before. This is a stepping stone in fully elucidating the pathogenesis and rupture of AAA. This information may lead to better medical targets or management of AAA in patients.

Table of Content

List of Tables

List of Figures

Abbreviations

AAA	abdominal aortic aneurysm
EVAR	Endovascular aneurysm repair
CFD	Computational Fluid dynamics
COPD	Chronic obstructive pulmonary disease
CT	Computed Tomography
CTA	Computed Tomography Angiography
HE	Hematoxylin and Eosin
HTN	Hypertension
IHC	Immunohistochemistry
ILT	Intraluminal Thrombus
MMP	Matrix Metaloproteinase
NRS	Normal Rabbit serum
RAAA	Ruptured Abdominal Aortic Aneuryms
REB	Research ethics board
VG	Van Geison Stain
WSS	Wall sheer stress

Acknowledgements

I would like to thank Dr. April Boyd, Dr. David Kuhn and Dr. Tom Klonisch for all the help and support they provided during the years to help me with this project. I would also like to thank and recognize all the members in Dr. Klonisch lab and our engineering department at the University of Manitoba specifically; Richard Lozowy's work, that helped make this project come to life.

Introduction

Currently, there is no truly reliable way to evaluate the susceptibility of particular abdominal aortic aneurysms (AAA) to rupture. Discovery of these criteria would vastly improve AAA management and prevent death due to rupture. There is interest in the literature on elucidating, the pathogenesis of AAA growth by correlating aortic blood flow changes with changes in the composition of the aortic wall and the enzymes that remodel it. Discovery of the factors that remodel the aortic wall would vastly improve our understanding of the development, growth and rupture of AAA.

Review of the Literature

Current understanding of AAA

Abdominal aortic aneurysms result in significant morbidity and mortality in men and women. In North america rupture of AAA is the 15th leading cause of death and increases to the 10th leading cause of death in men above age 55 [55]. Incidence of rupture in men and women older than 50 is 76 per 100,000 and 11 per 100,000 respectively [56].Rupture of an AAA (RAAA) is associated with a mortality rate of 90%. Currently, the decision to repair an AAA is based on aortic size. In men, AAA are repaired when they reach 5.5 cm, and in women at 5.0 cm. The annual risk of AAA rupture greater than 5.5 cm ranges from 9% to 32% (1), which supports the use of size as a primary criterion for the decision to repair; however, as many as 33% of RAAA have diameters smaller than 5 cm, while others can reach sizes of 10-12 cm without rupture (2). Currently, there is no truly reliable way to evaluate the susceptibility of an AAA to rupture. Discovery of these evaluation criteria would vastly improve AAA management.

The current understanding of the pathogenesis of AAA can be described by four main mechanisms; proteolytic degradation, inflammation and immune response, biomechanical wall sheer stress and molecular genetics. These four mechanisms constitute both a physical and biological interactions within the aortic wall that bring about the formation and eventual rupture of AAAs.(3-8).

Proteolytic degradation of elastin and collagen, occurs through biochemical mediators such as matrix metaloproteinases (MMPs), within the aortic wall and is a natural process the body uses to repair and replace the damaged aorta and maintain normal aortic strength and con-

formation (4). In disease states, such as aneurysm formation, there is accelerated and unregulated breakdown of collagen and elastin. MMPs are a large family of biochemical substances found throughout the body and in the aorta are mainly used for remodelling and in repair. MMPs have many biochemical mediators that up-regulate and down-regulate their activity, such as interlukins, cytokines and tissue inhibitors of MMPs. These substances are also very important in the repair and remodelling processes in AAA(5-7). We will discuss them in more depth later on.

The inflammation and immune response occurs at the aortic wall as a response to injury to the tissue. Injury can occur from biophysical forces, oxidative stress and environmental factors most importantly smoking, others are outlined in figure 1(5-11). The inflammatory response increases cytokines, interleukins and migration of macrophages and monocytes to the aortic wall. This increase in mediators and migration of inflammatory cells are key in starting and propagating the proteolytic process resulting in up regulating MMPs leading to elastin and collagen remodelling. Continued injury and inflammation is thought to be a main contributor to the unregulated proteolytic degradation without remodelling leading to aneurysm formation(5).

Biophysical factors including; the conformation of the aorta, hypertension (HTN), peripheral resistance are also important in aneurysm formation(9). By causing injury, inflammation and physical force contribute to the continued degradation, expansion and eventual rupture of the AAA. Aneurysmal formation usually occurs in the infrarenal aorta; where 95% of all aortic aneurysms develop(1). Of the many theories to explain the 5-fold greater incidence of infrarenal AAA than thoracic aortic aneurysms, the presence of differential hemodynamic conditions along the length of the aorta is potentially most significant(12). When compared with the suprarenal segments, the infrarenal aorta experiences increased peripheral resistance, increased oscillatory

wall shear stress (WSS), and reduced flow during resting conditions (9).

Finally a person's genetics are related to aneurysm formation in that each person's response to injury is dependant on how they up regulate and down regulate inflammatory factors, proteolytic mediators and types of collagen and elastin that are found in the aorta (fig. 1)(3).

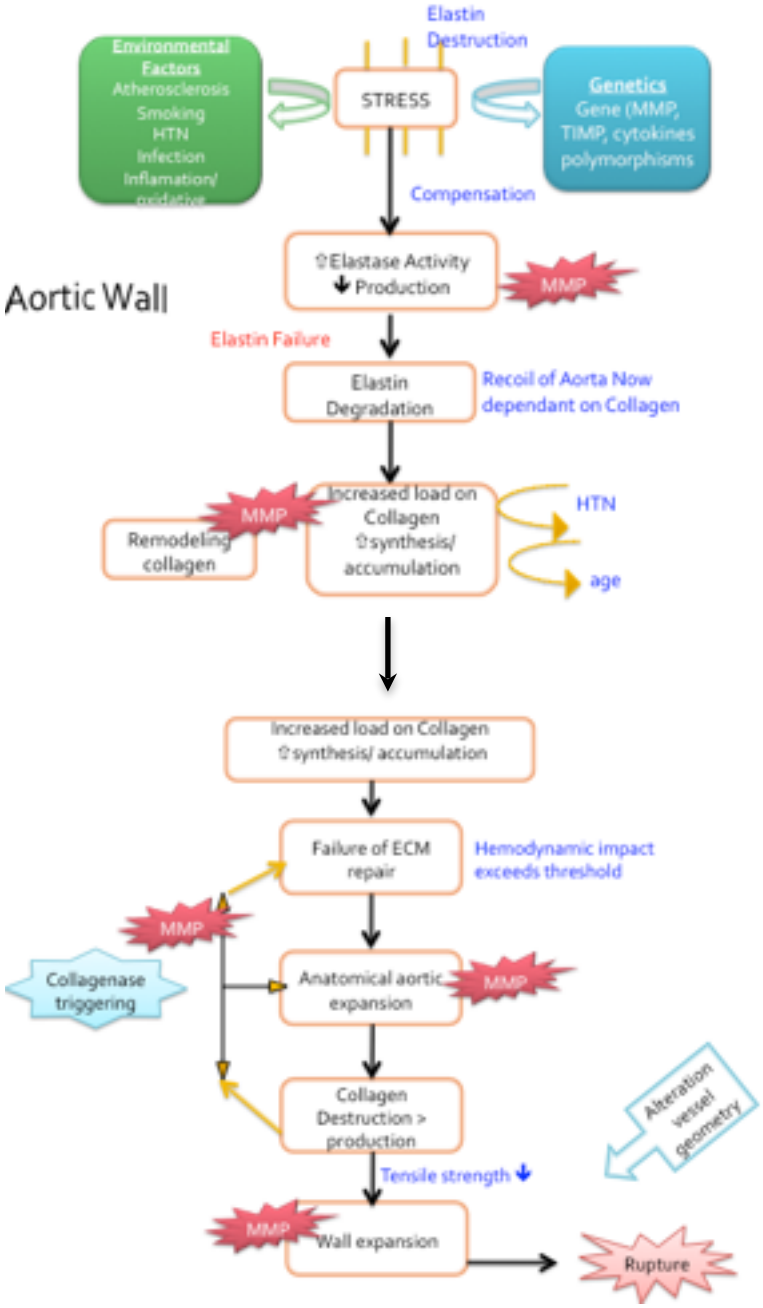

Fig. 1 Representation of the development of AAA through proteolytic degradation with MMPs.Highlighting a multistep process involving the patients genetics, environmental factors and the triggering of MMPs through continued activation.

Current understanding of Computational Fluid Dynamics

The potential for hemodynamic forces to influence AAA risk has been demonstrated in both experimental and clinical investigations. AAA diameter varies inversely with aortic flow in experimental rodent preparations where increasing flow, either before or after creation of an aneurysm, by allowing animals free access to an exercise wheel, significantly decreases AAA formation and size progression without measurable influences on aortic pressure (10, 11). It has also been recognized that major lower limb amputation (12) and, more recently, chronic spinal cord injury predispose patients to an increased risk for late AAA formation when controlled for typical risk factors (13). There has been considerable research modelling of the physical characteristics of AAA using CT reconstructions with computational methods designed to evaluate the effect on mechanical wall stress (14-21). These studies have revealed features that affect the biomechanical environment within AAA; these include tortuosity, asymmetry, presence of intraluminal thrombus, and wall thickness (18,19,22-24). Unfortunately, the correlation of the magnitude of wall stress, coupled with the tensile strength of the aneurysm wall have yet to consistently predict the outcome for specific AAA (19,23,25). Just as alterations in WSS may be an important predictor of rupture of AAA, the strength of the aortic wall is related to the elastin and fibrillar collagen types I and IV content.

Our group was the first to model blood flow in the geometry of human ruptured AAA (26). We showed that the site of rupture was not in the region of maximal pressure or WSS as predicted (26); instead, rupture occurred in all cases in flow recirculation zones where low WSS predominated. These results suggest that areas of recirculation may lead to thrombus deposition and aortic wall degeneration and eventual rupture (26).

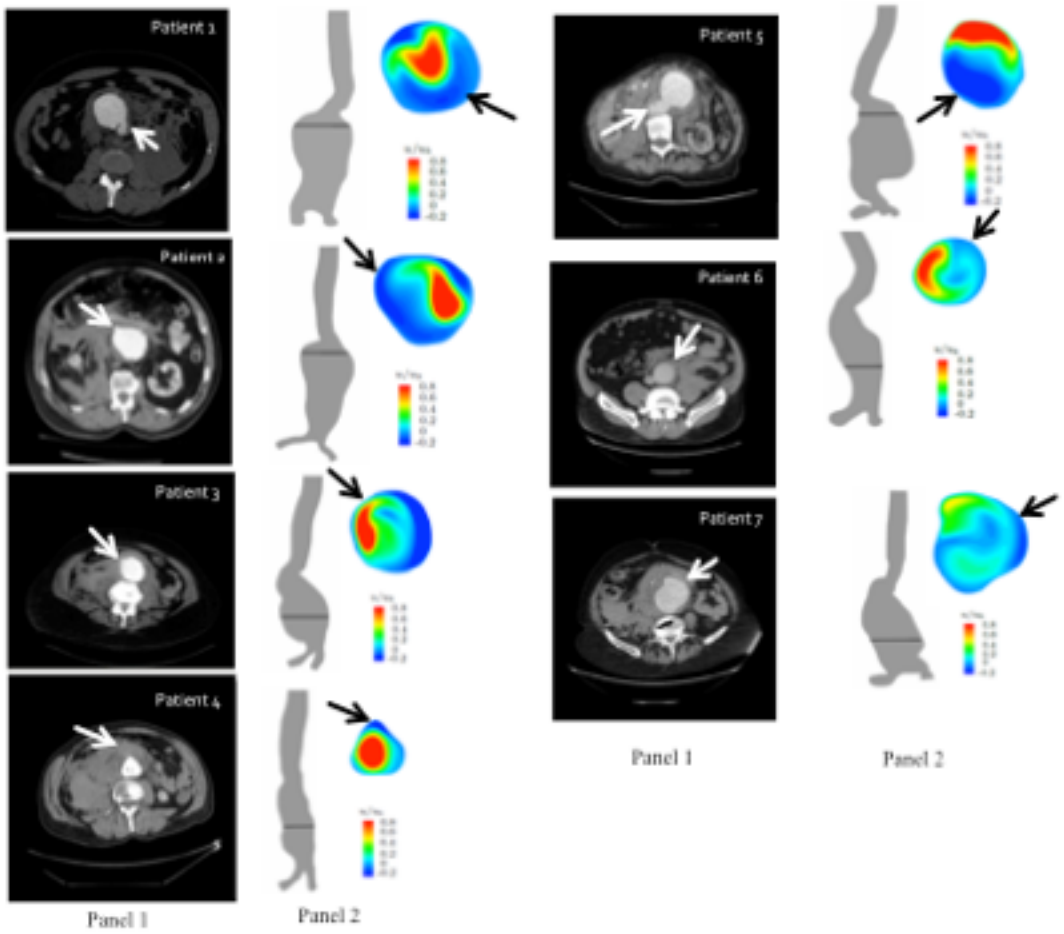

Fig.2 Rupture site of AAA as compared with WSS. This study shows the results of 7 ruptured AAA patient who underwent CT angiograms. Black and white images shows rupture on the CT (white arrow), grey silhouette show diameter of aorta at rupture (black line), velocity at rupture is seen in the colour image represented by black arrow. Demonstrating that rupture occurred in areas of high ILT, and flow recirculation and low velocity. Also demonstrating that rupture did not occur at the maximal diameter.(Used with permission from JVS)(26).

Matrixmetalloprotienases

Just as alterations in WSS may be an important predictor of RAAA, the strength of the aortic wall is related to the elastin and fibrillar collagen types I and IV content. The content of these components may not be uniform, and tissue failure leading to rupture may occur as a result of local loss of matrix strength secondary to the action of tissue enzymes that regulate proteolysis of matrix components. Matrix Metalloproteinases (MMP) are a family of extracellular matrix–degrading enzymes essential for homeostatic physiologic processes, including: wound healing, tissue remodelling and degradation of the extracellular matrix(28-29). They are a large family of calcium-dependent zinc containing endopeptidases that affect collagen, elastin, gelatin, matrix glycoproteins and proteoglycans. MMPs are regulated through inflammatory cells that respond to hormones, growth factors and cytokines. These cells include osteoblasts endothelial cells, macrophages, neutrophils and lymphocytes. Macrophages, neutrophils and lymphocytes are nucleated cells that can be found in the aortic wall after injury from wall stress, deposition of free radical from smoking and endothelial breakdown(7).

The evidence that supports MMPs' role in the pathogenesis of AAA is seen in multiple studies. There is over expression of the MMPs in aortic aneurysmal tissue as compared with normal aortic tissue (27-29). There is increased expression of activators of MMPs, such as cytokines and growth factors, found in aortic tissue (30,31). This suggests that there is a shift to a proteolytic state in damaged aortic tissue. This is also supported by the change in expression of tissue inhibitors of MMPs (TIMPs), specifically their down regulation in AAAs and further increase the shift toward proteolytic activity. Studies have also shown that knock out mice where there is inhibition of, or lack MMPs activity promotes preservation of elastin in the aortic wall.

Finally, when these elastases are infused into experimental models we see the development and growth of aneurysms(26,42).

Matrix dissolution is an essential pathophysiologic mechanism in AAA disease. The critical role of MMP activity in the pathogenesis of AAA has been recognized for more than a decade (26 ,32). Several MMPs have been implicated in AAA disease, in particular one that is present almost universally found in AAA is MMP-9, a serine elastases. MMP-9 is a zymogen that cleaves elastin, collagen types I and IV, and fibrinogen. Plasma MMP-9 levels are increased in AAA disease, and more MMP-9 mRNA is present in aneurysmal than in normal aortic tissue. Experimental data also suggest that MMP-9 needs to be present and in its active form to achieve maximal aneurysm progression (33). This gelatinase B is usually found in infiltrating adventitial macrophages, specifically in areas adjacent to the adventitial vasa vasorum (34,35). When focusing on infrarenal AAA there are regional factors that increase the production of MMP-9 and may be responsible for aneurysm development in this area (36). Recent data has shown that MMP-9 levels are significantly elevated in RAAA, particularly at the site of rupture compared with other sites in the aortic wall (37,38).

MMP-9 involvement in the formation of AAAs has also been studied in knock out mouse models where the MMP-9 gene is absent(39). Formation of aneurysms were induced through chemical means and then the aorta were analysed. The results demonstrated that without MMP-9 activity there is complete lack of dilatation of the aorta and histological analysis revealed preservation of the media's elastin content (39). This study strongly suggests that MMP-9 presence is directly responsible for the formation of elastase-induced AAAs. Even though MMP-9 seems to play a prominent role in the development of AAA there are other studies showing the

involvement of other enzymes and gene products contributing to and influencing MMP-9's activity in infrarenal aneurysms (40-42). Specifically MMP2 and MMP12 and tissue inhibitor of matrixmetalloproteinases (TIMP) all regulate the amount and activation of MMP-9. The mechanisms responsible for the local aortic wall elevations in MMP-9 remain unclear. Specifically the relationship between aortic peak WSS and MMP activity in the aortic wall remain unknown.

The objective of this research is to gain a better understanding of how flow, ILT and wall sheer stress within the aorta affects its break down of collagen, elastin through MMP-9's enzymatic processes. We hypothesize that flow recirculation leads to increased ILT deposition that results in decreased regional oxygen delivery which promotes increased inflammatory activity leading to AAA wall degeneration. The purpose of this study was to examine the correlation between predicted pulsatile flow dynamics and observed ILT deposition patterns in human AAA with regional differences in MMP-9, elastin, and collagen. Understanding the correlation between aortic blood flow and enzymatic wall decomposition would vastly improve our understanding the mechanisms involved in the development, growth and rupture of AAA.

Rationale and Hypothesis:

Alterations in abdominal aortic blood flow is important for the development, growth and rupture of AAA. We hypothesize that low wall shear stress, characterized by flow recirculation, leads to increase ILT depostion which promotes increased inflammatory activity that leads to regional wall degeneration. Specifically, we postulate low wall shear stress results in increased MMP-9 levels with associated decreases in elastin and collagen in the aneurysmal aortic wall.

Objectives and Goals

The objectives of this research is to gain a better understanding of how abdominal aortic aneurysms (AAA) develop. Specifically, how the flow and wall sheer stress within the aorta affects its break down of collagen, elastin through enzymatic processes.

Questions:

1. Is the composition of active and inactive MMP-9 different throughout the abdominal aorta in non-ruptured AAA?
2. Does wall sheer stress affect the composition of elastin, collagen and inflammatory cells at different locations of the aneurysmal abdominal aorta?
3. Is there a correlation between wall sheer stress and MMP-9 (active, non-active)?

Methods:

This study used a combination of basic science, mechanical engineering and clinical measurements to analyze data from patients with AAA. All tissue samples were collected with expressed written consent under study protocols REB B2013: 130. Patients who were diagnosed with AAA were referred to one vascular surgeon at Health Sciences Centre. These patients were enrolled in the study at their clinic visit after they had been consented for AAA repair. Consent was obtained by the Research Nurse in clinic. The consent form (appendix a) was read by the patients, questions and concerns were answered either by the research nurse or relayed to the principle investigator for further explanation.

The patients then underwent a CT angiogram completed at the Health Sciences Center (HSC) The raw images were blinded as to personal data and delivered to the Department of Mechanical Engineering at the University of Manitoba. Our engineering group then numerically simulated aortic blood flow in non-ruptured AAA using the open foam computational fluid dynamic model. Intra-aortic areas of high and low wall shear stress (WSS) were identified in laminar and pulsatile flow states.

At the time of open repair, redundant aortic tissue and thrombus samples were harvested throughout the aorta in stereotyped locations (Fig. 3). Prior surgery risk factors were recorded from all the patients and entered into a database for basic patient demographics. A schematic diagram was also created to help co-ordinate with engineering data to better localize WSS and blood flow at sample locations. The excision of the tissue was carried out by the surgeon (Principle investigator). We then documented on our diagram the estimated locations of the samples (Fig 3). The infrarenal aortic length from just below the renal arteries to the bifurcation of the iliacs was

used to divide the aorta into quarters. Samples were taken at one quarter and three quarters posteriorly and taken anteriorly at one half the distance of the infrarenal aorta. The aortic tissue was then placed on a sterile mayo stand and divided into halves. The tissue that was less disrupted was placed into a sterile test tube with formalin. The other half of the aortic tissue sample was place into cry- tubes and snap frozen by immediately placing them into liquid nitrogen. The cryo-tubes were then stored at -80^{o}C. The tissue in the formalin tubes were allowed to sit for 48 hours.

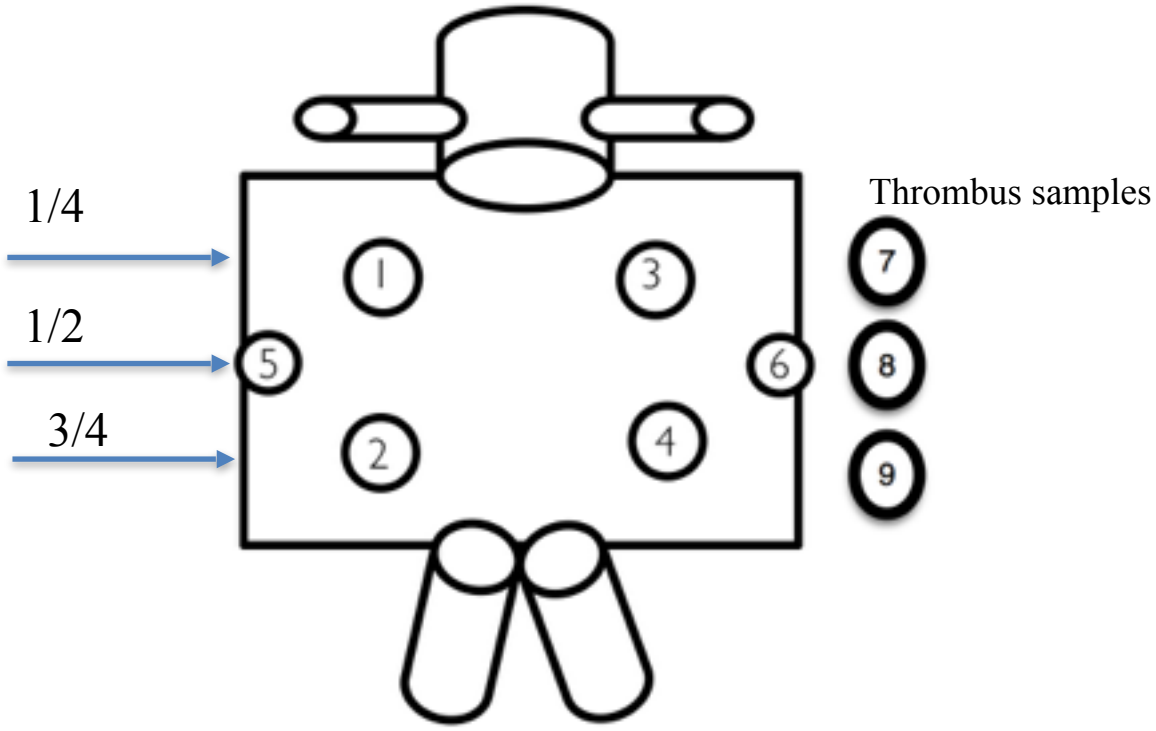

Figure 3. Diagram of estimated aortic sample locations taken at the time of elective repair of AAA. Thrombus samples were taken at various location in the aorta and recorded to compare with flow velocities.

The tissue that was stored in the formalin was then prepared for embedding with Paraffin. Prior to embedding the tissues were cut to achieve a size of 10 x 10 x 3 mm. If the tissues were too large for one block the were divided into two samples for that one site of aortic tissue. Once the tissue was cut it was placed into plastic cassettes and labeled appropriately. Cassettes with tissue were then placed into 70% ethanol to prevent drying out. Processing the tissue was carried out using a standard tissue processor embedding machine (Shandon Citadel® Tissue processor). Labels were placed on the discs to indicate patient, sample site and sample number from that site.

The embedded tissue was prepared for the microtome by shaving excess wax around the tissue to achieve similar size wax and tissue portions. The wax blocks were then placed in the microtome and large portions of 20 µm were cut until the sample of tissue was exposed and a complete section of tissue was visible. The embedded tissue was then cut with a microtome to 5 µm thickness. to include intima, media and adventia then placed on APTES ((3-Aminopropyl)triethoxysilane) coated slides. For each sample there were ten slides with up to three sections of tissue . The slides where dried overnight on a slide dryer. Labeled slides where sorted by sample and patient and placed into separate slide cases for further analysis.

Hematoxylin and Eosin staining

Prior to preparing the slides Hematoxylin and Eosin staining solutions were prepared (appendix b). The slides were deparaffinized using two, five minute washes with Xylene. Rehydration was carried out with sequential ethanol treatments to the slides with decreasing ethanol concentrations to 90% then placed in a water bath for 5 minutes. I then placed the slides into hematoxylin bath for 7 minutes for the primary staining. Slides were then washed with running

water for 5 minutes. Slides were then placed in a ethanol solution to remove excess stain. Slides were washed again prior to being placed into a Eosin staining solution. After staining was complete dehydration of the slides using sequential ethanol washes was carried out. The slides were then cleared with Xylene and coverslips were applied to the slides with permount (Fisher Scientific) in a fume hood.

Analysis of the slides stained with hematoxylin and eosin was carried out under 100x and 200x magnifications. Each sample had 2-3 sections that were stained and analyzed. Multiple pictures (7-10) were taken of the slides to represent the tissue sample. A qualitative analysis, performed by one person was performed for each sample to estimate the amount of nucleated cells within the samples. Nucleated cells where assumed to be neutrophils, monocytes, lymphocytes and fibroblast, and represented inflammation within the tissue. ZEN pro image analyzer was used to label dark staining nuclei. The designation of minimal (0-20% stained slide) , moderate (20-70% stained slide) or abundant (>70% stained) amounts of tissue where assigned to the sample by taking the average of all the pictures analyzed for each sample. A number value of 1-3 was then assigned; minimal (1), moderate (2), and abundant (3) to the samples to allow further analysis.

Verhoeff-Van Geison staining

Prior to preparing the slides Weigert Iodine solution, 10% aqueous ferric chloride, 5% alcoholic hematoxylin, Verhoeff's staining solution and Van Geison (VG) counterstain were prepared (appendix b). The slides were deparafinnized using Xylene washes. Ethanol washes were then used to rehydrate the slides and completed with a tap water rise. The rehydrated slides were then placed into the Verhoeff's staining solution for an hour then quickly rinsed with water.

Differentiation of the slides was done with 2% ferric chloride solution for 1-2 minutes. The differentiation was stopped with several changes of tap water and were microscopically checked for the appearance of the black elastic fibres. After confirmation that the slides were staining they were placed in sodium thiosulfate to remove excess iodine. The slides were counterstained with Van Gieson Counterstain for 3.5 to 4 minutes. Dehydration of the slides was then carried out with sequential ethanol washes and then cleared with Xylene. Coverslips were applied with permount (fisher scientific) in a fume hood.

Analysis of the slides stained with Verhoeff-Van Gieson was carried out under 100x magnifications with the ZEN imaging capture computer system. Each sample had 2-3 slices that were stained and analyzed. Multiple pictures (7-10) were taken of the slides to represent the tissue sample. A qualitative analysis was performed for each sample to estimate the amount of elastin and collagen present within the samples. Elastin was stained black in the sample and was seen between the intimal and media layers and the media and advential layers of the aortic tissue. Collagen was stained pink and was seen throughout the aortic tissue. ZEN pro image analyzer was used to estimate the amount each collagen and elastin present within each imaged captured. The designation of minimal (0-20% presence of elastin/collagen) , moderate (20-70% presence of elastin/collagen) or abundant (>70% presence of elastin/collagen) amounts of this extracellular matrix element where assigned to the sample by taking the average of all the images analyzed for each sample. A number value of 1-3 was then assigned; minimal (1), moderate (2), and abundant (3) to the samples to allow further analysis.

Immunohistochemistry MMP-9 total and active

MMP-9 total and MMP-9 active antibodies were purchased from the supplier (appendix b) and recommended laboratory products and protocols were used to perform immunohistochemistry on (appendix b) these antibodies.

De-paraffination of the slides was performed by placing the slides into a glass slide rack wrapping it with foil and heating it to 60 ^{o}C in an oven for two hours. Warmed slides were then immediately placed into three sequential Xylene baths for ten minutes. Rehydration was carried out with descending ethanol baths for 3 mins and then rise with double-distilled (dd)H20. Equilibration of the slides occurred for 10 minutes in a Tris-buffered sodium tween buffer (1x TBST) (appendix b).

Blocking of the endogenous enzyme was performed in the dark with Horse-Radish peroxidase/biotin protocol; 3% hydrogen peroxide in methanol mixture (appendix b) . Ten slides at a time were placed into a Coplin jar and then added to the above mixture for 20 mins in complete darkness. The slides were then washed with 1x TBST buffer for 2 separate washes of 5 minutes.

Antigen retrieval was then performed with a citrate Buffer solution (appendix b) and heated to around 90 °C in, then kept in a water bath for 30 minutes. Slides, were removed from water bath and placed in a fume hood for 20 minutes. Washing of the slides was then carried out first with a 10 minute TBST buffer bath then followed by two subsequent 5 minutes TBST buffer baths.

Protein-Protein interaction were avoided by blocking unspecific interactions with a normal rabbit serum (NRS) (appendix b) blocking buffer. Prior to placing the blocking solution on the slides tissue samples on slides were encircled with a paraffin blocking pen to isolate each

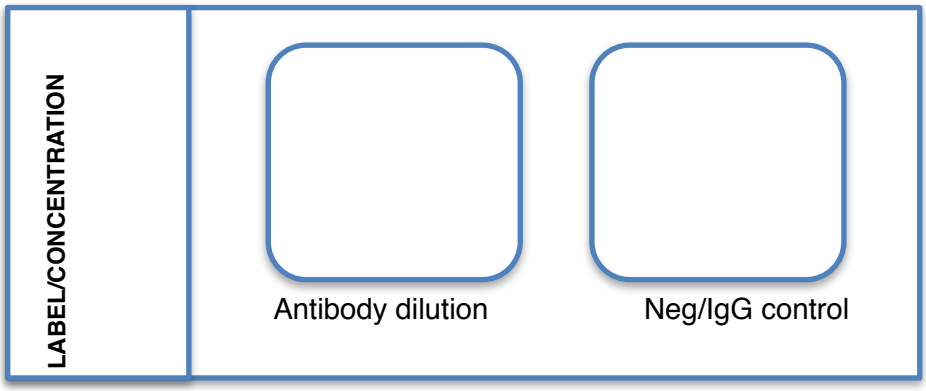

Fig. 4 Slides representing tissue samples for antigen staining in IHC process. Each slide had the selected antibody dilution with either a negative (neg) or IgG control. Batches of tissue samples included both negative (NRS) and IgG controls.

sample. Then150 µL of 5% NRS solution was applied to the encircled tissue sample (fig 4). Attention was taken to ensure the tissue on the slide did not dry out. The slides were then placed in a moist chamber and covered for 1 hour.

Applying our primary antibody and IgG control was preceded by determining the correct concentration/dilutions of each MMP9 total, MMP-9 active and IgG that were needed to obtaine appropriate analysis of aortic tissue MMP-9. Dilutions for the MMP-9 active and total started at 1:100, 1:250, 1:500 and 1:1000 (Antibody : 5%NRS blocking buffer) antibody dilutions were tested on extra slides containing our patients tissue sample (AB95-7 and JP11-2). IgG dilution was carried out according to the product data sheet of 1:1000 (NB720-B).

When the blocking step was complete and our primary antibody and IgG dilutions were made I removed the buffer from the slides by gently taping it off onto a clean paper towel. After ensuring that the paraffin encircling was still in place and fixed if necessary we then applied 150 μL of primary antibodies (MMP-9 total or Active all mouse anti-human) solutions and IgG and

blocking buffer as indicated (Fig. 4) . The slides were placed back into the moist chamber and stored overnight at 4^{o} C. To remove excess solutions and clean the slides they were washed 3 times in 1x TBST buffer solution. Secondary antibody (rabbit anti mouse)(appendix b) was diluted to according to the product data sheet recommendations (1:1000) with the 5% NSR in TBST buffer. Antibody dilutions were then incubated for 1 hour in the moist chamber. The secondary antibody was washed off with 3 washes of 1x TBST solution.

Development of the slides was done first by placing streptavidin-HRP reagent (appendix b) to each of the sections encircled by paraffin. Then the reagent was washed in 3 baths of TBST for 10 minutes each. DAB substrate kit (appendix b) were prepared according to the manufacturer's instructions. To ensure that the slides did not over-develop, the staining intensity was observed under the microscope with a maximal incubation for 30 mins, as recommended by the manufacture of the DAB substrate kit (appendix b). Quenching was then carried out by placing the developed slides into 1x TBST buffer for 1-2 seconds. The slides were counter stained with hematoxylin for 1 second and cleaned with running tap water for 5 minutes. Dehydration was carried out with sequential ethanol baths (3 minutes each) and then two Xylene baths. Permount™ was used with a plastic cover slip over each tissue sample on the slides.

Analysis of the tissue samples was carried out with a bright field microscope and Zen™ imaging processor to semi-quantitatively assess the amount of MMP9 total and active was staining on each tissue sample. Magnifications of 200X with the ZEN imaging capture computer system were used. Each slide had 1 tissue stained with MMP-9 (total or active) and 1 tissue sample that were stained with IgG or NRS toassess the specificity of the staining. Multiple images (3-5) were taken of the slides for a representative collection of images. A qualitative analysis was per-

formed for each sample to estimate the amount of MMP9 that was present within the samples. MMP-9 total and active stained brown and was seen in areas of inflammatory cells. Careful inspection of the slides was carried out to not mistake areas of high calcium, which stained beige (fig. 7) These areas were removed form the ZEN™ quantitative analysis. ZEN pro-image analyzer was used to estimate the amount MMP-9 total and active present within each image captured. The designation of minimal (0-20% total area) , moderate (20-70% total area) or abundant (>70% total area) amounts of MMP-9 were assigned to the sample by taking the average of all the iamge analyzed for each sample. A number value of 1-3 was then assigned; minimal (1), moderate (2), and abundant (3) to the samples to allow further analysis.

Quantitative protein analysis

Quantitative analysis of the amount of MMP-9 in each aortic tissue sample was carried out by extraction of the protein then sending the protein samples for multiplex immunoassay with Bioplex200™ through a commercial company Eve technologies (Calgary, Alberta). For protein extraction, tissue was weighed (40 mg) and then placed in a mortar. Liquid nitrogen was poured onto the tissue and the tissue was ground into a fine powder using a pestle. Then 1200 µL (30 µL/mg of tissue) of 0.1% Triton-X-100 50mM Tris-HCl lysis buffer was added to the ground tissue and allowed to sit for 15 minutes. The protein extract was then transferred into 1.5 mL microfuge tubes and spun for 20 minutes at 13000 rpm. This separated the extract into a pellet (bottom), a supernatant containing protein, and a fat layer (top). The supernatant (protein) was pipetted into a new 1.5 mL microfuge tube and sonicated for 10 seconds. The protein was then stored in aliquots at -80^{o}C until analyzed. Concentration of MMP9 were analyzed with multiplex immunoassay with bioplex200 beads and results were obtained in ng/mg.

Analysis of Thrombus deposition

All patients enrolled in the study had CT scans of their aortas prior to AAA repair. Those CT scans were analyzed by two separate investigators to assess size of the aneurysm and where thrombus deposition occurred throughout the aorta. To ensure correlation of these results, they were compared. If any results did not match a third investigator was used to tie break. Tissue samples from the aortas were assigned concentrations of MMP-9 in ng/mg protein by quantitative analysis Bioplex200 assay and were sorted to areas of thrombus and areas of no or little thrombus. This was done by two separate investigator and results were compared. Averages with standard deviation were calculated at areas of high and low thrombus of the aorta

Computational fluid dynamic models

CT angiogram (CTA) images of the infrarenal aorta were obtained for one non-aneurysmal aorta and all elective AAA patients. Three-dimensional (3D) AAA geometry was generated from CTA images using the commercial medical imaging software *Mimics* (version 14.0) (*Materialize,* Helm Court, Plymouth, MI 48170). Once completed these scans were sent to our engineering department and flow velocity models were returned to the primary investigator to correlate velocity with tissue factors.

The upstreams aorta including the visceral arteries were excluded to simplify the geometry. The aorta proximal to the aneurysm was also modelled as a constant diameter transitioning into the patient-specific AAA anatomy.

The open source finite-volume code *OpenFOAM-2.2.0* (Open CFD Ltd, Bracknell, UK, RG12 1BW) was used to solve the governing equations, in a Cartesian coordinate system $x = (x; y; z)$, using the SIMPLE algorithm. The solution was considered converged when the residuals were less than 1 x 10^{-6}. The blood was assumed to be an incompressible fluid with Newtonian properties. Blood density and dynamic viscosity are ρ = 1050 kg m^{-3} and μ = 0:0035 kg m^{-1} s^{-1}, respectively. A no slip condition was applied on the inner walls of the aorta.

Pulsatile flow was considered and the flow rate was fixed at Q = 15.7 ml s^{-1}; equivalent to a resting cardiac output of 5 l/min. This value is representative of the mean value that occurs during a pulse and simulates in laminar flow conditions. The bulk Reynolds number is Re_b = 250 and is defined as $Re_b = 2\ \rho u_b R/\mu$; where length scale R = 0.012 cm is the upstream aorta radius and u_b is the bulk velocity. The velocity field is given by $u = (u, v, w)$ and the pressure was defined as P. At the upstream inlet fully developed *Poiseuille* flow was assumed. The WSS at the inlet is 0.04 Nm^{-2} and was calculated from $WSS_{inlet} = 4\ \mu Q/\ \pi\ R^3$. Unstructured grids composed of tetrahedral and prism cells were generated using commercial grid generation software (*Pointwise*, Fort Worth, Texas, USA, 76104). The number of cells varied from 1.9 million to 4.6 million depending on the size of the AAA. For the surface contours, pressure was expressed as $P^* = (P - P_{inlet})/P_D$; where $P_D = 0{:}5\rho u^2_b$ and WSS* indicates wall shear stress has been normalized by WSS_{inlet}.

Once the models were generated areas of high and low WSS where calculated using a scale and colour model. These areas were then assigned to sample locations for each patients aorta visually with the help of the CTA preformed prior to surgery. To more accurately assign flow

velocities to location in the aorta at points of tissue sampling the areas were reviewed with the engineers.

Statistical Analysis

We first compared the amount of Elastin and collagen content within the tissue samples to see if that correlated with MMP9 content. This was done using SPSS to carry out a univariate regression correlating the two variables. First Elastin versus MMP-9 active and then total, and collagen versus MMP9 active and then total. Using a pearson correlation and SPSS we compared velocity (m/sec) within the aorta and MMP-9 total, MMP-9 active, elastin, and collagen. We then correlated presence of thrombus with the same variables, MMP-9 total, MMP-9 active and Elastin and collagen. Pearsons regression statistics was used to correlate the amount of thrombus deposition (mm) to the velocity (m/sec) within the aorta at that location.

An independent t-test was used to compare regional differences in MMP-9 levels between regions of high and low ILT deposition. Pearson correlation coefficients were calculated to determine the relationship between ILT deposition and MMP-9 levels, and between flow velocity and ILT deposition. Values were considered statically significant at $P<0.05$.

The areas of thrombus that were sampled were also analyzed. Levels of MMP-9 in sampled areas of thrombus were compared to flow velocity; specifically areas of recirculation were compared with areas of flow impingement. Averaged in each type of flow area were taken and compared in paired t-tests. Values are presented as mean +/- standard error of the mean.

Results

Demographics

Twenty-four men (n=18) and women (n= 6) undergoing open AAA repair for AAA > 5.0 cm between May 2014 and February 2015 were enrolled in this study. One additional patient was a planned pilot case used to assess the safety of multi-site aortic tissue harvest; data for this patient are not included. All patients were consented to open AAA repair with aortic tissue harvest, either due to lack of EVAR suitability, or based on patient preference. Patients details were collected including; age, sex, medications, cardiovascular risk factors, and smoking history. All except 1 AAA patient underwent preoperative CTA imaging. The CTA images were used to assess AAA morphology and for CFD analysis of infrarenal aortic blood flow

Those that had a CTA were sent for CFD analysis of the aortic blood flow. One patient was not included because their tissue samples were not put in liquid nitrogen and quantitative analysis of their MMP-9 could not be carried out, however, the tissue that was placed in the formalin was analyzed with the rest of the tissue sample and included in the qualitative analysis. The pilot patient was used to ensure patient safety and for testing dilution of samples for IHC staining, and results were not included in the final analysis.

All patients had their medical history data taken at the time of aortic aneurysm repair, this information is displayed in Table 1. The majority of the patients enrolled in the study were male (79%). The average age of the patients enrolled in the study was 73 $\pm$ 7.3 years and the average size of the aortas that underwent elective repair was 6.39 cm with at standard deviation of $\pm$1.2 . Preoperative CTAs showed that 24 patient enrolled, 88% had thrombus found in the AAA. There was a large portion of the patients that had smoked or were currently smoking (92%). Risk

factors for atherosclerosis disease, such as hypertension (HTN) 67%, hyperlipidemia 83% , diabetes 33% and COPD 38% were also prevalent in our patient population. The most common medications were statins, with 83% of patients currently on this treatment.

Table 1. Demographics of patients and aortic tissue samples

	Number of patients	deviation/ precentage
Age	73	±7.25
Size	6.39	±1.2
Gender male	19	79
Samples	7.6	1.0
Thrombus	21	88
Smoking	22	92
HTN	16	67
Hyperlipidemia	20	83
Diabetes	8	33
COPD	9	38
Statin	20	83
Peripheral Vascular disease	12	15

Analysis of Aneurysm through imaging

Prior to tissue harvest 24 patients underwent CT scanning and 21 were included in the final analysis. As previously mentioned one patient did not have their tissue placed in liquid nitrogen and was removed from further quantitative analysis and two had non-contrast imaging due to poor renal function. Of the remaining 21 AAA, 17(81%) had an eccentric thrombus, meaning thrombus was not distributed equally. Two aortas had very little to no thrombus and 2 had dense circumferential thrombus. All CTA scans were analyzed with open foam CFD analysis. Models for each patient were generated showing the true lumen or flow channel of the aorta in both sagittal and coronal views. Flow diagrams showing velocities (m/sec) within the flow channels were generated in a colour scheme system with high velocities/ impingement were represented at the red end of the colour spectrum and low velocities/recirculation were represented at the blue end of the colour spectrum(Fig 5). All flow diagrams at represented in appendix D. The velocity values recorded from the models are reported in appendix c; table 1.

To more accurately estimate velocities at tissue sample location the colour scan was expanded. Results showing velocities at tissue locations are demonstrated in table 1 in (appendix d). All models generated for patients in the study are included in (appendix d). Analysis of the models showed that flow within the aorta was laminar in nature but became turbulent when they aortic diameter and lumen expanded. High velocities followed the dominant flow channel and low velocities were associated with zones of recirculation when the aorta expanded and became aneurysmal. Measurements of thrombus thickness were correlated with velocities. A moderate correlation of r= - 0.41 was observed. Indicating that in areas of thick ILT flow was more likely

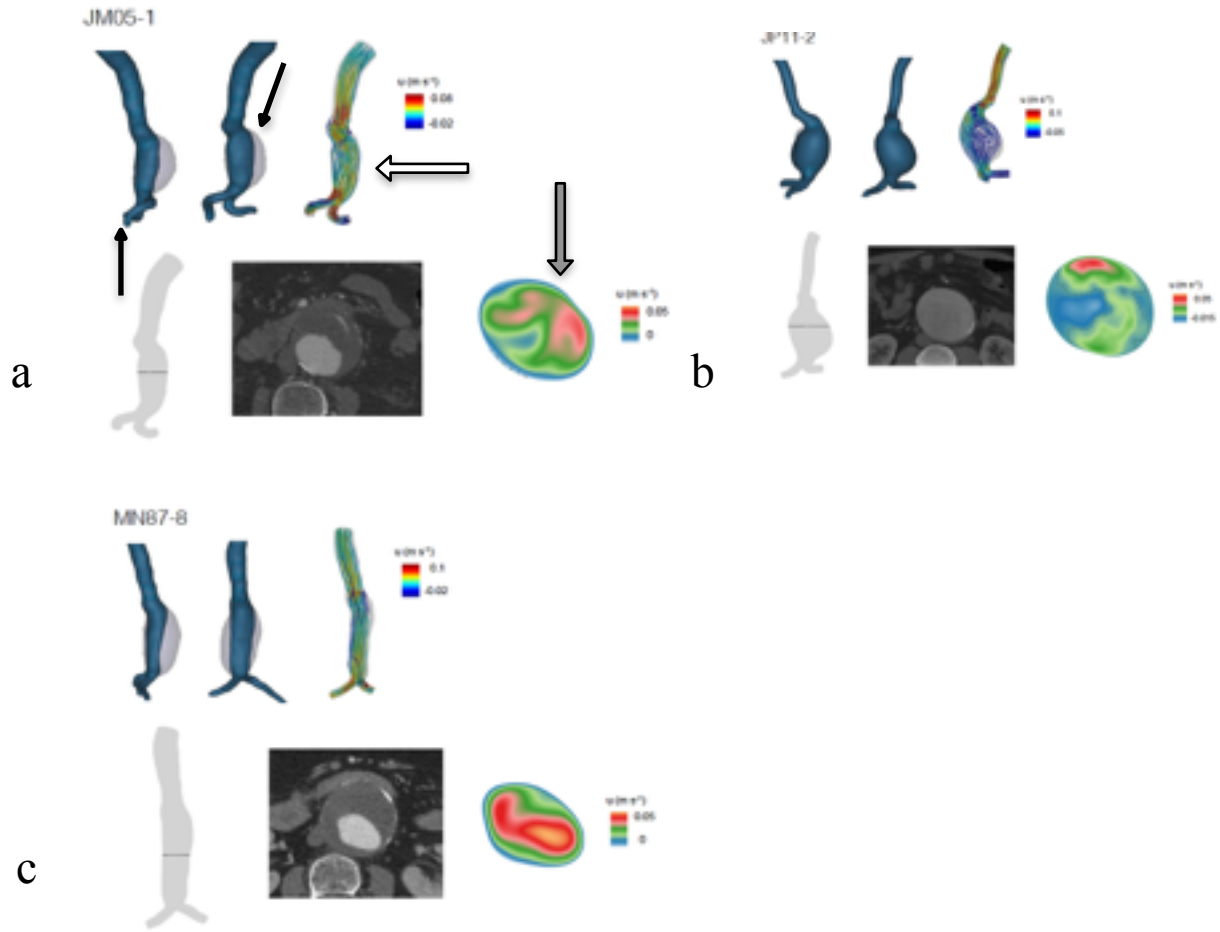

Fig 5. Examples of CFD models of three patients. a. AAA with eccentric ILT. JM05-1 tissue sample 1-6 velocity values m/s (0.02,0.02,0.02,0.02,0.02, 0.06,0.06), b) AAA without ILT. JP11-2 tissue samples 1-6; velocity values (0.01,0.01,0.01,0.01,0.05,0.05) and c) AAA with circumferential ILT MN87-8 tissue samples 1-6; velocity values m/s (0.028,0.028,0.028,0.028,0.028,0.028). All models included silhouettes of aortas in blue and grey for coronal (black arrow down pointing) and sagittal (black arrow up pointing) views. Flow channels measured in (m/sec) shown in colour (white arrow). Cross sectional flow represented with colour diagram (grey arrow), grey aortic silhouette showing cross section and CTA reference.(a) representing in a patient with eccentric thrombus. A patient with no thrombus (b) and a patients with concentric circumferential thrombus within their AAA (c).

to have lower velocities and those at thin (mms) thrombus were more correlated with higher velocity Flow (fig 5)

All patients enrolled in the study underwent AAA repair. There were no mortalities from AAA repair within the 30 days, and no major post-operative complications. No complications from tissue harvest occurred intra-operatively or post-operatively that affected the post-operative course. Tissue samples were harvested from the aorta with the average 7.6 $\pm$ 1 samples per patient. Up to 6 samples were harvested from aortas and up to 3 samples were harvested from thrombus within the aorta. Four patients did not have one tissue sample included in the qualitative analysis and and two patients did not have tissue samples included in the quantitative analysis. The four patient tissues samples either did not have any aortic tissue seen within the sample or there was too much calcium to have an accurate staining and assessment of the tissue or there was no tissue to harvest from the aorta at the location predetermined as seen in fig 3. The two tissue sample that were not included in the quantitative analysis were absent in the aortic tissue. All samples of the 24 patients were divided into equal halves approximately 10 cm^2 and thickness varied from 3 mm to 15 mm one sample did not get placed in liquid nitrogen before storage at -80 ^{0} C and that tissue was not included in the final analysis. All 24 groups of tissue samples were placed in formalin after harvest.

Qualitative analysis of tissue samples

All tissue samples in formalin from the 24 patients were placed in paraffin blocks and sectioning completed for further staining. H&E, VG and IHC staining was completed on all patients. An example of all types of histologic staining for one location is seen in Fig 7. In total five samples were not included in the final analysis. For patient MC47-6, sample 3 had too much calcium in

the tissue and could not be prepared properly for staining. For patient AR49-6, sample 1, JM05-1 sample 2, JS98-8 sample 2 did not have tissue harvested at time of surgery. For patient NJ24-1 sample 2 did not show aortic tissue.

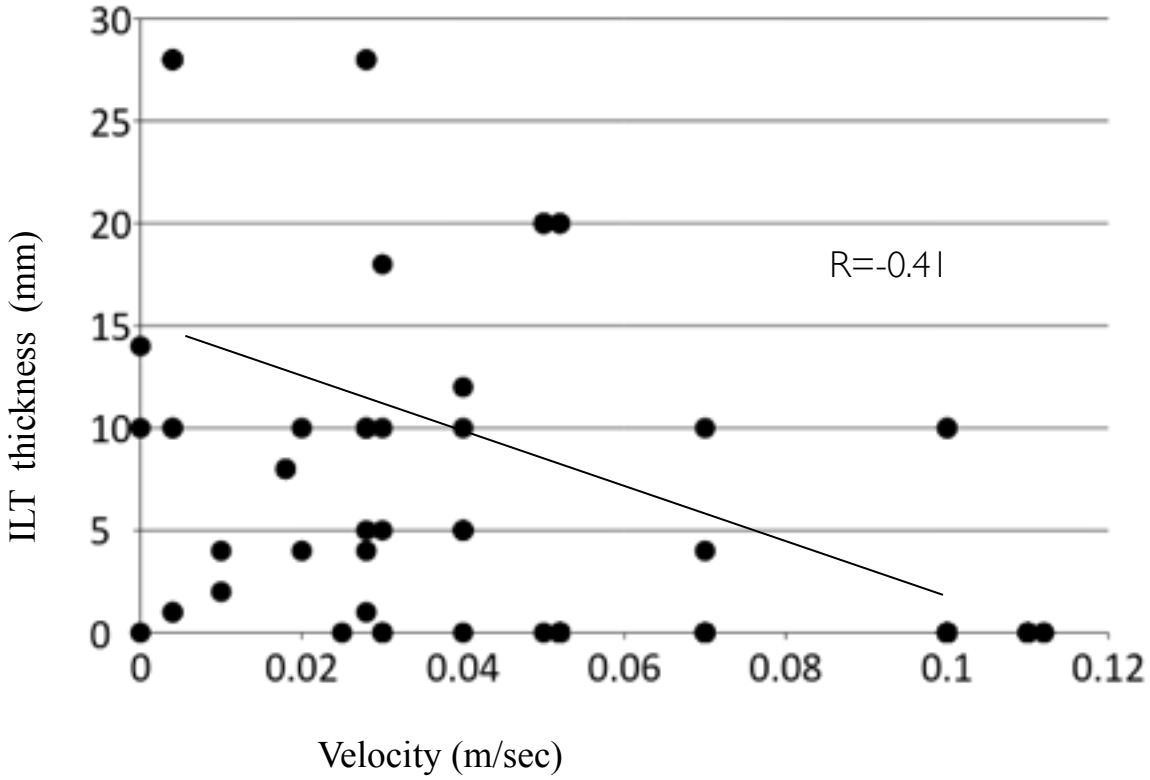

Fig 6. Correlation of blood flow velocity (m/sec) with ILT deposition (mm) in 17 AAA with eccentric ILT. R value of 0.41 and p value <0.05.

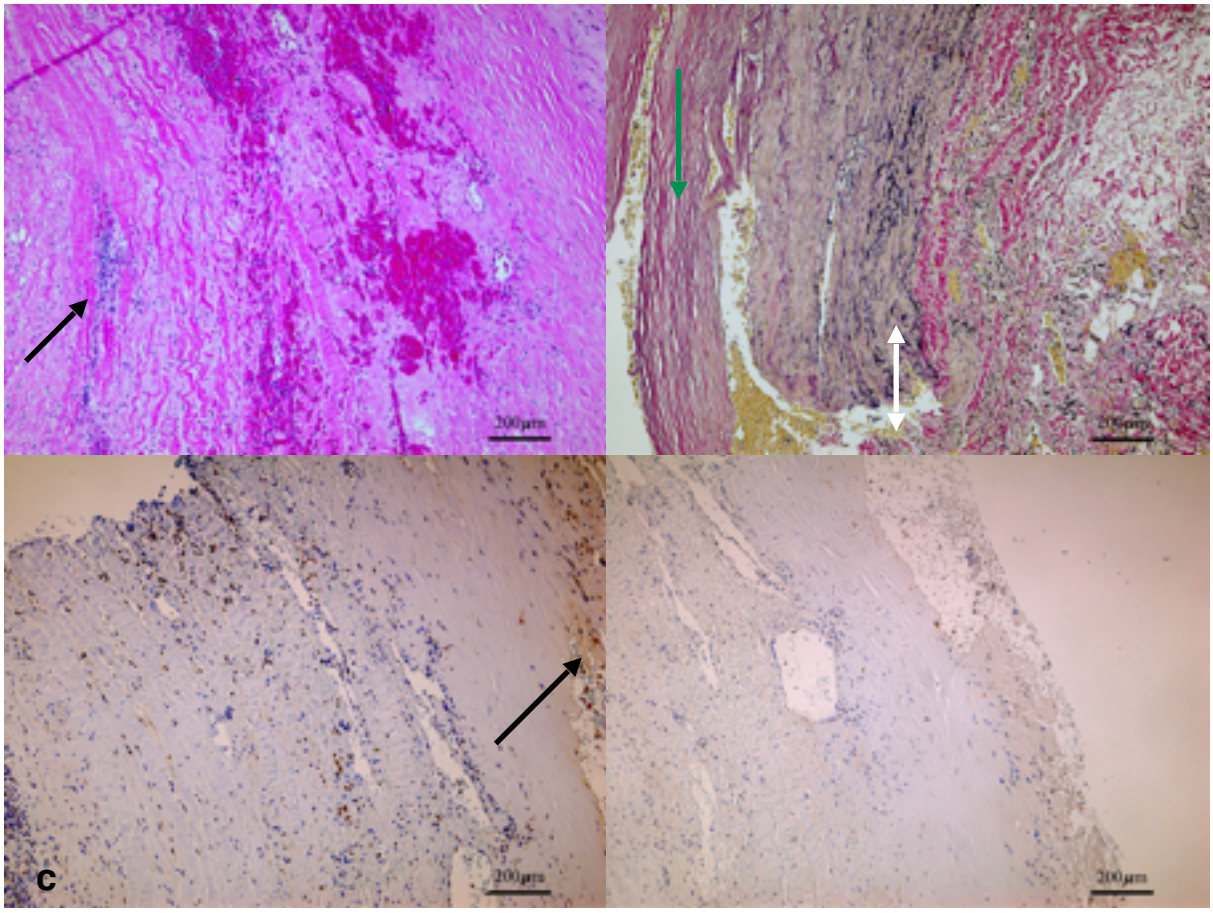

Fig. 7 Histology representation of aortic tissue for patient RC18-1 Histology at 200x magnification examples of nucleated inflammatory cells on H&E stain (black arrow) a., VG staining showing collagen (green arrow) and elastin (white arrow) (b), IHC staining of MMP-9 total brown areas staining positive for MMP9 and beige areas demonstrating areas of calcium artifact(black arrow)(c.), IHC staining for MMP-9active (d.) These samples were assessed as having low inflammation and high elastin content with low amounts of MMP9 total and active.

Univariate analysis showed a $r = -0.43$ ($p < 0.001$) correlation with elastin and MMP-9 total and $r = -0.47$ ($p < 0.001$); suggesting that elevated levels of MMP-9 active and total were associated with less elastin within the aortic tissue at that location. When collagen was correlated with MMP-9 total a negative relationship of $r = -0.243$ ($p = 0.02$) was seen. Collagen and MMP-9 active also showed a negative relationship with $r = -0.37$ ($p < 0.001$); these are moderate to strong relationships (table 2).

Table2. Univariate analysis with Pearsons regression between elastin and collagen and qualitative amounts of MMP-9 total and MMP-9 active.

	MMP-9 total	P- value	MMP -9 active	p-value
Elastin	r = -0.43	<0.001	r = -0.47	<0.001
Collagen	r = -0.243	0.02	r = -0.37	<0.001

Pearson regressions were also used to correlate velocities and amounts of MMP-9 total, active and elastin and collagen. These results are shown in table 5. With this qualitative analysis there was no statistically significant correlation between any variables and velocity. Of note is that MMP-9 was mildly correlated in a positive direction and Collagen and elastin had negative correlation.

We also examined the presence of ILT with the presence of MMP-9 active, total and elastin and collagen in our qualitative analysis. The correlation showed a mild to moderate positive correlation to the total MMP-9 $r = 0.201$ p value of < 0.01 and MMP-9 active had a mild to moderate correlation, $r = 0.227$ ($p < 0.05$). Suggesting that in areas of high ILT there were increased amounts of MMP9 total and active. Presence of thrombus was correlated with less elastin within the aortic tissue $r = -0.100$ ($p < 0.05$) at that AAA location. Collagen was mildly increased in regions of increased ILT but the value was not statistically significant in the quantitative analysis.

Table 3. Pearsons correlation of velocity (m/sec) versus ILT deposition and qualitative variables MMP-9 Total, active and content of collagen and elastin (*p < 0.10 and **p < 0.05)

	Velocity (m/sec)	Thrombus
MMP-9 Total	.072	0.201 *
MMP-9 active	0.053	.227**
Collagen	-.066	0.170
Elastin	-.173	-.100**

Quantitative analysis of aortic tissue and thrombus deposition

Twenty-one sets of aortic tissue samples were sent for quantitative MMP9 total analysis. A summary of the MMP-9 concentrations are seen in appendix c. Up to 6 tissue sample from each patient were included, 0-3 samples of ILT from the aortic tissue were included. In 17 patients there was eccentric ILT. AAA with eccentric thrombus showed that 14/17 (82%) had highest mean levels of MMP-9 associated with higher levels of ILT (Fig.8). The mean MMP-9 concentration in areas of high thrombus was 42.1 ng/mg with a standard error of 10.2, the mean concentration of MMP-9 in areas of low thrombus was 22.4 +/-5.4.

A total of 30 samples of ILT were harvested from the various patients. Samples of harvested thrombus were distributed throughout the aorta and different locations were associated with different mean velocities. Theses samples were sorted into areas of impingement (high flow velocity) and recirculation (low velocity or reverse flow). Of 23(79%) samples were harvested in areas associate with recirculation, and 7 (21%) in areas of impingement. The mean MMP-9 concentration in areas of recirculation was 53.6 ng/mg +/-10.6 and mean MMP-9 concentration of impingement of 9.5 +/- 3.4 (Fig 9).

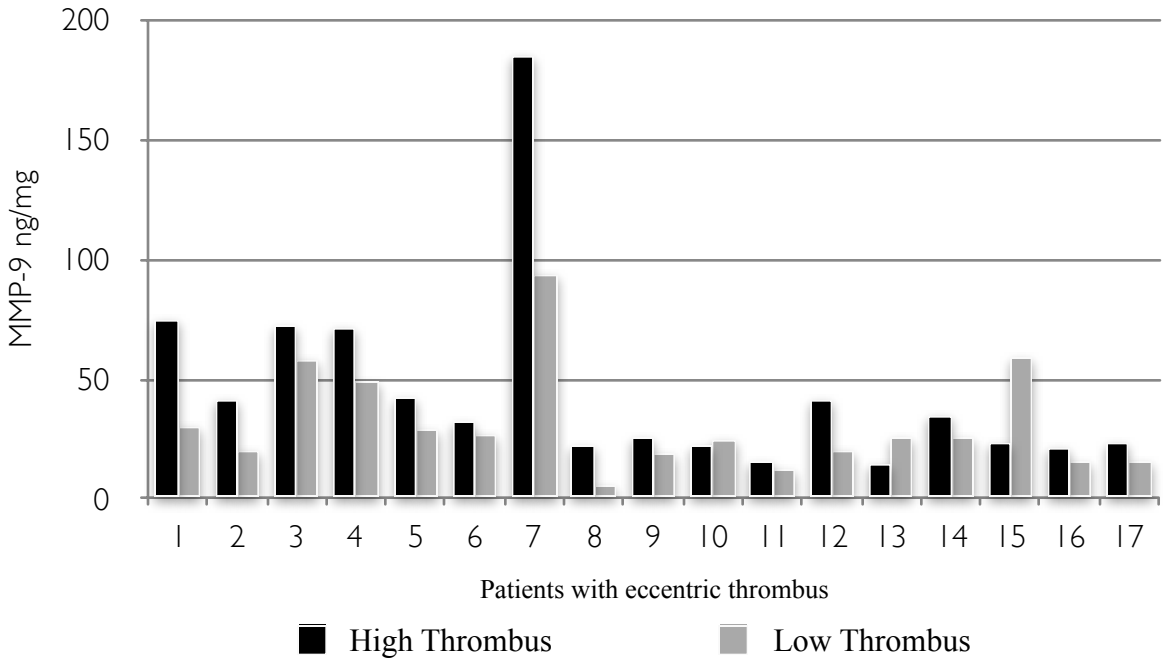

Fig8: Full thickness aortic MMP-9 levels (ng/ mg protein) in areas of low and high ILT deposition in 17 patients with eccentric ILT deposition.

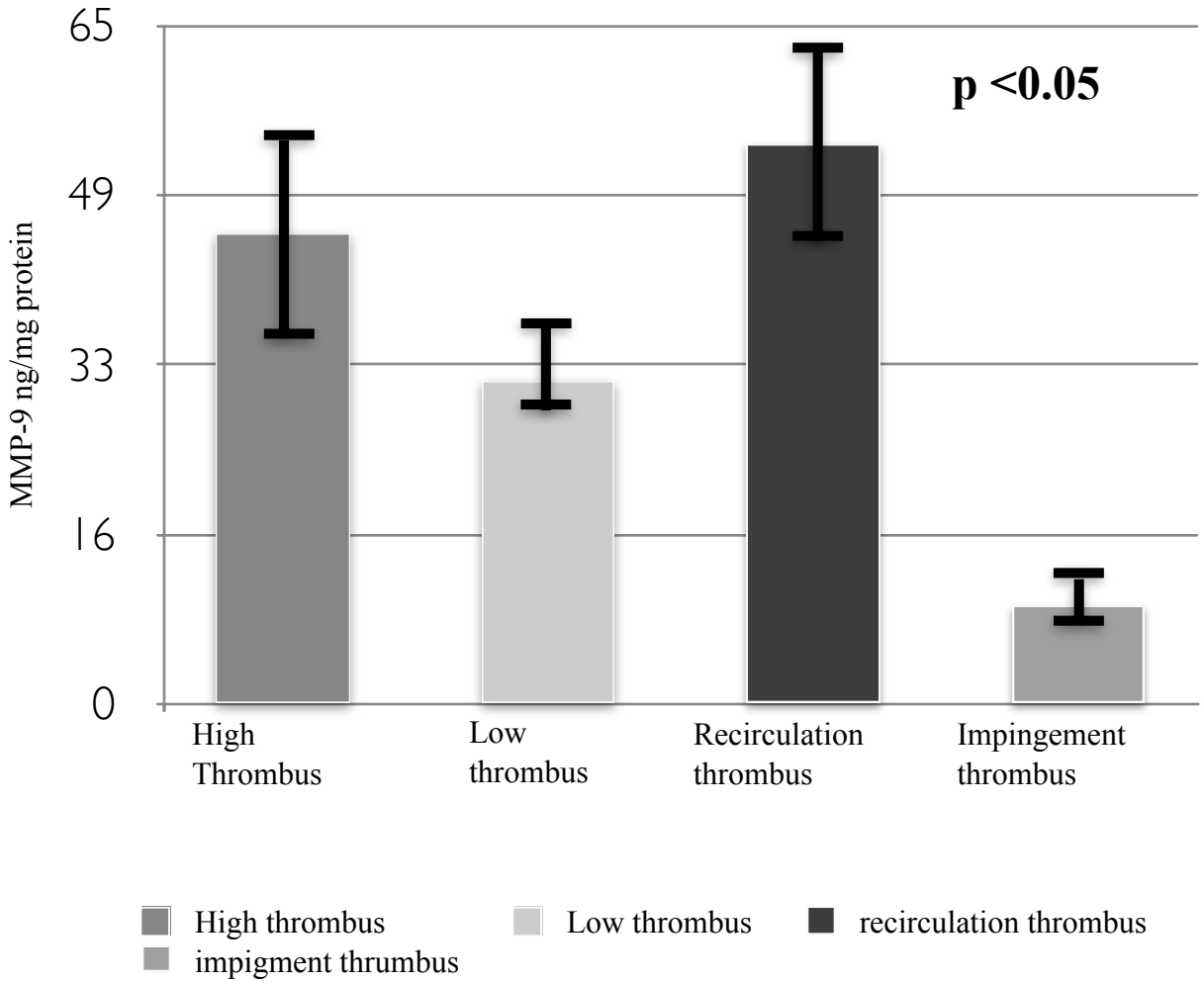

Fig 9.Mean (+/-standard error) MMP-9 tissue levels (ng/mg) protein in regions of high (43.6 +/-10.2) and low ILT (30.7 +/-5.4) deposition ($p<0.05$). Mean (+/- standard error) MMP-9 thrombus levels in regions of impingement 9.5 +/- 3.4 and recirculation 53.6 +/- 10.6 (ng/mg).

Discussion

Size, inflammation, biomechanical forces and patient genetics are now accepted as the main pathophysiologic factors that lead to the formation and rupture of AAA. Many previous investigations have looked at how each individual factor contributes to the formation and rupture of AAA, but none have examined how biomechanical forces,-inflammation, and proteolytic degradation are related; specifically, how biomechanical forces contribute to the dynamic remodelling that create and propagate the formation of AAA, and eventually lead to their rupture. Even though we accept that there is more to rupture than size alone, we still use it as our clinical marker in directing the surgical management of aneurysms. This research successfully incorporated an investigation of the effect of inflammatory cells, ILT, proteolytic factors, and MMP-9s, with an investigation of predicted pulsatile aortic flow and wall sheer stress within AAA. MMP-9, specifically, has been studied in AAA populations, as it has been most associated with the formation and rupture of AAA. The ability to incorporate and compare more contributing factors in AAA pathogenesis improves our model of AAA, and may lead to more accurate understanding of the core biologic factors responsible in the formation and rupture of AAA. By understanding the precise pathophysiology of AAA, there is the potential for targeted therapies that may significantly improve the management of AAA disease.

Demographics

This study included 24 patients, excluding 1 pilot patient (data not included) all patients were accounted for by the end of the study. This is a relatively large number aortic tissue samples compared with trials that study the presence of MMPs within aortic tissue. Most research on AAA tissue have significantly fewer subject and do not harvest in a stereotyped manner. Tissue

in those trials tends to be harvested from variable location and in some cases the samples are not full-thickness. The rational for our study was to have a large population of AAA with enough tissue to represent the entire AAA, This was reasoned to be more accurate in delineating the pathogenesis of the formation of AAA. which should be relatively consistent in our population. The characteristics of the population of patients in this study were similar of most patients that undergo AAA repair; male, 7th decade of life, smokers and hypertension. Our AAA population is an accurate representation of the standard AAA population in non-ruptured aortas undergoing elective repair. One could argue that; there may have been less variability in the genetic background for the population of AAA studied as it was done at a single centre in one province in Canada, however, Canada is relatively genetically diverse and we do not feel this played a signigicant role in biasing the types of AAA. This research did not examine inflammatory aneurysms, which are known to involve 10% of all AAA. Inflammatory AAA are clinically very different from typical AAA and have many similarities to retroperitoneal fibrosis. An inflammatory AAA is densely inflamed and may involve surrounding tissues, such as renal vein, ureters and duodenum. Although there may be a similar pathogenesis of the two types of aneurysms, we believe that the inclusion of inflammatory aneurysm would no represent the typical process of AAA formation.

CTA modelling and analysis of Flow and ILT

We successfully generated *Open-Foam CFD* models for 21 patients in our study. Our study is similar to other flow analyses of AAA areas with larger intraluminal diameter showing more turbulent flow. We also showed that turbulent flow and recirculation were also correlated with thicker ILT whereas impingement and the high velocities correlated with thinner ILT depo-

sition. Until recently ILT was thought to passively accumulate in AAA, and possibly provide protection against rupture by reducing peak wall stress. There is increasing evidence that ILT is biologically active and may promote aortic wall degeneration and rupture; either by stimulating inflammatory and proteolytic mechanisms, or by providing a barrier to aortic wall oxygenation. AAA with higher ILT are associated with faster growth rates and higher risk of rupture (53). Conversely, areas of low ILT may allow better penetration of circulation inflammatory factors that may promote wall degeneration (54). Variation in ILT deposition may also be flow-mediated; with flow impingement preventing ILT accumulation, and recirculating flow favouring ILT deposition (3). Although there is increasing evidence of ILT involvement in AAA, it's role remain controversial.

We are aware that there may be some inaccuracy in the location of aortic tissue harvest and the velocity. This is because the flow diagrams generated by the CFD studies cannot give exact velocities at the sampling locations just a general sense of what wall stress that the aorta is experiencing at that location of the aorta. We used the flow diagrams to assume that there is very little variability within a 5 cm range in the aorta, so on average the flow we measured at our sample locations was reasonably accurate. There are studies in animal models using more advanced imaging systems that are able to look at much smaller portion of the aorta to more accurately estimate WSS, which maybe the next step in analyzing AAA pathogenesis (52). The estimation of velocity from the diagrams in this study was based on previous validated studies. The data generated from the models was sufficient for us to answer the question of the direction on flow and WSS that the aorta was experiencing at each location

Qualitative analysis of tissue samples

MMP-9 is thought to play a key role in AAA formation and rupture; this has been shown in the literature (27-29,47). We have shown in this patient population that MMP-9's is associated with lower levels of collagen and elastin in aortic tissue which is consistent with current literature for MMPs(50). Although, there are concerns with accuracy in qualitative analysis, it was used more to confirm that our population was behaving in the same way that was previously seen in the literature and to histologically confirm quantitative method. Specifically the analysis of the tissue with H&E, VG and IHC allowed us to assess the aortic histology not only in different locations within the aorta but also with different modalities. The goal of this qualitative analysis was to get a general understanding of variability throughout an AAA. The histologic analysis of the tissue samples was sometimes incomplete because of the qualities of the aortic tissue. Specifically, increased amounts calcium in a sample would make it difficult to ensure good quality aortic tissue that could be-histologically analyzed. We did not include the tissue samples that had excessive calcium disruption of the tissue. A total of 5 samples (all from different aortas) were excluded from out qualitative analysis. Exclusion of tissue samples created incomplete data in when we were doing our correlations. The overall effect of having missing data was most likely small. Increased calcium within tissue samples may have had an impacted on IHC analysis as well. This is because the tissue samples that were grossly calcified in paraffin wax cassette required decalcification with low pH substance that may have changed the configuration of MMP-9 within our tissue samples. MMP-9 is synthesized in the cell as a proenzyme and introduction of H^+ ions may cause changes to the structure of the protein in its active and latent form. IHC relies on antigen binding and if there is change to the structure from changing in pH binding locations may be affected, causing inaccurate amounts of MMP-9 total and active seen. When looking at

the qualitative analysis we see that there is little difference between MMP-9 total and MMP-9 active which suggests that even if there was an effect on the zymogen MMP-9 it was little and may not have impacted the overall results. Our quantitative results were expressing total MMP-9 and calcium was not an issue in the analysis of lyophilized tissue because when the crude protein is removed from the aortic tissue it does not include the calcium during ELIZA analysis .

Quantitative analysis of aortic tissue and thrombus deposition

This study was the first to correlate flow-mediated increase in ILT deposition with increased tissue levels of MMP-9 activity, and decreased elastin and collagen content in human AAA. These findings suggest that ILT deposition may promote local increases in MMP-9 proteolytic activity in the AAA wall that may selectively weaken these regions and promote rupture. Other trials have shown amounts of MMP within aortic tissue but none have examined multiple sampling sites from one aorta. This trial is unique in that it gives a more representative map of the inflammatory and proteolytic process in an AAA. It also takes into account the role that WSS and ILT may play within that same AAA. We know from previous studies that areas of turbulent or recirculating blood activates platelets and increases thrombus deposition (47,49). We can now say that turbulent flow may contributes to an increase in proteolytic activity by increasing ILT deposition at that location in the aorta.

When we examined predicted pulsatile flow and MMP-9 concentrations in ILT, we found that in areas of low flow and recirculation (low WSS) there were higher concentrations of MMP-9. This suggests that in areas of impingement/ high flow there is less proteolytic degradation than in the areas where blood flow recirculates. An explanation for this may be in knowing that blood flows in a Newtonian way; constant viscosity at all shear rates, and that cells within the blood

are separated throughout the lumen with erythrocytes found mostly in the centre and platelets and white blood cells being pushed near the luminal wall (53-56). When whole blood is subject to turbulent flow and recirculation this Newtonian flow is disrupted. This disruption in flow may increase interactions between erythrocytes and fibrinogen leading to increase in viscosity (57-58). The interactions of mediators in the blood can contribute to platelet adhesion, increased density of inflammatory mediator migration and activation or proteolytic enzymes.

Flow and MMP-9 in Thrombus

Finally, we examined the amount of MMP-9 ng/mg found in thrombus at high and low velocities. We found that in areas where there was recirculation, ILT (low WSS) on average had significantly lower amounts of MMP-9 total than in areas of impingement/ elevated velocities. This is in keeping with finding higher levels of MMP-9 in areas of high thrombus and recirculation in our aortic tissue samples. This study is the first to demonstrate flow and deposition of MMP-9 within thrombus.

Our results are comparable to other studies that showed the presence of MMPs throughout diseased aortas (46,47); however, we not only showed the presence of MMP-9, but also found that levels of MMP-9 varied considerably throughout the aorta, suggesting again that the remodelling occurring within AAAs is a dynamic process. Not only, did we see variation in MMP-9 in the aorta, but also an increase in the amount of MMP-9 in areas of highest intraluminal thrombus deposition. This has been demonstrated in the literature with MMP-2 (47) but not with MMP-9. Polzer et al. 2011 showed that MMP-2 and MMP-9 in areas of thickest thrombus but did not sample tissue from the rest of the aorta. The reasoning for sampling areas of thickest ILT is to see if they had increased inflammatory/proteolytic mediators, however this model is not

representative of the entire aorta. Limiting sampling to one location limits your ability to assess the dynamic remodelling of the entire aorta. We have shown with sampling of multiple locations of an AAA that areas of thicker,not just thickest ILT, have higher concentrations of MMP-9. The difference in the results may be a reflection of the dynamic process that AAA go through during remodelling, and sampling the aorta at multiple locations creates a more representative model. Our results further reinforces that ILT contributes to the inflammatory state that creates and propagates formation of AAA.

Conclusion and Future directions

We set out to show the variability of aortic tissue concentration of MMP-9 within AAA and also how differences in intraluminal thrombus and wall sheer stress impacted the biologic activity in the aorta. Our data showed that there is great variability in concentrations of MMP-9 through the aneurysmal aorta. We also showed that in areas of thick intraluminal thrombus is associated with higher levels of MMP-9 and lower WSS and flow recirculation. Lastly we found that flow recirculation is associated with higher levels of MMP-9 in ILT.

The ultimate goal of this work is to develop a greater understanding of the pathogenesis of AAA which will allow us to create management plans that ultimately better serve patients by preventing death due to rupture. A clearer-understanding-of AAA pathogenesis will also help pinpoint areas in the process that can be targeted to more effectively halt growth of the expanding aorta. The goal would be to further understand the cellular mediators involved in in expansion and rupture in the hope that targeted therapies might be developed.This work may even be helpful in explaining the continued growth of AAA after repair with endovascular grafts.

The role of MMP-9 has been more clearly delineated in ILT deposition and how it is related to flow in the aneurysmal abdominal aorta. An understanding of the factors that create AAA may also help us predict failures in treatment with EVAR or open repair. This work is another step in the direction of a more complete understanding of how AAA form and rupture.

References

[1] Choke E, Cockerill G, Wilson WRW, Sayed S, Dawson J, Loftus I,et al. A review of biological factors implicated in abdominal aortic aneurysm rupture. Eur J Vasc Endovasc Surg 2005;30(3):1–18.

[2] Crawford CM, Hurtge-Grace K, Talarico E, Marley J. Abdominal aortic aneurysm: an illustrated narrative review. J Manip Physiol Ther 2003;26(3):184–95.

[3] Thompson RW. Reflections on the pathogenesis of abdominal aortic aneurysm. Cardiovasc Surg 2002;10(4):389–94.

[4] Ailawadi G, Eliason JL, Upchurch Jr GR. Current concepts in the pathogenesis of abdominal aortic aneurysm. J Vasc Surg 2003;38(3):584–8.

[5] Kadoglou NP, Liapis CD. Matrix metalloproteinases: contribution to pathogenesis, diagnosis, surveillance, and treatment of abdominal aortic aneurysms. Curr Med Res Opin 2004;20(4):419–32

[6] Panek B, Gacko M, Palka J. Metalloproteinases, insulin-like growth factor—I and its binding proteins in aortic aneurysm. Int J Exp Pathol 2004;85(3):159–64.

[7] Treska V, Kocova J, Boudova L, Neparsova P, Topolcan O, Pecen L, et al. Inflammation in the wall of abdominal aortic aneurysm and its role in the symptomology of aneurysm. Cytokine, Cell Mol Therapy 2002;7(3):91–7.

[8] Satta J, Mennander A, Soini Y. Increased medial tunel-positive staining associated with apoptotic bodies is linked to smooth muscle cell diminution during evolution of abdominal aortic aneurysms. Ann Vasc Surg 2002;16(4):462–6.

[9] Gimbrone Jr MA, Topper JN, Nagel T, et al: Endothelial dysfunction, hemodynamic forces, and atherogenesis. Ann N Y Acad Sci 2000; 902:230.

[10] Hoshina K, Sho E, Sho M, et al: Wall shear stress and strain modulate experimental aneurysm cellularity. J Vasc Surg 2003; 37:1067.

[11] Greve JM, Les AS, Tang BT, et al: Allometric scaling of wall shear stress from mice to humans: quantification using cine phase-contrast MRI and computational fluid dynamics. Am J Physiol Heart Circ Physiol 2006; 291:H1700.

[12] Vollmar JF, Paes E, Pauschinger P, et al: Aortic aneurysms as late sequelae of above-knee amputation. Lancet 1989; 2:834.

[13] Yeung JJ, Kim HJ, Abbruzzese TA, et al: Aortoiliac hemodynamic and morphologic adaptation to chronic spinal cord injury. J Vasc Surg 2006; 44:1254.7

[14] Vorp DA, Raghavan ML, Webster MW. Mechanical wall stress in abdominal aortic aneurysm: influence of diameter and asymmetry. J Vasc Surg 1998;27(4):632–9.

[15] Finol EA, Di Martino ES, Vorp DA, Amon CH. Fluid–structure interaction and structural analyses of an aneurysm model. In: Proceedings of the 2003 summer bioengineering conference SBC2003, Key Biscayne, FL, 2003. p. 75–6.

[16] Finol EA, Keyhani K, Amon CH. The effect of asymmetry in abdominal aortic aneurysms under physiologically realistic pulsatile flow conditions. J Biomech Eng 2003;125:207–17.

[17] Finol EA, Shkolnik AD, Scotti CM, Amon CH. Computational modeling of abdominal aortic aneurysms: an assessment of rupture potential for presurgical planning. In: Payan Y, editor. Biomechanics applied to computer assisted surgery. India: Research Signpost Publisher;

2005. p. 243–60.

[18] Di Martino ES, Guadagni G, Fumero A, Ballerini G, Spirito R, Biglioli P, et al. Fluid–structure interaction within realistic threedimensional models of the aneurysmatic aorta as a guidance to assess the risk of rupture of the aneurysm. Med Eng Phys 2001;23(9):647–55.

[19] Fillinger MF, Marra SP, Raghavan ML, Kennedy FE. Prediction of rupture risk in abdominal aortic aneurysm during observation: wall stress versus diameter. J Vasc Surg 2003;37(4):724–32.

[20] Fillinger MF, Raghavan ML, Marra SP, Cronenwett JL, Kennedy FE. In vivo analysis of mechanical wall stress and abdominal aortic aneurysm rupture risk. J Vasc Surg 2002;36(3):589–97.

[21] Raghavan ML, Vorp DA, Federle MP, Makaroun MS, Webster MW. Mechanical Wall stresses on three-dimensionally reconstructed models of abdominal aortic aneurysm. In: Proceedings of the first joint BMES/EMBS conference, Atlanta, GA, 1999.

[22] Scotti CM, Shkolnik AD, Muluk S, Finol EA. Fluid–structure interaction in abdominal aortic aneurysms: effects of asymmetry and wall thickness. Biomed Eng 2005;4:64. [19] Di Martino ES, Bohra A, Vande Geest JP, Gupta N, Makaroun M, Vorp DA. Biomechanical properties of ruptured versus electively repaired abdominal aortic aneurysm wall tissue. J Vasc Surg 2006;43(3):570–6.

[23] Fillinger MF, Racusin J, Baker RK, Cronenwett JL, Teutelink A, Schermerhorn ML, et al. Anatomic characteristics of ruptured abdominal aortic aneurysm on conventional CT scans: implications for rupture risk. J Vasc Surg 2004;39(6):1243–52.

[24] Thubrikar MJ, Robicsek F, Labrosse M, Chervenkoff V, Fowler BL. Effect of thrombus on

abdominal aortic aneurysm wall dilation and stress. J Cardiovasc Surg 2003;44(1):67–77.

[25] Kleinstreuer C, Li Z. Analysis and computer program for rupture risk prediction of abdominal aortic aneurysms. Biomed Eng 2006;5(1):19.

[26] Boyd, AJ, Kuhn, D, Lozowy, R, Kulbisky G P, Low wall shear stress predominates at sites of abdominal aortic aneurysm rupture. JVS, 2016 Jun, 63(6): 1613-1619

[27] Yamashita A, Noma T, Nakazawa A, et al. Enhanced expression of matrix metalloproteinases-9 in abdominal aortic aneurysms. World J Surg 2001;25:259-65

[28]. Tamarina NA, McMillan WD, Shively VP, Pearce WH. Expression of matrix metalloproteinases and their inhibitors in aneurysms and normal aorta. Surgery 1997;122:264-72

[29.] Palombo D, Maione M, Cifiello BI, Udini M, Maggio D, Lupo M. Matrix metalloproteinases. Their role in degenerative chronic diseases of abdominal aorta. J Cardiovasc Surg. 1999;40:257-60

[30.] Deng GG, Martin-McNulty B, Sukovich DA, et al. Urokinasetype plasminogen activator plays a critical role in angiotensin IIinduced abdominal aortic aneurysm. Circ Res 2003;92:510-7

[31.] Carmeliet P. Proteinases in cardiovascular aneurysms and rupture: targets for therapy? J Clin Invest 2000;105:1519-20

[32] Lorelli DR, Jean-Claude JM, Fox CJ, et al: Response of plasma matrix metalloproteinase-9 to conventional abdominal aortic aneurysm repair or endovascular exclusion: implications for endoleak. J Vasc Surg 2002; 35:916.

[33] Longo GM, Xiong W, Greiner TC, et al: Matrix metalloproteinases 2 and 9 work in concert to produce aortic aneurysms. J Clin Invest 2002; 110:625.

[34] Thompson RW, Holmes DR, Mertens RA, et al. Production and localization of 92-kilodalton gelatinase in abdominal aortic aneurysms. J Clin Invest 1995;96:318-26

[35] McMillan WD, Patterson BK, Keen RR, Shively VP, Cipollone M, Pearce W. In situ localization and quantification of mRNA for 92-kD type IV collagenase and its inhibitor in aneurysmal, occlusive and normal aorta. Arterioscler Thromb Vasc Biol 1995;15:1139-44

[36] Ailawadi G, Knipp BS, Lu G, et al. A nonintrisic regional basis for increased infrarenal aortic MMP-9 expression and activity. J Vasc Surg 2003;37:1059-66

[37] Wilson WR, Anderton M, Schwalbe EC, et al: Matrix metalloproteinase-8 and -9 are increased at the site of abdominal aortic aneurysm rupture. Circulation 2006; 113:438-445.

[38] Wilson WR, Anderton M, Choke EC, et al: Elevated plasma MMP1 and MMP9 are associated with abdominal aortic aneurysm rupture. Eur J Vasc Endovasc Surg 2008

[39] Pyo R, Lee JK, Shipley JM, et al. Targeted gene disruption of matrix metalloproteinase-9 (gelatine B) suppresses development of experimental abdominal aortic aneurysms. J Clin Invest 2000;105:1641-49

[40] Allaire E, Hasenstab D, Richard D, et al. Prevention of aneurysm development and rupture by local overexpression of plasminogen activator inhibitor – 1. Circulation 1998;98:249-55

[41] Deng GG, Martin-McNulty B, Sukovich DA, et al. Urokinasetype plasminogen activator plays a critical role in angiotensin IIinduced abdominal aortic aneurysm. Circ Res 2003;92:510-7

[42] Saito S, Zempo N, Yamashita A, Takenaka H, Fujoka K, Esato K. Matrix metalloproteinase expressions in arteriosclerotic aneurysmal disease. Vasc Endovasc Surg 2002;36:1-7

[43] Boyd, AJ, Lozowy, RJ, and Kuhn, DSC CFD analysis of abdominal aortic aneurysm

growth: the effect of iliac stenosis. Full manuscript in Proceedings of CANCAM, 2010.

[44] Boyd, AJ, Lozowy, RJ, and Kuhn, DSC Phase-averaged velocity and turbulence statistics in a stenosed tube. Full manuscript in Proceedings of CANCAM 2012.

[45] Duncan ME, Richard JP, Murry et al. Human matrix mettalloproteinase-9: activation by limited trypsin treatment and generation of monoclonal antibodies specific for the activated Human matrix metalloproteinase-9: activation by limited trypsin treatment and generation of monoclocal antibodies specific for the activated. Eur J Biochem. 1998 Nov 15 [PMID: 9851689]

[46] Shang T et al. Journal of Surgical Research, volume 178, issue 2, December 2012 Pages 1029-1037 Fig 3

[47] S. Polzer, T.C. Gasser, J. Swedenborg, J. Bursa. The Impact of Intraluminal Thrombus Failure on the Mechanical Stress in the Wall of Abdominal Aortic Aneurysms. Eur J Vasc & Endovas. Vol 41, Issue 4, Pages 467–473 april 2011

[48] Koole D1, Zandvoort HJ, Schoneveld A, Vink A, Vos JA, van den Hoogen LL, de Vries JP, Pasterkamp G, Moll FL, van Herwaarden JA.Intraluminal abdominal aortic aneurysm thrombus is associated with disruption of wall integrity.J Vasc Surg. 2013 Jan;57(1):77-83. doi

[49] Biasetti J, Hussain F., Gaseer C. Blood flow and coherent vortices in teh normal and aneurysmatic aortas: a fluid dynamical approach to intraluminal thrombus formation. J. R. Soc. Interface Vol. (8) 1449-1261 april 2011

[50] G. Matthew Longo,1 Wanfen Xiong,1 Timothy C. Greiner,2 Yong Zhao,1 Nicola Fiotti,1 and B. Timothy Baxter1,3 Matrix metalloproteinases 2 and 9 work in concert to produce aortic aneurysms, J Clin Invest. 2002 Sep 1; 110(5): 625–632.

[51] Lozowy R., Kuhn D. , Boyd A., The relationship between pulsatile flow impingement and intraluminal thrombus deposition in abdominal aortic aneurysms. Cardiovascular Engineering and Technology. 2016 Nov, 8(1):57-69.

[52] Shepherd, Robert D. et al.A Novel In Vitro Model Predicts Aortic Stent Graft Hemodynamic Alterations After Endovascular Repair. Journal of Vascular Surgery , Volume 62 , Issue 5 , 1376

[53] Speelman L, Schurink GW, Bosboom EM, Buth J, Breeuwer M, van de Vosse FN, Jaco MH. The *mechanical role of thrombus on the growth rate of an abdominal* aortic aneurysm. Vasc Surg. 2010 Jan;51(1):19-26.

[54]Adolph R, Vorp DA, Steed D 1 L, Webster MW, Kameneva MV, Watkins SC. Cellular cotent and permeability of intraluminal thrombus in abdominal aortic aneurysm. J VascSurg1997;25:916-26.

[55] Silverberg E, et al: Cancer statistics, 1990. CA Cancer J Clin 40(1):9–26, 1990

[56]Choksy SA, et al: Ruptured abdominal aortic aneurysm in the Hunt- ingdon district: a 10 year experience. Ann R Coll Surg Engl 81(1):27–31, 1999.

Appendix A

Health Sciences Centre
Winnipeg

Dr. April J. Boyd* MD, PhD, FRCSC
*Practicing as a Medical Corporation

Section of Vascular Surgery
April J. Boyd, MD
Gregory E. J. Harding, MD
Joshua Koulack, MD

Health Sciences Centre

RESEARCH PARTICIPANT INFORMATION AND CONSENT FORM

Title of Study: "Computational Fluid Dynamics Analysis of Pulsatile Flow in Non-Ruptured Abdominal Aortic Aneurysms: A Correlation between Aortic Hemodynamics and Matrix Metalloproteinase Levels.

Principal Investigator: Dr. April J Boyd, GF 546 HSC
Co-Investigator : Prof David C.S. Kuhn, Dept. of Mechanical Engineering,
Sponsor: Application Submitted to Thorlakson Award

You are being asked to participate in a research study. Please take your time to review this consent form and discuss any questions you may have with the study staff. You may take your time to make your decision about participating in this study and you may discuss it with your friends, family or (if applicable) your doctor before you make your decision. This consent form may contain words that you do not understand. Please ask the study staff to explain any words or information that you do not clearly understand.

Purpose of Study

Currently, there is no truly reliable way to evaluate the susceptibility of particular abdominal aortic aneurysms (AAA) to rupture. Discovery of these criteria would vastly improve AAA management. We plan to simulate aortic blood flow from CT scans of non-ruptured AAA and to correlate matrix metalloproteinase (MMP) levels with site-specific flow measurements. This work will improve our understanding of the interaction between the mechanical effect of shear and the local biological factors responsible for AAA wall degeneration and eventual rupture.

A total of 25 participants will participate in this study

Study procedures

Before undergoing repair of your abdominal aortic aneurysm, a blood sample of 5 ml (1 teaspoon) will be withdrawn from a vein in your arm. You may experience bruising at the site of blood withdrawl. At the time of your surgery, several small fragments of your aneurysm sac will be collected from various sites. Removal of this aortic tissue will not affect the quality of your aneurysm repair, nor will is significantly lengthen the duration of your operative procedure.

Routine CT scan images of your aneurysm will be converted to a computer format where flow can be simulated within each aneurysm. From this flow information we can calculate the pressure and wall shear stress profiles within each aneurysm and compare it to the tissue study samples above.

All blood and tissue samples will be coded for confidentiality, with the code known only to Dr. Boyd, and stored in a locked laboratory at the Bannatyne campus of

the University of Manitoba.

Participation in the study will be for 1 day (the day of your aneurysm repair)

Risks and Discomforts

The only discomfort will be related to the sampling of blood from your arm. You may develop bruising at this site. Rare complications include serious skin infections and blood infection.

The aortic tissue will be taken while you are under general anesthetic for your aneurysm repair. The aneurysmal aortic sac tissue samples taken do not affect your aneurysm repair as this tissue is excluded from the graft which is used to replace your aorta. Generally the sac of the excluded aneurysm is wrapped around the fabric graft repair to protect the graft from becoming adherent to surrounding bowels. Removal of small pieces of excluded aneurysm sac will not affect the wrapping of your aortic graft.

Benefits

There will be no direct benefit to you from participating in this study. We hope the information learned from this study will benefit other people by helping to better predict the factors which may promote abdominal aortic aneurysm growth and rupture.

Costs

No cost to you.

Confidentiality

Information gathered in this research study may be published or presented in public forums, however your name and other identifying information will not be used or revealed. Despite efforts to keep your personal information confidential, absolute confidentiality cannot be guaranteed. Your personal information may be disclosed if required by law.

Medical records that contain your identity will be treated as confidential in accordance with the Personal Health Information Act of Manitoba.

The University of Manitoba Biomedical Research Ethics Board may review records related to the study for quality assurance purposes.

All records will be kept in a locked secure area and only those persons identified will have access to these records. If any of your medical/research records need to be copied to any of the above, your name and all identifying information will be removed. No information revealing any personal information such as your name, address or telephone number will leave the Health Sciences Centre.

Voluntary Participation/Withdrawal from the Study

Your decision to take part in this study is voluntary. You may refuse to participate or you may withdraw from the study at any time. Your decision not to participate or to withdraw from the study will not affect your care at this centre. We will tell you about any new information that may affect your health, welfare, or willingness to stay in this study.

Questions

You are free to ask any questions that you may have about your treatment and your rights as a research participant. If any questions come up during or after the study or if you have a research-related injury, contact the study doctor and the study staff: *Dr. April Boyd* at

For questions about your rights as a research participant, you may contact The University of Manitoba, Bannatyne Campus Research Ethics Board Office at

Do not sign this consent form unless you have had a chance to ask questions and have received satisfactory answers to all of your questions.

Statement of Consent

I have read this consent form. I have had the opportunity to discuss this research study with *Dr. April Boyd* and or his/her study staff. I have had my questions answered by them in language I understand. The risks and benefits have been explained to me. I believe that I have not been unduly influenced by any study team member to participate in the research study by any statements or implied statements. Any relationship (such as employer, supervisor or family member) I may have with the study team has not affected my decision to participate. I understand that I will be given a copy of this consent form after signing it. I understand that my participation in this study is voluntary and that I may choose to withdraw at any time. I freely agree to participate in this research study.

I understand that information regarding my personal identity will be kept confidential, but that confidentiality is not guaranteed. I authorize the inspection of any of my records that relate to this study by The University of Manitoba Research Ethics Board.

By signing this consent form, I have not waived any of the legal rights that I have as a participant in a research study.

Participant signature_____ **Date** _____
(day/month/year)

Participant printed name: _____

I, the undersigned, attest that the information in the Participant Information and Consent Form was accurately explained to and apparently understood by the participant or the participant's legally acceptable representative and that consent to participate in this study was freely given by the participant or the participant's legally acceptable representative.

Witness signature_____ **Date** _____
(day/month/year)

Witness printed name: _____

I, the undersigned, have fully explained the relevant details of this research study to the participant named above and believe that the participant has understood and has knowingly given their consent

Printed Name: _____Date _____
(day/month/year)

Signature: _____

"**Role in the study: _____***[This must be done by an authorized/ qualified member of the research team i.e. investigator, study nurse, etc.]*".

Relationship (if any) to study team members:**_____**

Appendix B

10x TBS

80 g NaCl Simga (C1909)

24.4 g Tris - Trizma Base Sigma (T1503)

ddH_2O

pH adjust 7.6 with HCl

1xTBST

100 ml 10x TBS

900 ml ddH_2O

1 ml Tween 20 (polyoxyethylene sorbitan monolaurate) Omnipur/EMD 9480

mixed until combined

Horse-Radish Peroxidase/ Biotin preparation for blocking of endogenous enzyme

20 ml 3% H_2O_2

180 ml Methanol - EMD millipore (MX0488-1)

Mix in the Dark

Citrate Buffer

9 ml Solution A

21.01 g Citric Acid -Sigma (S4641)

1 L ddH_2O

41 ml Solution B

29.441 g Tisodium Citrate Dihydrate - Sigma (24641)

1L

450 ml ddH_2

mixed right before use

Blocking Buffer 5% NRS

25 μL - Normal Rabbit Serum - NOVUS NBP1 -716816

475 μL - TBST

mixed and kept cool 4 °

Streptavidin -Horseradish peroxidase reagent - NOVUS (NBP2 -29370)

2 μL of Streptavidin- HRP

1000 μL 5% NRS in TBST

Secondary Anitbody: rabbit anti-mouse IgG antibody Biotin - NOVUS (NB720-B)

Isotype : mouse IgG1 isotype Control : NOVUS (NBP2 - 24894)

MMP9 Total Antibody - abcam (ab58803)

publications -

Njie eG et al. PLoS one. 2012 7(4) Epub 2012 Apr4 Fig 2 doi 10.137/journal pone. 0034097; april 4 2012

Shang T et al. Journal of Surgical Research, volume 178, issue 2, December 2012 Pages 1029-1037 Fig 3

MMP9 Active Antibody - NOVUS (NBP2 -13173)

publications -

Duncan ME, Richard JP, Murry et al. Human matrix mettalloproteinase-9: activation by limited trypsin treatment and generation of monoclonal antibodies specific for the activated Human matrix metalloproteinase-9: activation by limited trypsin treatment and generation of monoclocal antibodies specific for the activated. Eur J Biochem. 1998 Nov 15 [PMID: 9851689]

Development of Slides

DAB (3, 3'-diaminobenzidine tetrahydrochloride)

120 μL DAB 10x

460 μL Stable peroxide Substrate Buffer

Fisher Scientific (34002)

Appendix C

Table 1. Summary of 24 patients tissue sample analysis for inflammatory cells (H&E), Elastin (VG-E), collagen (VG-C) and MMP-9 active (MMP-9a) and Total (MMP-9t). Velocities at each location are also shown in m/sec (m/s)Values represent relative amounts of the above variables; 0-30% (1) 31-60% (2), >60(3)

Patient	Sample #	H&E	MMP-9t	MMP-9a	VG -E	VG -C	Velocity m/s
AB95-7	1	2	2	2	2	2	0.01
	2	2	2	2	1	3	0.01
	3	2	1	1	3	3	0.07
	4	1	3	3	0	1	0.07
AM42-2							
	1	4	2	1	3	3	0.025
	2	3	1	1	2	3	0
	3	1	1	1	1	1	0
	4	1	1	1	3	3	0
AR49-6							
	1	NA	NA	NA	NA	NA	0.036
	2	1	1	2	1	1	0.036
	3	1	1	1	2	2	0.036
	4	2	1	0	3	3	0.036
CS94-7							
	1	3	1	1	3	3	0.02
	2	1	1	1	3	3	0.02
	3	2	2	2	2	2	0.04
	4	2	2	2	2	2	0.04
EG86-3							
	1	2	1	1	3	3	0.024
	2	3	2	2	1	2	0.024
	3	3	2	2	1	2	0.076
	4	2	2	1	1	2	0.076
ES58-5							
	1	2	3	2	0	2	0.05
	2	2	2	2	0	1	0.05
	3	2	1	1	3	3	0.1
	4	2	1	1	1	3	0.1
FD29-5							
	1	2	2	2	1	2	0.004
	2	3	2	3	1	2	0.028
	3	3	3	2	0	1	0.052
	4	2	1	1	3	3	0.028
JP11-2							
	1	2	2	2	1	2	0.01
	2	2	2	2	3	3	0.01
	3	3	3	3	2	2	0.01
	4	3	2	2	1	2	0.01
JM05-1							
	1	3	1	1	2	3	0.02
	2	NA	NA	NA	NA	NA	0.02
	3	1	1	1	1	2	0.02
	4	3	2	2	3	3	0.02
JS98-8							
	1	2	1	1	2	2	
	2	NA	NA	NA	NA	NA	
	3	3	2	2	0	1	
	4	2	1	1	0	2	
LQ01-2							
	1	1	1	1	1	2	0.018

	2	2	2	2	0	2	0.018
	3	1	1	1	2	2	0.052
	4	2	2	2	1	2	0.052
MC47-6							
	1	2	1	1	1	3	0.028
	2	2	2	2	2	3	0.028
	3	NA	NA	NA	NA	NA	0.028
	4	2	2	2	2	2	0.028
MN87-8							
	1	2	1	1	1	2	0.028
	2	2	2	2	1	2	0.028
	3	3	3	1	1	2	0.028
	4	2	2	2	2	2	0.028
NJ24-1							
	1	2	1	1	1	2	0.03
	2	NA	NA	NA	NA	NA	0.03
	3	1	2	2	2	2	0.03
	4	2	1	1	1	1	0.03
RB85-4							
	1	2	2	2	1	1	0.052
	2	2	2	1	2	3	0.052
	3	1	1	1	2	2	0.052
	4	2	2	2	1	1	0.052
RC18-1							
	1	2	1	1	3	3	0.004
	2	3	2	1	2	3	0.004
	3	2	2	2	1	2	0.028
	4	1	3	1	2	3	0.028
RL43-3							
	1	3	1	1	1	2	0.004
	2	2	2	2	1	2	0.004
	3	2	2	1	2	2	0.004
	4	3	1	1	3	3	0.004
RH47-4							
	1	1	1	1	3	3	0.04
	2	2	1	1	2	3	0.04
	3	3	1	1	2	2	0.04
	4	5	1	1	2	2	0.04
RD65-5							
	1	2	2	2	1	2	
	2	1	1	1	1	1	
	3	1	1	1	2	2	
	4	2	2	2	0	1	
TF04-1							
	1	1	2	2	1	1	0.02
	2	2	2	2	1	2	0.02
	3	3	1	1	1	1	0.02
	4	1	1	1	2	2	0.02
TS21-4							
	1	1	2	2	0	2	0.07
	2	2	2	2	0	2	0.03
	3	2	1	1	2	3	0.07
	4	2	1	1	3	3	0.03
WB25-4							
	1	2	1	1	2	2	0.004
	2	2	1	1	2	2	0.004
	3	1	1	1	1	1	0.028

	4	2	2	1	1	2	0.028
WS07-0							
	1	3	2	2	0	1	0.04
	2	2	3	3	0	2	0.04
	3	2	2	3	1	2	0.04
	4	1	1	1	2	2	0.04
WS76-6							
	1	2	1	1	3	3	
	2	1	2	2	1	2	
	3	2	2	2	0	2	
	4	2	1	1	0	2	

Appendix C

Table 2. Bioplex immunoassay quantities of MMP9 (ng/mg) of aortic tissue separated by right and left sides of the aorta and areas of highest ILT highlighted in orange.

Patient ID	Side	Impingement	Thrombus	Recirculation	sample 1	sample 2	sample 3	Average	stdev
AB95-7	R		R	R	78	86	61	75	12.8
	L	L			31	33	25	29.7	4.2
	Trombus			97					
AM42-2	R	R	R		9	77	36	40.7	34.2
	L				21	22	17	20	2.6
	Trombus			56					
AR49-6	R	R			29	14		21.5	10.6
	L		L	L	4	13	30	15.7	13.2
	Trombus		2						
CS94-7	R	R			11	26	21	19.3	7.6
	L		L	L	29	11	35	25	12.5
	Trombus			7					
EG86-3	R		-	-	30	35	15	26.7	10.4
	L	L	-	-	29	17	23	23	6
	Trombus	-	-	-					
ES58-5	R		R	R	15	16	15	15.3	0.6
	L	L			12	10	13	11.7	1.5
	Trombus			41					
FD29-5	R			-	1	8	9	6	4.4
	L	L	L	-	18	25	24	22.3	3.8
	Trombus	18		8					
JP11-2	R	R			11	5	65	27	33.0
	L		L		5	6	33	14.7	15.9
	Trombus			167					
JM05-1	R	R		-	15	24	35	24.7	10.0
	L		L	-	10	10	21	13.7	6.4
	Trombus	7							
JS98-8									
LQ01-2	R		R	-	23	33		28.0	7.1
	L	L		-	67	52		59.5	10.6
	Trombus			78					
MC47-6	R	-		-	15	7	24	15.3	8.5
	L	-	L	-	5	18	47	23.3	21.5
	Trombus	2		11.5					
MN87-8	R	-	-	-	19	42	57	39.3	19.1
	L	-	-	-	8	31	28	22.3	12.5
	Trombus		8						
NJ24-1	R	R			34	20	18	24	8.7
	L		L	L	15	28	22	21.7	6.5
	Trombus			32					
RB85-4	R	R		-	50	39		44.5	7.8

	L		L	-	62	81		71.5	13.4
	Trombus			15					
RC18-1	R		R	R	82	21	112	71.7	46.4
	L	L			35	30	109	58	44.2
	Trombus			64					
RL43-3	R		R	-	122	119	314	185	111.7
	L	L		-	71	116	92	93	22.5
	Trombus			57					
RH47-4	R		R	-	19	24	82	41.7	35.0
	L	L		-	23	18	46	29	14.9
	Trombus			34					
RD65-5	R								
	L								
TF04-1	R		-	-	26	21	41	29.3	10.4
	L	L	-	-	76	21	16	37.7	33.3
	Trombus	-	-	-					
TS21-4	R		R	R	23	5	75	34.3	36.4
	L	L			18	46	12	25.3	18.1
	Trombus			50					
WB25-4	R	r			14	22	25	20.3	5.7
	L		l	l	32	25	55	37.3	15.695009
	Trombus			6					
WS07-0	R	-	-	-	15	16	4	11.7	6.7
	L	-	-	-	24	7	9	13.3	9.3
	Trombus	11		86					
WS76-6	R								
	L								
		9.5		53.6					
		6.8	std devia	42.6					
		3.4	std error	10.6					

Appendix C

Table 3. Bioplex immunoassay quantities of average MMP-9 (ng/mg) of aortic tissue separated high and low amounts of intraluminal thrombus

	High Thrombus	Low thrombus		
	75	29		
	40	20		
	21.5	15.7		
	25	19.3		
	15.3	11.7		
	22.3	6		
	14.7	27		
	13.7	24.7		
	28	59.5		
	23.3	15.3		
	21	24		
	71	44.5		
	185	93		
	41.7	58		
	34.3	29		
	37.3	25.3		
	71.7	20.3		
Average	43.5764705882353	30.7		
Stdv	42.1095852112873	22.4		
stderror	10.21	5.4		
ttest two tailed	0.24			
ttest one sided	0.13			

Annie Ducas
Masters Thesis

Appendix D

Computational Flow models of all patients undergoing CTA.

AB95-7

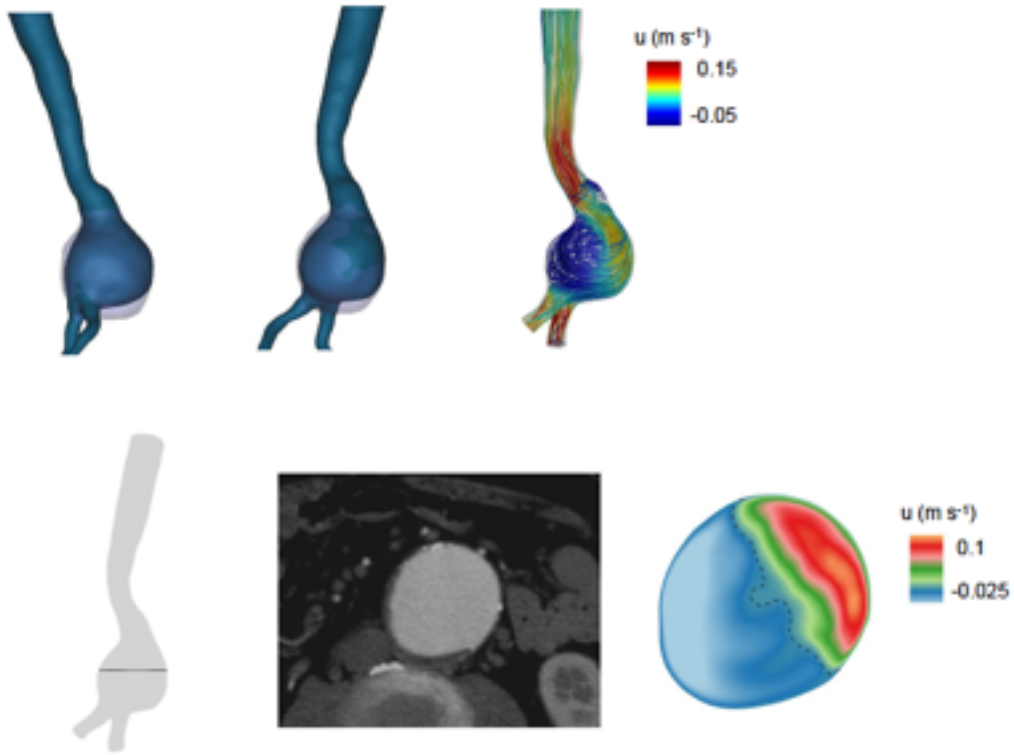

AM42-2

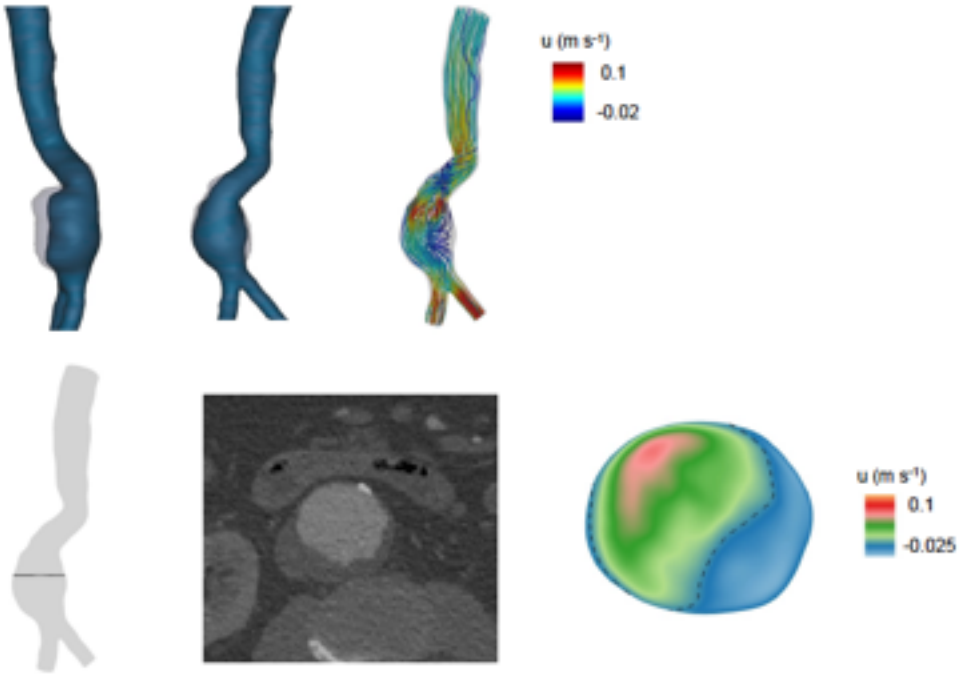

AR49-6

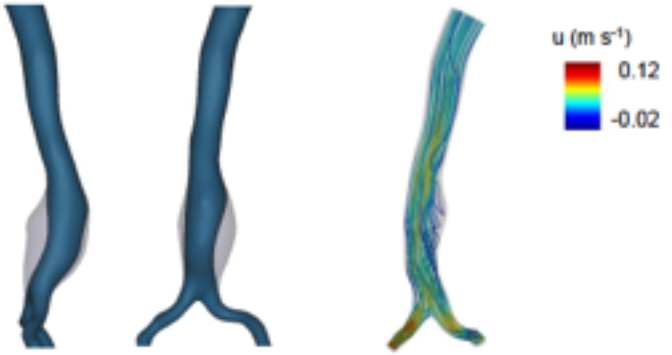

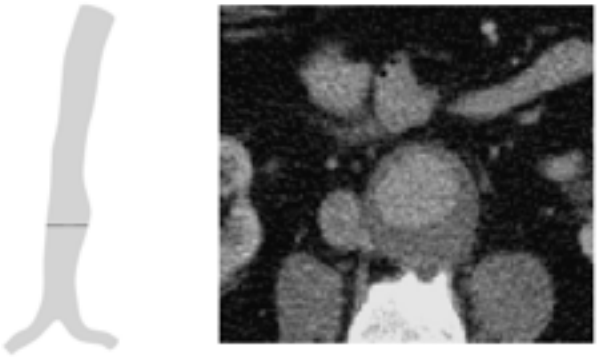

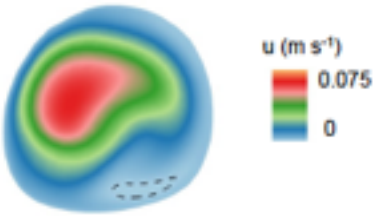

CS94-7

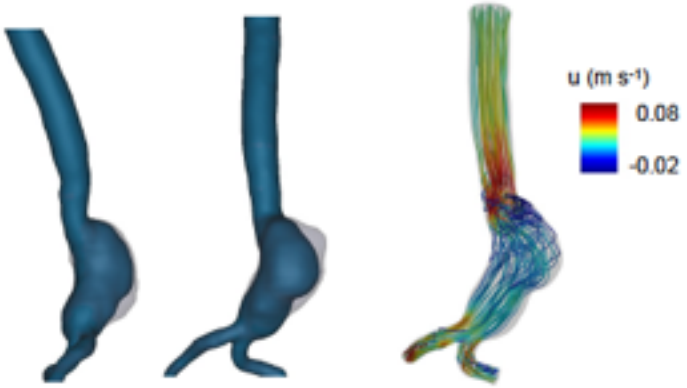

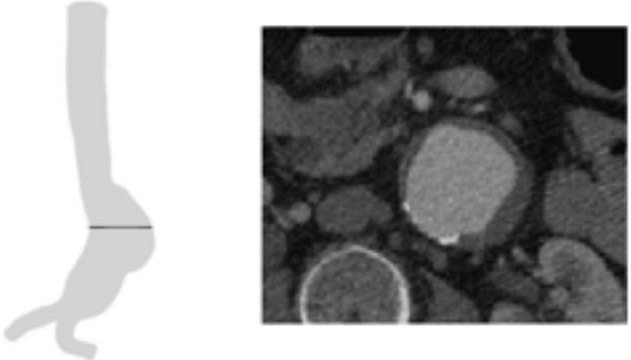

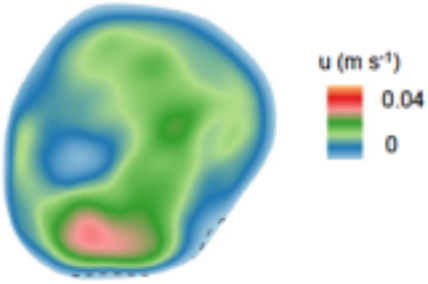

EG86-3

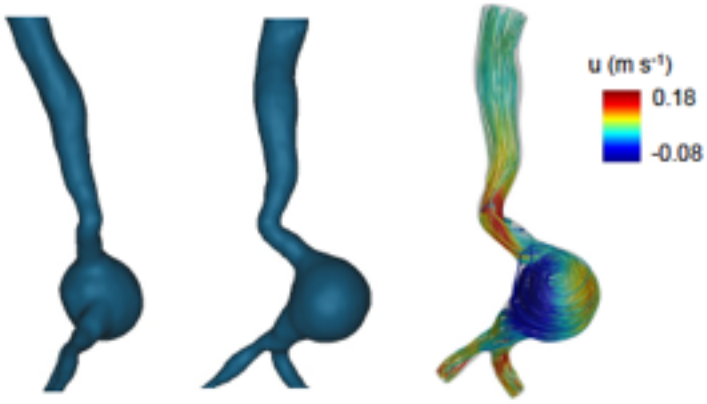

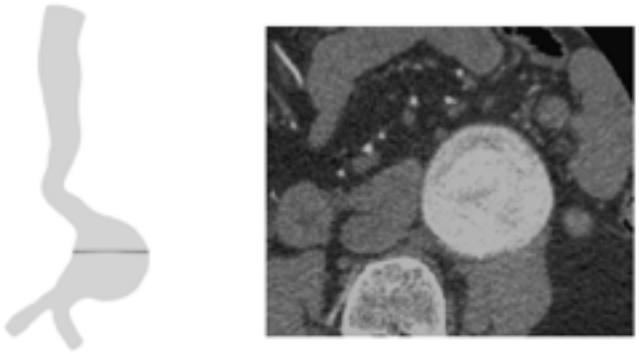

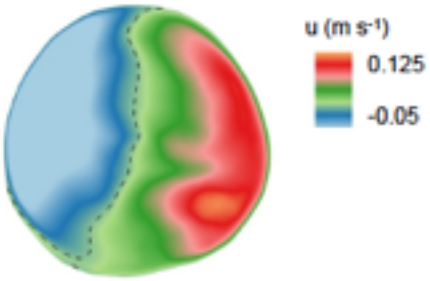

ES58-5

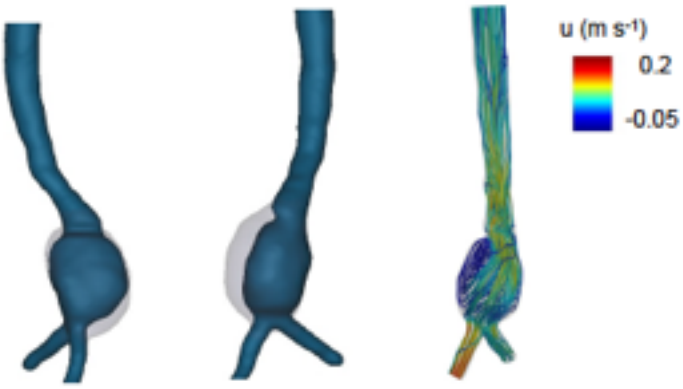

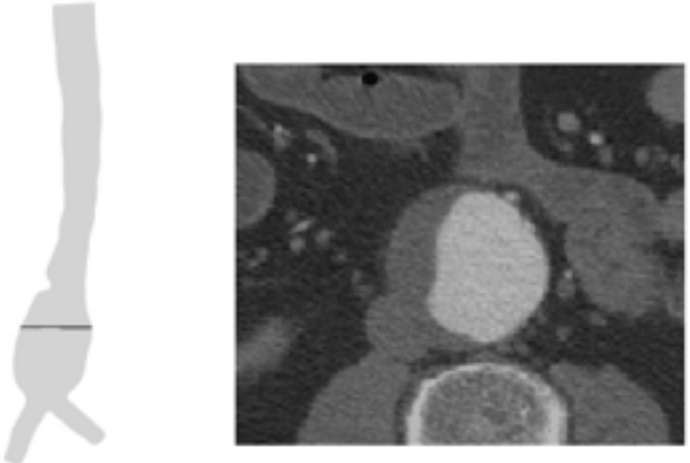

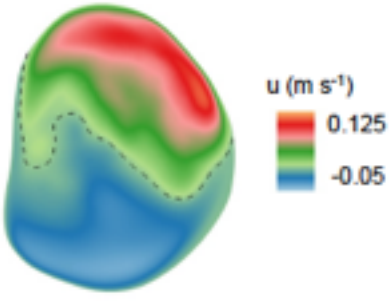

FD29-5

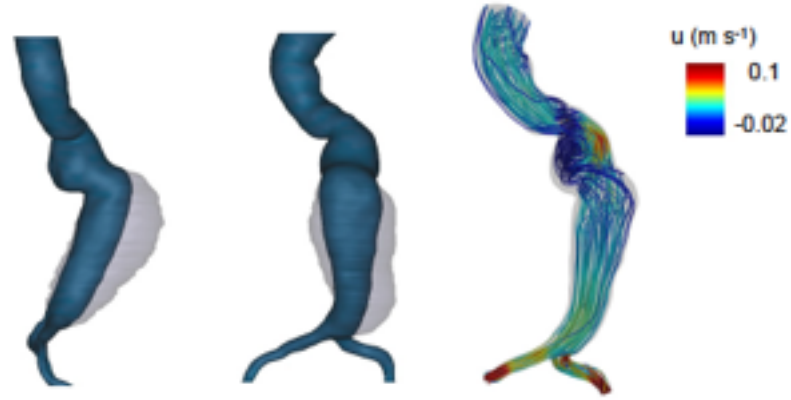

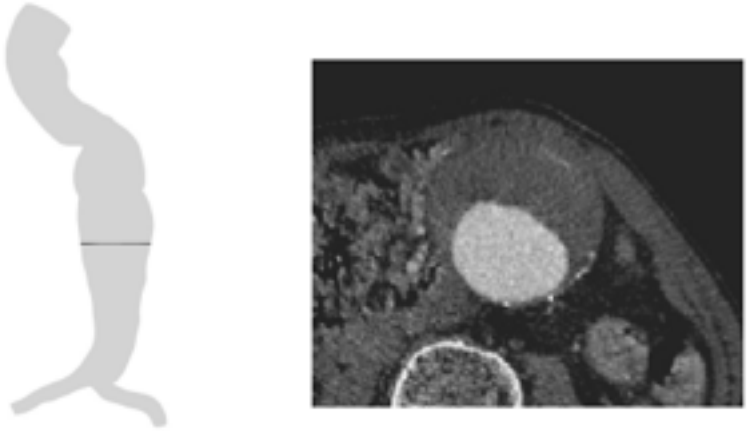

JM05-1

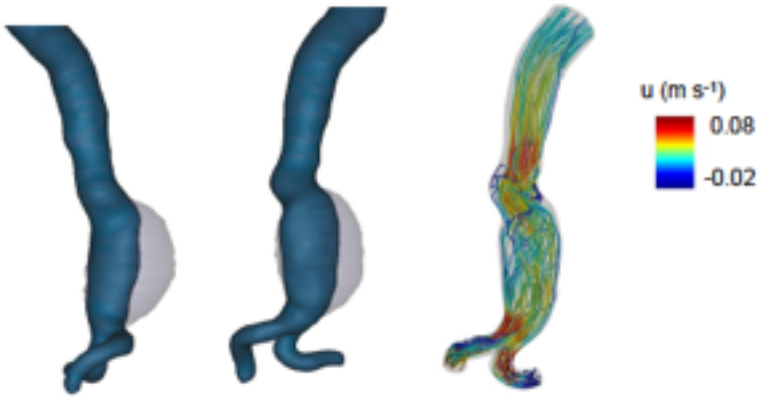

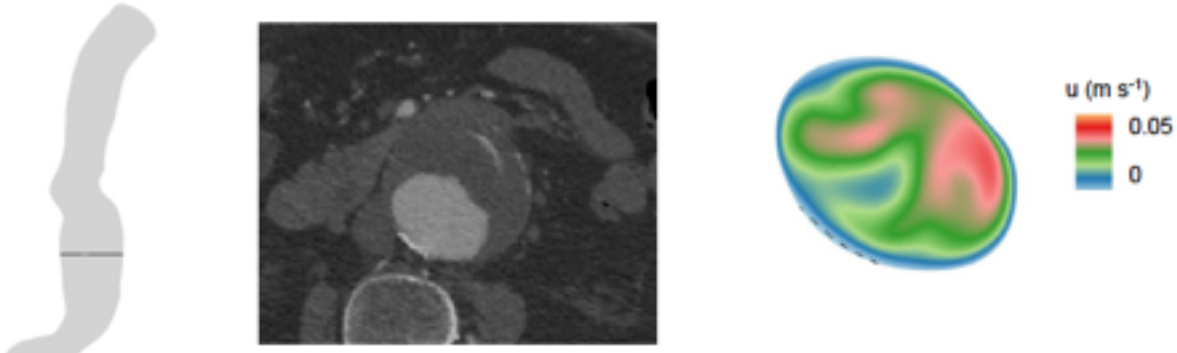

JP11-2

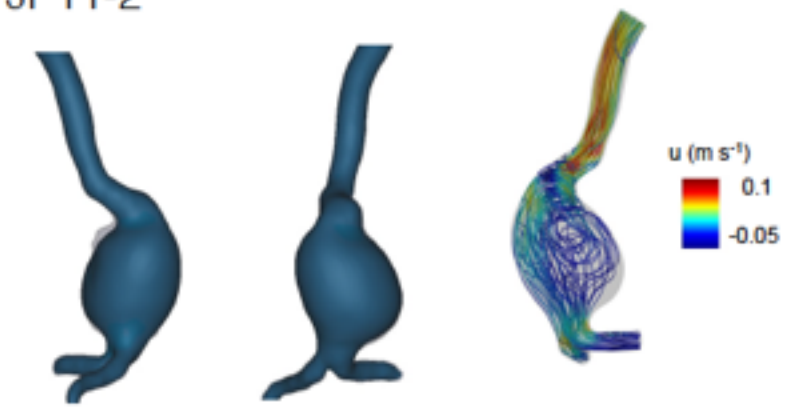

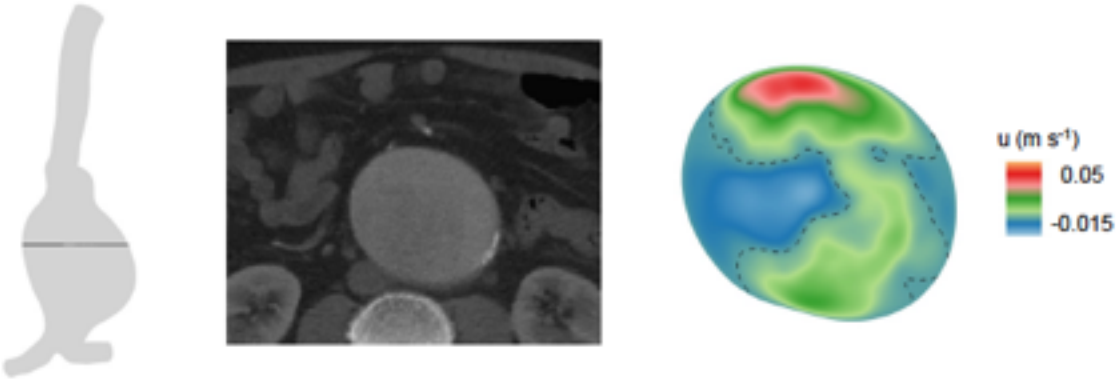

LQ01-2

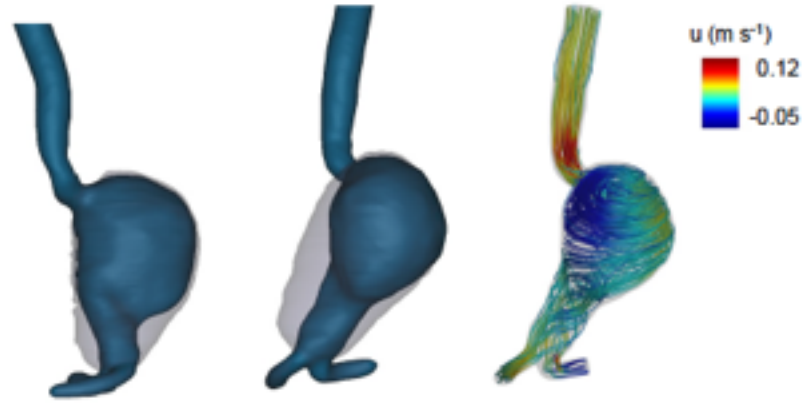

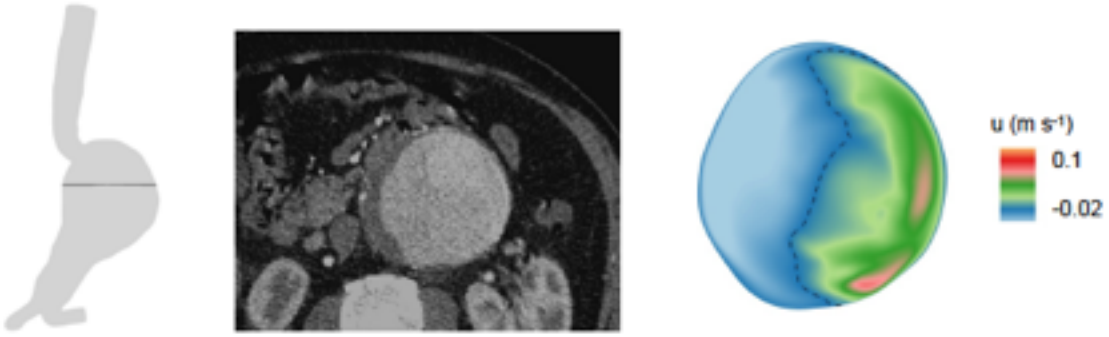

MC47-6

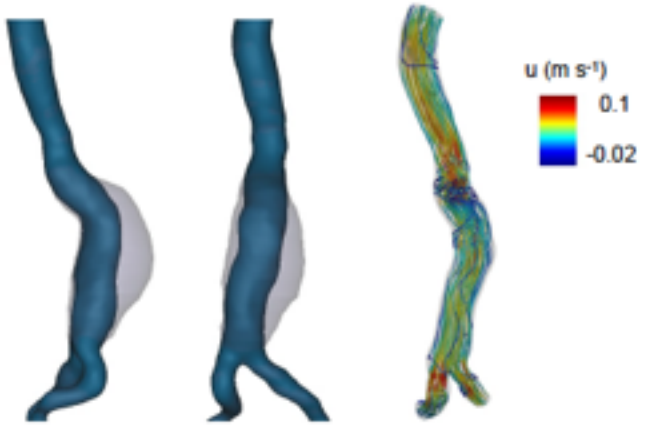

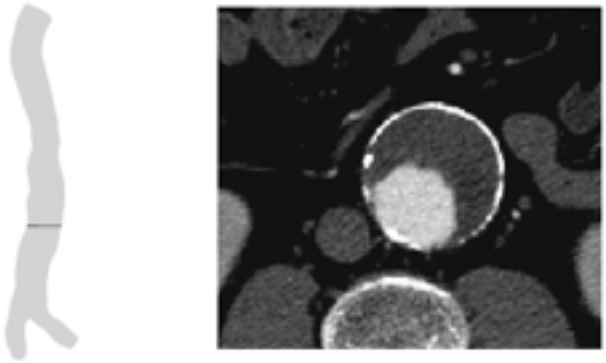

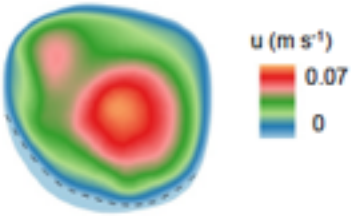

MN87-8

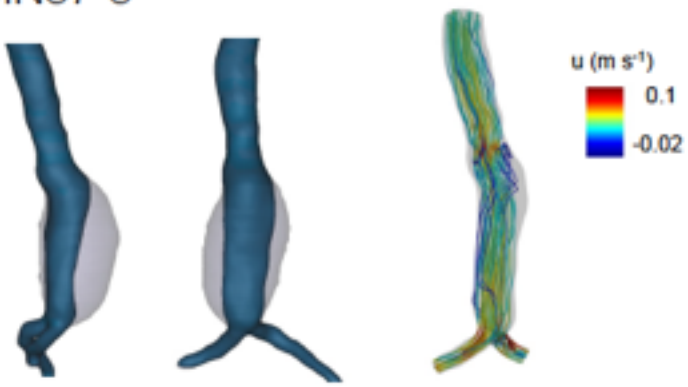

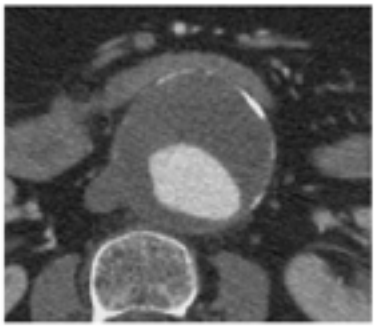

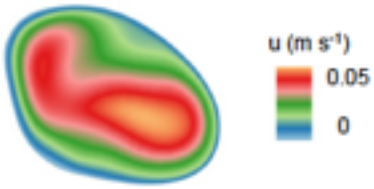

NJ24-1

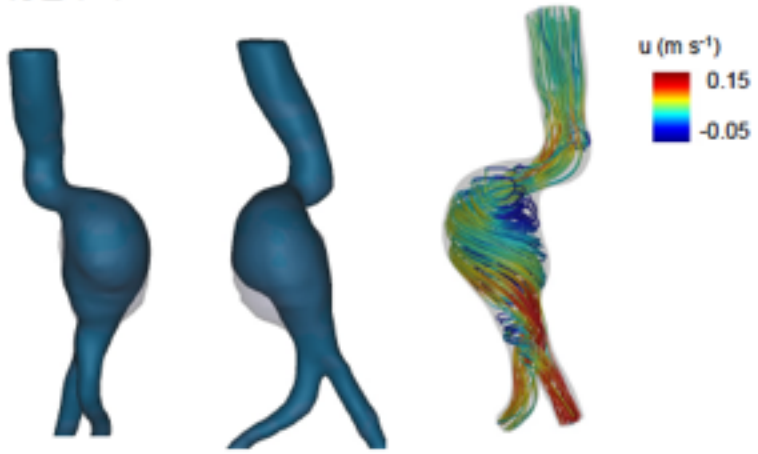

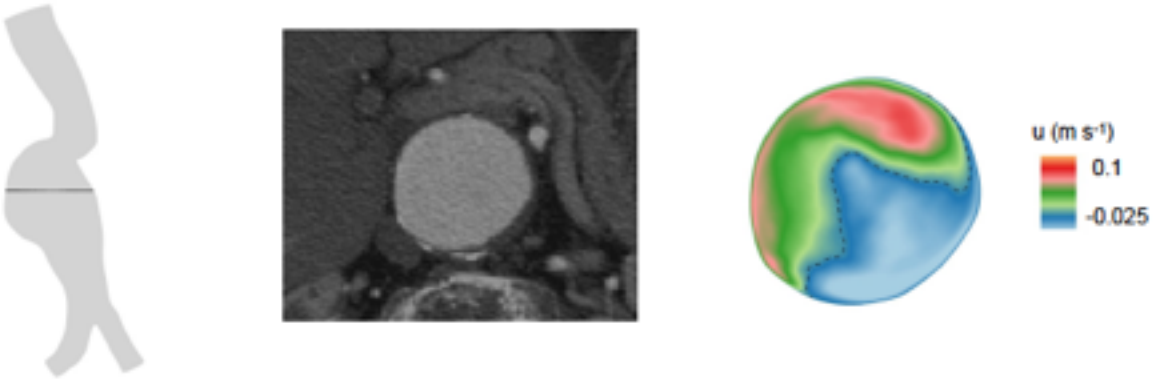

RB85-4

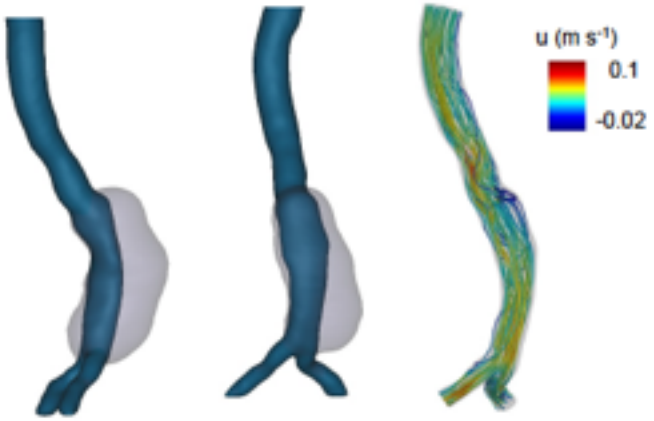

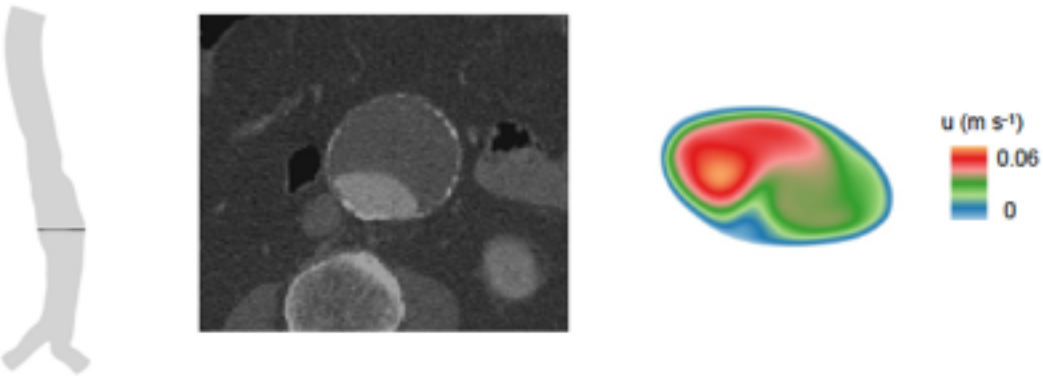

RC18-1

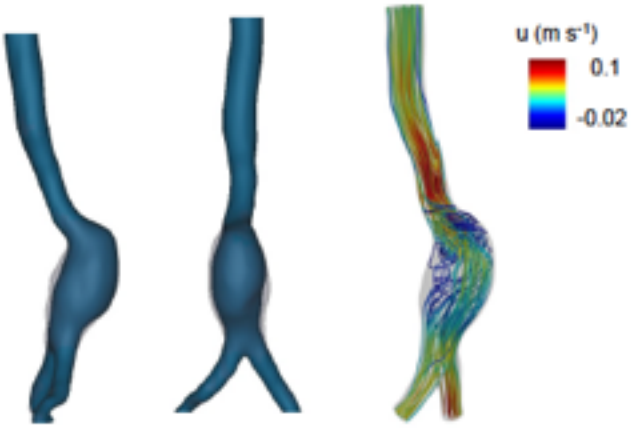

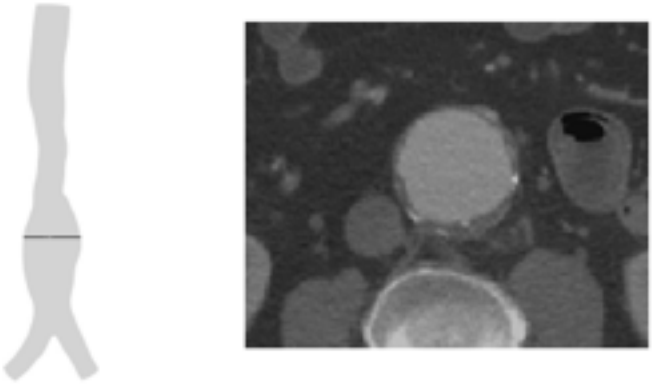

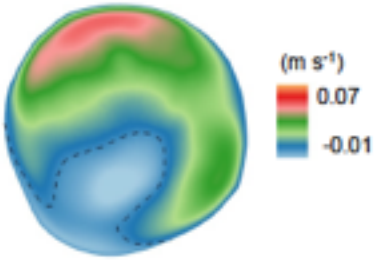

RH47-4

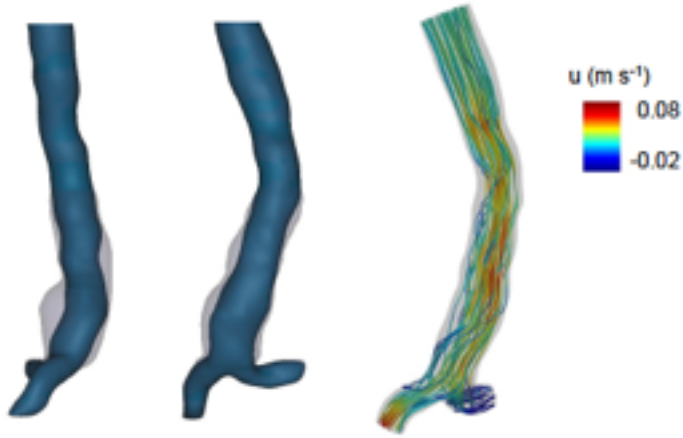

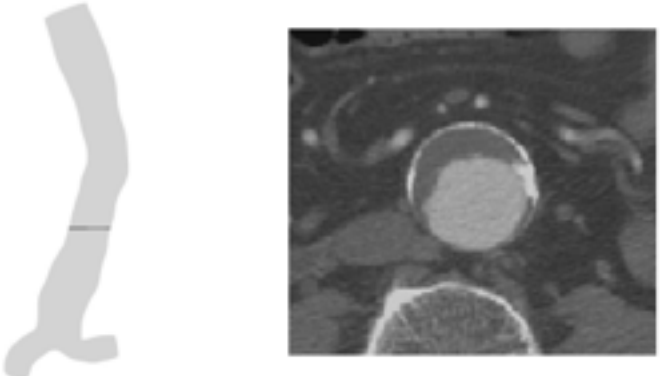

RL33-3

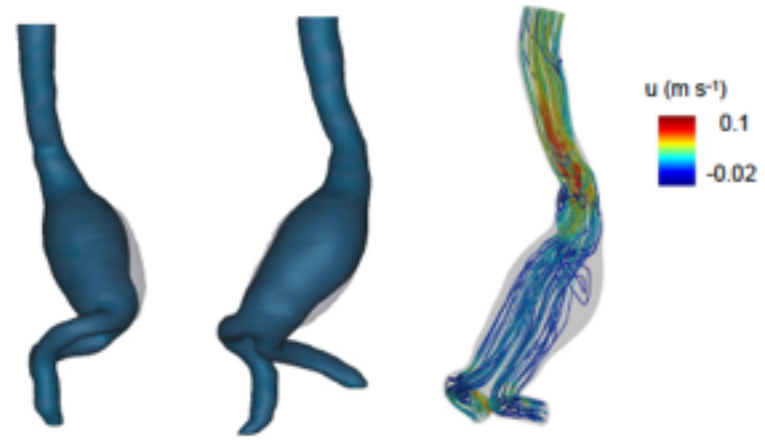

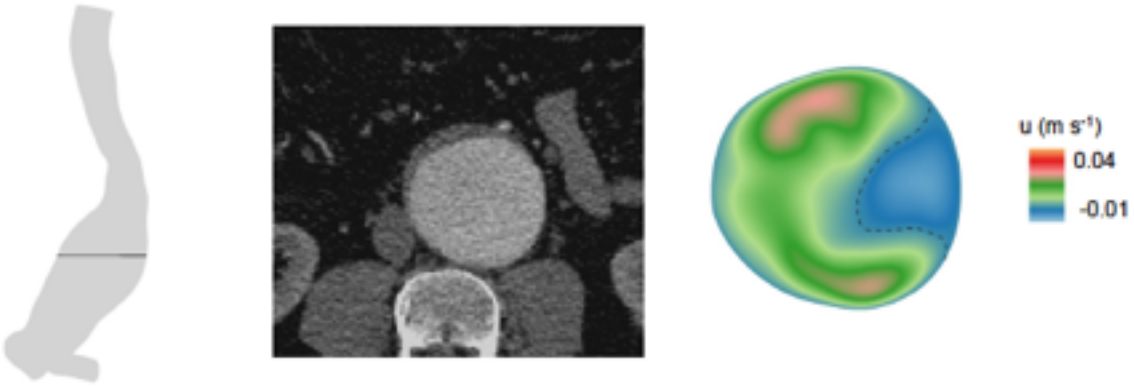

TF04-1

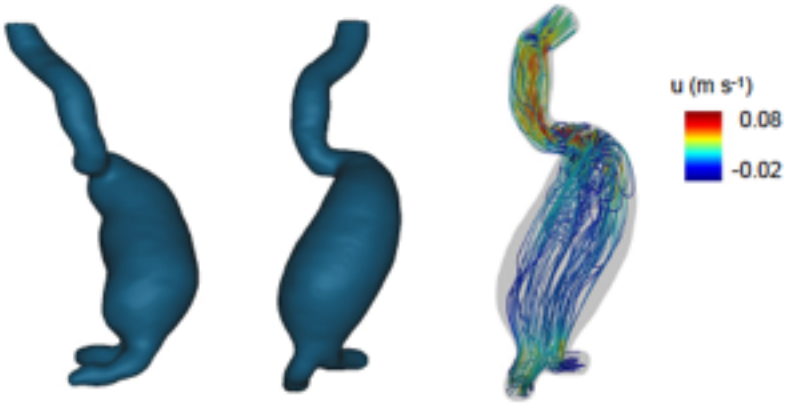

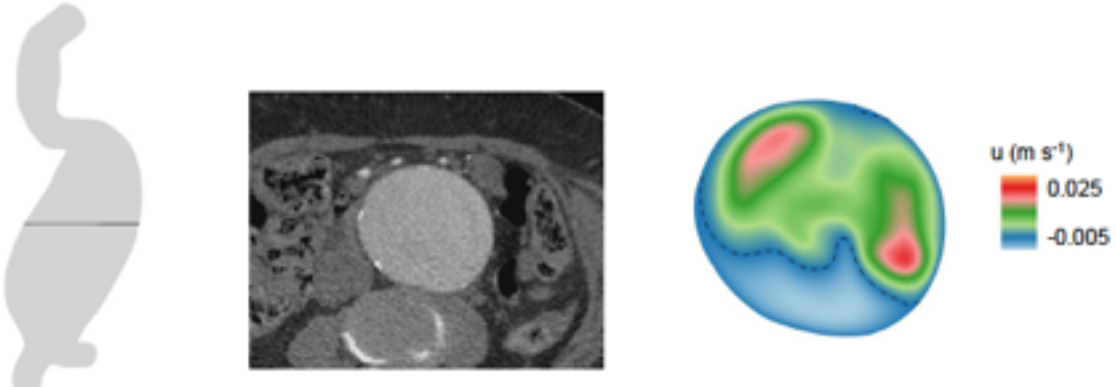

TS21-4

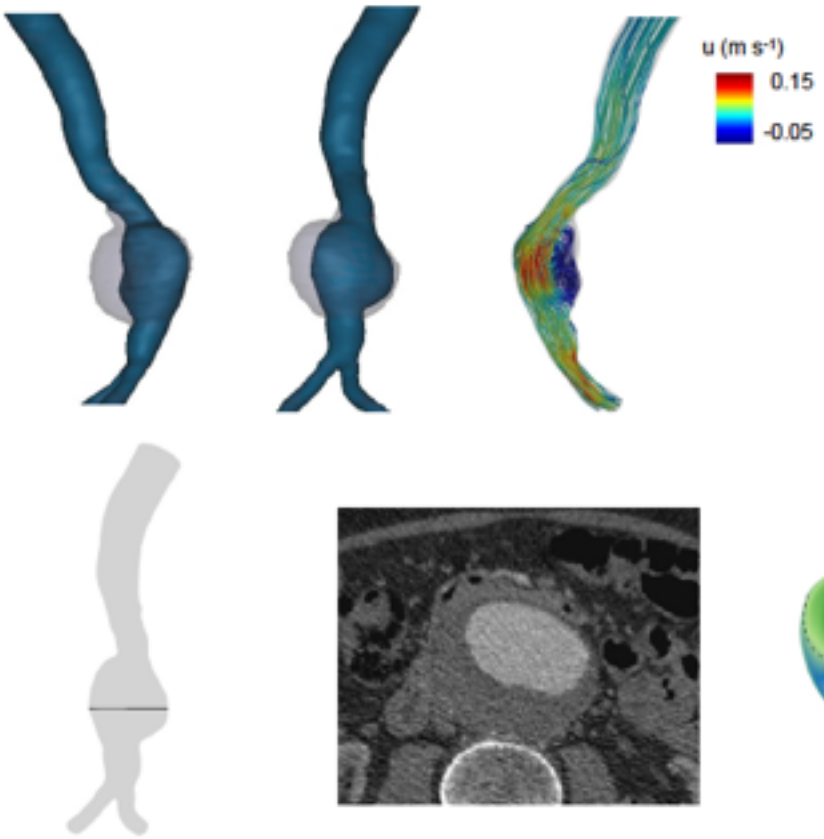

VB27-7

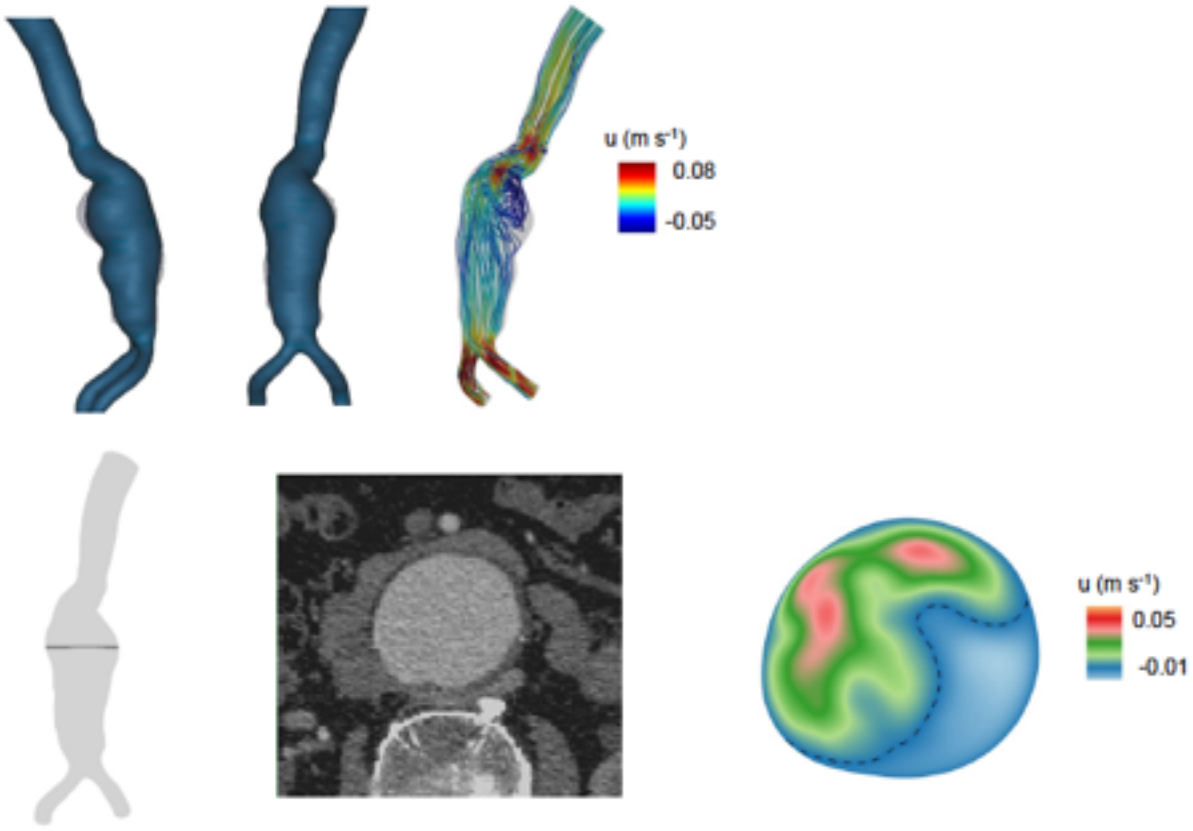

WB24-5

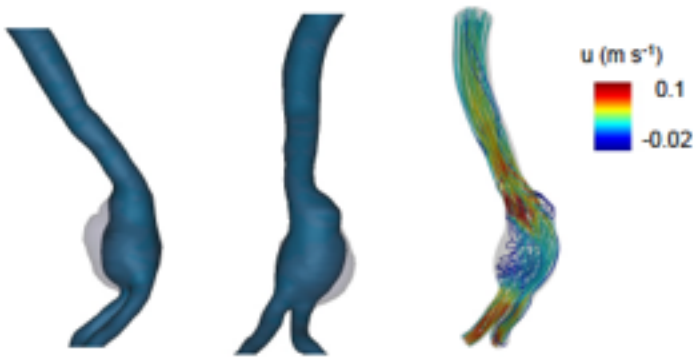

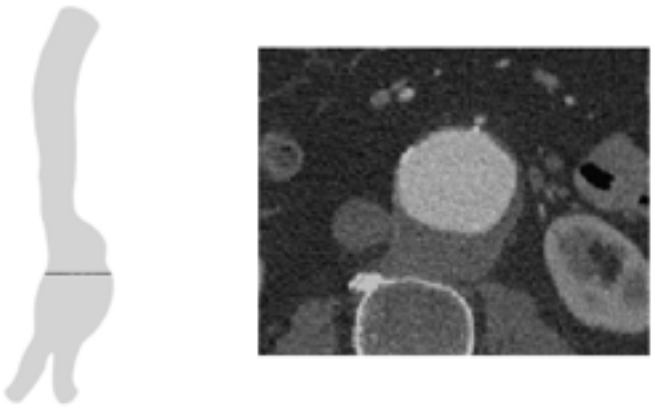

WS07-0

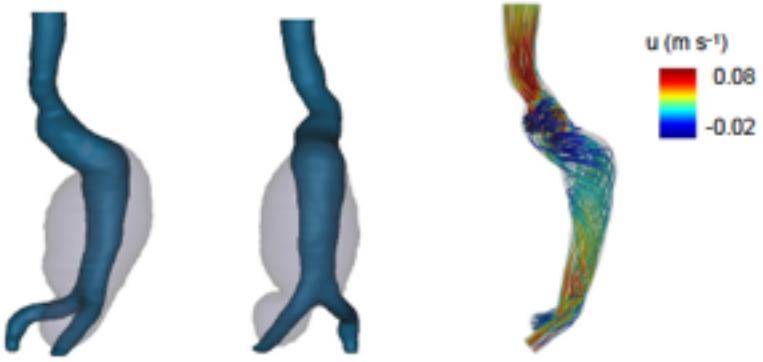

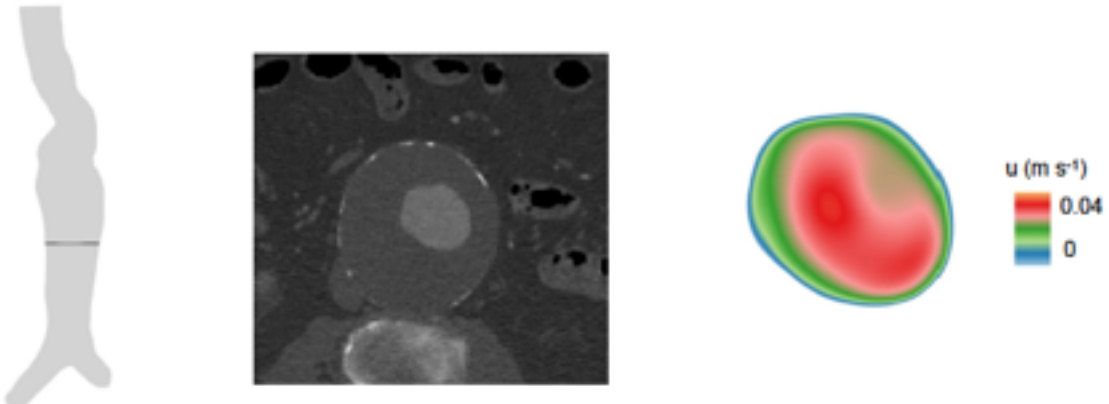

Annie Ducas
Masters thesis

Appendix E

Histologic samples

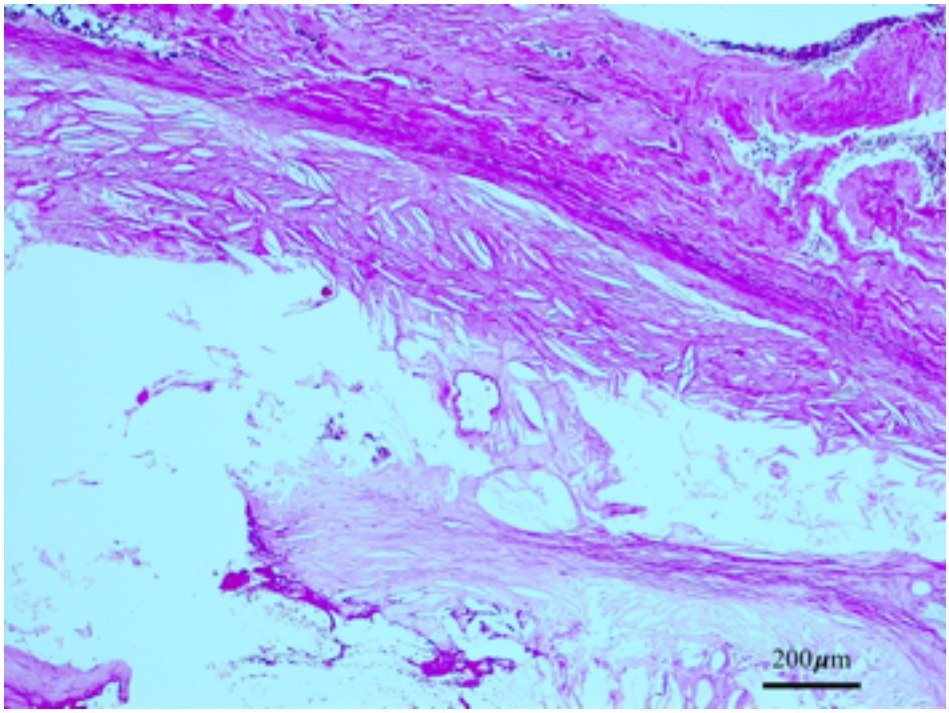

Fig 1 Histology slide at 200x magnification of H&E stained AAA (JS98-8) showing tissue that was highly calcified and very difficult in analysis of the tissue.

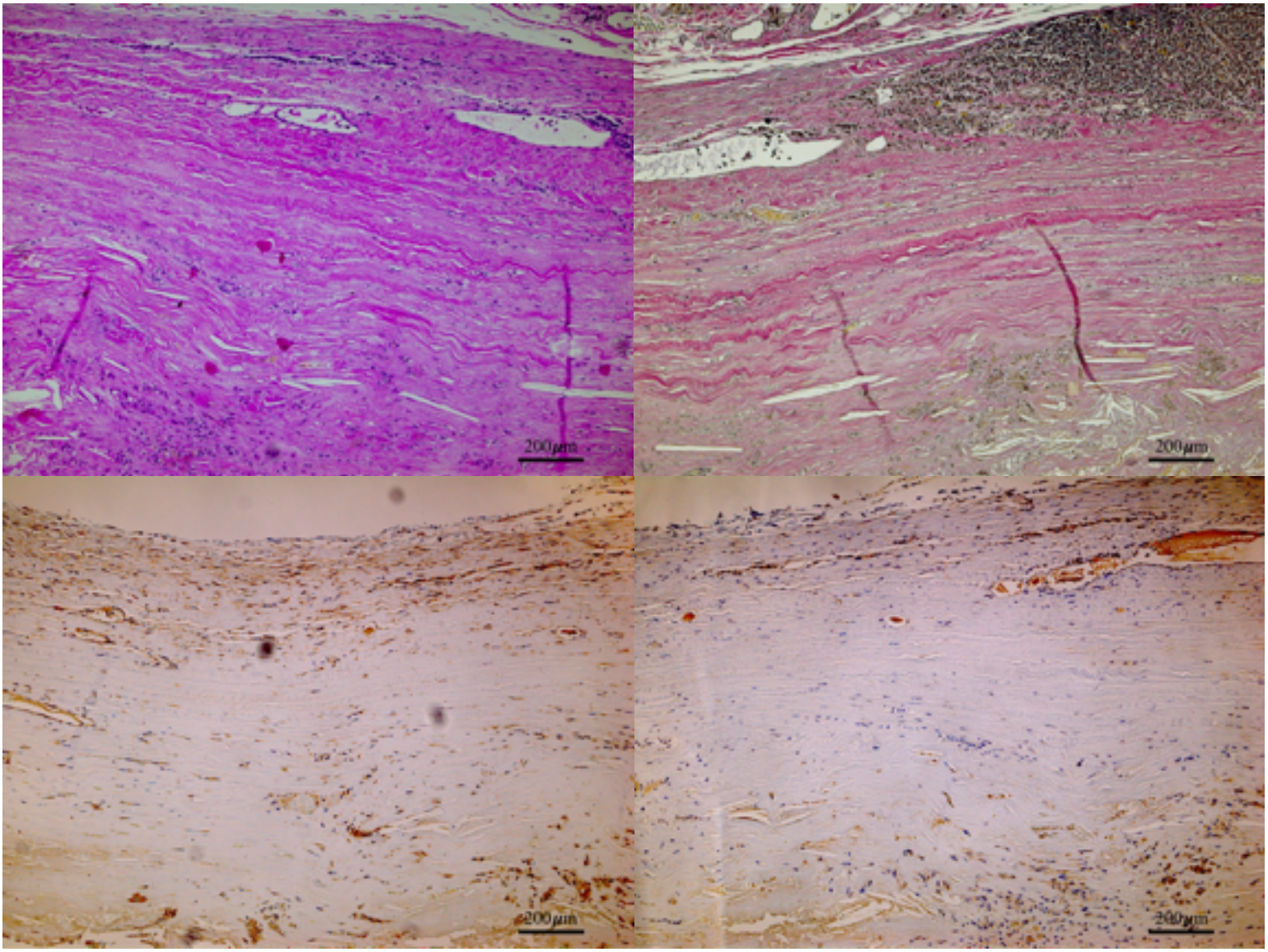

Fig. 2 Histology representation of aortic tissue.patient FD 29-5Histology at 200x magnification examples of nucleated inflammatory cells on H&E stain a., VG staining showing collagen and elastin b., IHC staining of MMP9 total brown areas staining positive for MMP9 and beige areas demonstrating areas of calcium artifact c., IHC staining for MMP9active d. These samples were assessed as having low inflammation and high elastin content with low amounts of MMP9 total and active

Cardiovascular Engineering and Technology, Vol. 8, No. 1, March 2017 (© 2016) pp. 57–69
DOI: 10.1007/s13239-016-0287-5

Appendix F ark

The Relationship Between Pulsatile Flow Impingement and Intraluminal Thrombus Deposition in Abdominal Aortic Aneurysms

RICHARD J. LOZOWY ,[1] DAVID C. S. KUHN,[1] ANNIE A. DUCAS,[2] and APRIL J. BOYD[2]

[1]Department of Mechanical Engineering, University of Manitoba, Winnipeg, MB, Canada; and [2]Department of Surgery, University of Manitoba, Winnipeg, MB, Canada

(Received 24 August 2016; accepted 7 November 2016; published online 28 November 2016)

Associate Editors Tim McGloughlin and Ajit P. Yoganathan oversaw the review of this article.

Abstract—Direct numerical simulations were performed on four patient-specific abdominal aortic aneurysm (AAA) geometries and the resulting pulsatile blood flow dynamics were compared to aneurysm shape and correlated with intraluminal thrombus (ILT) deposition. For three of the cases, turbulent vortex structures impinged/sheared along the anterior wall and along the posterior wall a zone of recirculating blood formed. Within the impingement region the AAA wall was devoid of ILT and remote to this region there was an accumulation of ILT. The high wall shear stress (WSS) caused by the impact of vortexes is thought to prevent the attachment of ILT. WSS from impingement is comparable to peak-systolic WSS in a normal-sized aorta and therefore may not damage the wall. Expansion occurred to a greater extent in the direction of jet impingement and the wall-normal force from the continuous impact of vortexes may contribute to expansion. It was shown that the impingement region has low oscillatory shear index (OSI) and recirculation zones can have either low or high OSI. No correlation could be identified between OSI and ILT deposition since different flow dynamics can have similar OSI values.

Keywords—Abdominal aortic aneurysm, Intraluminal thrombus, Pulsatile flow, Oscillating wall shear stress.

INTRODUCTION

An abdominal aortic aneurysm (AAA) is a dilatation of the aorta between the renal arteries and the iliac bifurcation. Dilatation weakens the aortic wall making it susceptible to rupture and currently the decision to repair an AAA is based on a diameter criterion of 5.5 cm in men and 5 cm in women. The risk of rupture is significant at sizes $>$ 5.5 cm and increases with diameter[18]; however, ruptured AAA (RAAA) can have diameters smaller than 5 cm, while others can reach sizes of 10–12 cm without rupture. The fact that rupture can occur at a wide range of sizes indicates additional criteria could be used to evaluate the susceptibility of AAA rupture.

The tangential force exerted on the arterial wall by blood flow, referred to as wall shear stress (WSS), is thought to be an important hemodynamic factor that regulates arterial health. Low WSS and oscillations in blood flow direction are dominant mechanisms that can lead to a deterioration of the arterial wall.[36] The fact that the majority of aortic aneurysms are infrarenal suggests hemodynamics specific to this region trigger the initial aortic dilation. Under resting conditions, only one third of the supraceliac flow rate is directed into the legs[16] and WSS is substantially lower in the abdominal segment of the aorta.[35] Interestingly, it has been shown that patients with a single above-knee leg amputation are more likely to develop AAA.[40] In addition to further lowering WSS in the abdominal aorta, due to reduced blood requirement from the amputated leg, a single above-knee leg amputation causes an asymmetrical flow pattern at the aortic bifurcation. The majority of the blood flow being directed down a single iliac artery of the non-amputated leg causes a higher wall-normal pressure force to be applied along the side with the amputation and expansion was found to be more prevalent on this side.

It is common for intraluminal thrombus (ILT) to accumulate within AAA. Once a layer of ILT forms the aortic wall is no longer directly exposed to low and oscillating WSS and this can not be considered the cause of wall deterioration.[17] The aortic wall receives oxygen primarily from luminal blood flow and a layer

Address correspondence to David C. S. Kuhn, Department of Mechanical Engineering, University of Manitoba, Winnipeg, MB, Canada. Electronic mail: david.kuhn@umanitoba.ca

of ILT may decrease the flow of oxygen (hypoxia), which in turn may decrease wall integrity, making it more susceptible to further expansion or rupture.[42] It has been shown that ILT deposition increased AAA growth rate,[25,44,48] and that regions of the AAA wall with ILT experienced localized hypoxia[41] and were thinner with more inflammation.[14] Alternatively it has been suggested that ILT is protective and shields the aortic wall from pressure forces.[5,23,43,47] In Speelman *et al.*[32] AAA wall stress was lower when a large ILT volume was present but growth rate was also higher. The authors stated that the deterioration of the aortic wall from ILT may be more significant than the hemodynamic forces acting on the wall. It has been suggested that ILT thickness could be used as a criterion, in addition to diameter, when determining risk of rupture[31] and ILT deposition in small-sized AAA should be a factor when considering early surgical repair.[33,44]

It is possible that zones of stagnant blood, turbulent fluctuations and flow impingement produce a hemodynamic environment that contributes to AAA expansion, ILT deposition and rupture. As an AAA increases in size adverse hemodynamic conditions may worsen, further increasing the risk of rupture. Since AAA can have a wide variety of shapes, it is possible that particular geometries have greater disturbances in blood flow. Some AAA may dilate to very large sizes while maintaining stable non-disturbed blood flow and therefore could potentially be at a lower risk for rupture. It would be beneficial to be able to identify the flow dynamics associated with particular aortic geometries.

In this current work we computationally investigated pulsatile blood flow dynamics in patient-specific AAA. The study consisted of 23 cases and we will be focusing our presentation on cases 1–4. The results indicate that the impingement of blood flow may prevent ILT deposition and influences the overall aneurysm shape. The remaining 19 cases will be referenced to further support this observation.

MATERIALS AND METHODS

Model Description

Case 1–3 have diameters of 6.8, 6.0 and 11 cm, respectively, and posterior-eccentric ILT of maximum thickness 1.8, 0.4 and 4.4 cm, respectively. For case 3 the ILT becomes circumferential-eccentric in the lower AAA segment. Case 4 has a diameter of 7.4 cm and is devoid of ILT. The models are generated from computed tomography angiography (CTA) images using the commercial medical imaging software Mimics-17.0 (Mimics, Materialise, Leuven, Belgium). To simplify the geometry, arteries that branch off of the aorta, such as the visceral arteries, are excluded and the common iliac arteries are modeled to the bifurcation of the internal and external iliac arteries.

The non-dimensional parameters that govern blood flow are the bulk Reynolds number Re_b, Womersley number Wo and the oscillating-to-mean flow rate ratio β, which are, respectively,

$$Re_b = \overline{u}_b D_h / \nu, \tag{1}$$

$$Wo = D_h / 2\sqrt{\omega/\nu}, \tag{2}$$

$$\beta = u_{osc} / \overline{u}_b. \tag{3}$$

Here $\nu = \mu/\rho$ is the kinematic viscosity, with μ and ρ being the dynamic viscosity and density, respectively, $\omega = 2\pi/T$ is the angular frequency, u_{osc} is the amplitude of the oscillating component of the pulse and $\overline{u}_b$ is the time-average of the bulk velocity at the inlet boundary. The length scale used to define Re and Wo is the inlet hydraulic diameter $D_h = 4A/P$, where A and P are the cross-sectional area and perimeter of the upstream aorta inlet, respectively. Although blood is a non-Newtonian fluid it can be assumed to behave like a Newtonian fluid in large arteries.[16] The governing equations for the conservation of mass and momentum, in a Cartesian coordinate system $\boldsymbol{x} = (x, y, z)$, are as follows:

$$\nabla \cdot \boldsymbol{u} = 0 \tag{4}$$

$$\partial \boldsymbol{u}/\partial t + \boldsymbol{u} \cdot \nabla \boldsymbol{u} = -\nabla p + \nu \nabla^2 \boldsymbol{u} \tag{5}$$

where the velocity field is given by $\boldsymbol{u} = (u, v, w)$, t is the time unit and $p = P/\rho$, with P being the pressure. Using physiologically-realistic flow conditions $\beta = 5.5$, $\mu = 0.0035$ kg m^{-1} s^{-1}, $\rho = 1050$ kg m^{-3} and $T = 1$ s. The mean and maximum bulk flow rate is 20 and 130 ml s^{-1}, respectively. For the cases in this study, Re_b varied from 254–313 and Wo varied from 16.5–20.5. The x-axis is placed perpendicular with the axial plane and is referred to as the streamwise direction.

The temporal variation in the infrarenal bulk flow rate used in this study is shown in Fig. 1a. The term infrarenal refers to the segment of the aorta below the renal arteries. The pulse profile is from Les *et al.*,[20] where it was calculated from patients with AAA and the mean infrarenal flow rate was found to be 17.5 ± 5.44 ml s^{-1}. The flow rate used in our study is then slightly above average for patients with AAA.

Systole refers to cardiac contraction and diastole to cardiac relaxation. At the end of systole, the infrarenal bulk flow rate reverses direction and throughout diastole the flow rate is effectively zero.

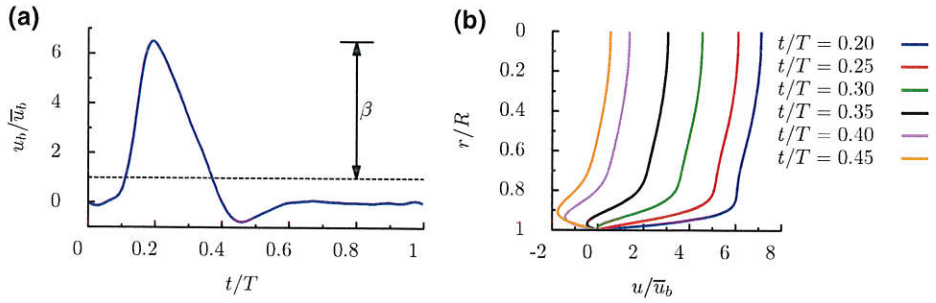

FIGURE 1. (a) Temporal variation in infrarenal bulk flow rate. (b) Analytical solution to a fully-developed pulsatile velocity profile in a pipe. Profiles calculated using bulk flow rate data from Les *et al.*[20]

Simulation Details

The open source finite-volume code OpenFOAM-2.2.2 (OpenCFD Ltd, Bracknell, United Kingdom) is used to directly solve the governing equations. The code uses the PISO algorithm[13] for pressure-velocity coupling, a second-order central difference scheme for the spatial derivatives and a second-order implicit Euler method for the time derivative. To satisfy a criterion of having the Courant-Friedrichs-Lewy (CFL) number <1 the time-step is fixed at $\Delta t = 0.25 \times 10^{-5}$ s for case 1 and $\Delta t = 0.5 \times 10^{-5}$ s for cases 2–4. At each time-step the equations are considered converged when the residuals become less than 1×10^{-6}. The time-dependent bulk velocity from Fig. 1a is implemented at the upstream inlet boundary. A uniform velocity is used as the boundary condition, as opposed to a fully developed profile, since within the aorta only several cm are required for an oscillating boundary layer to develop[46] and at no point does the mean component reach a fully developed state.[4] At the outlet boundaries, downstream in the iliac arteries, a reference pressure of $p = 0$ is imposed and the arterial walls are assumed to be rigid with a no-slip condition. The initial flow field is set to zero and statistics are collected after 5 pulses simulated to remove the effect of initial conditions. The time average of a flow quantity is represented by an overbar and is calculated by averaging over a period defined by $t_i = 5$ s and $t_f = 13$ s.

Unstructured grids composed of prism cells extruded from the wall and tetrahedral cells occupying the interior of the domain are generated using the commercial grid generation software Pointwise-17.2 (Fort Worth, Tex, US). The wall tangent edge length of the first prism cell adjacent to the wall is fixed at 0.002 cm and 15 prism cells are extruded at an expansion rate of 1.25. The edge length of the interior tetrahedral cells is fixed at 0.065 cm. The size of the grids used in this study varied from 6494498 to 13173579 and is comparable to those from previous studies.[1,19,48] The grid resolution is assessed by comparing the average edge length of a grid cell Δ to the time-averaged Kolmogorov length scale $\overline{\eta} = (\nu^3/\overline{\epsilon})^{1/4}$, where the term $\overline{\eta}$ gives the smallest scale of turbulent motion.[29] The term $\overline{\epsilon}$ is the time-averaged rate of turbulent kinetic energy (TKE) dissipation and is calculated using the triple decomposition method introduced by Hussain and Reynolds.[12] The instantaneous velocity field can be decomposed into

$$\boldsymbol{u} = \overline{\boldsymbol{u}} + \widetilde{\boldsymbol{u}} + \boldsymbol{u}', \tag{6}$$

where $\overline{\boldsymbol{u}}$ is the time average, $\widetilde{\boldsymbol{u}}$ is the periodic flucuation, $\boldsymbol{u}'$ is the turbulent fluctuation. Each period is segmented into $M = 50$ equidistant phase positions and at each phase $N = 25$ snapshots of the velocity field are collected. The average of $\boldsymbol{u}$ locked at a phase is calculated as

$$\langle \boldsymbol{u} \rangle = \overline{\boldsymbol{u}} + \widetilde{\boldsymbol{u}} = \frac{1}{N}\sum_{n=0}^{N-1} \boldsymbol{u}|_{t+nT} \tag{7}$$

and the turbulent fluctuation is $\boldsymbol{u}' = \boldsymbol{u} - \langle \boldsymbol{u} \rangle$. The instantaneous rate of TKE dissipation is calculated as $\epsilon = 2\nu \mathbf{s}' : \mathbf{s}'$, with $\mathbf{s}' = (\nabla \boldsymbol{u}' + \nabla \boldsymbol{u}'^{\mathrm{T}})/2$ being the fluctuating strain-rate tensor and the time-average of ϵ is calculated by averaging the 1250 instantaneous snapshots. This procedure has been performed for case 3 and the maximum $\Delta/\overline{\eta}$ is found to be 3.1 with a majority of the domain containing values <2.5. This indicates that the smaller turbulent fluctations are sufficiently resolved by the grid.

Hemodynamics Analysis

Turbulent coherent structures are defined as spatial regions of high vorticity that maintain their shape for an extended period of time. Here they are visualized using the Q-criterion,[11] where Q is defined as $(\boldsymbol{\Omega}^2 - \mathbf{S}^2)/2$, the tensors $\mathbf{S} = (\nabla \boldsymbol{u} + \nabla \boldsymbol{u}^{\mathrm{T}})/2$ and $\boldsymbol{\Omega} = (\nabla \boldsymbol{u} - \nabla \boldsymbol{u}^{\mathrm{T}})/2$ are the strain and rotation-rate tensor, respectively. The quantity Q measures the amount the local vorticity magnitude exceeds the strain rate. The WSS vector $\boldsymbol{\tau}_w = (\tau_{w,x}, \tau_{w,y}, \tau_{w,z})$ is defined as

the tangential component of the surface traction vector $\mathbf{t} = \boldsymbol{\tau}\boldsymbol{n}_s$, where $\boldsymbol{n}_s$ is a unit vector normal to the surface, $\boldsymbol{\tau} = 2\mu\mathbf{S}$ is the shear stress tensor. The tangential component of $\mathbf{t}$ is isolated by subtracting out the normal component through

$$\boldsymbol{\tau}_w = \mathbf{t} - (\mathbf{t}\cdot\boldsymbol{n}_s)\boldsymbol{n}_s. \tag{8}$$

The time-averaged WSS (TAWSS) is a scalar defined as

$$\mathrm{TAWSS} = \frac{1}{t_f - t_i}\int_{t_i}^{t_f} \|\boldsymbol{\tau}_w\| dt, \tag{9}$$

where $\|.\|$ is the magnitude of a vector. The oscillatory shear index (OSI)[10] quantifies the oscillation in the WSS vector's direction and is defined as

$$\mathrm{OSI} = 0.5\left(1 - \|\bar{\boldsymbol{\tau}}_w\|\mathrm{TAWSS}\right). \tag{10}$$

Low OSI indicates a single dominate flow direction and high OSI indicates oscillations in the flow direction. The transverse time-averaged WSS (transTAWSS)[27] quantifies the disturbance in the WSS vector and is defined as

$$\mathrm{transWSS} = \frac{1}{t_f - t_i}\int_{t_i}^{t_f} \left\| \boldsymbol{\tau}_w \cdot \left(\boldsymbol{n}_s \times \frac{\bar{\boldsymbol{\tau}}_w}{\|\bar{\boldsymbol{\tau}}_w\|}\right)\right\| dt. \tag{11}$$

Low transWSS indicates the WSS vector is predominately parallel with a single axis during the cardiac cycle and high transWSS indicates the WSS vector fluctuates about the dominate flow axis. Since a large range of TAWSS values can occur in AAA, transWSS was normalized by the local value of TAWSS.

RESULTS

Velocity Field

To better understand the expected flow dynamics in the abdominal aorta, the analytical solution to a fully-developed pulsatile velocity profile is calculated for a pipe segment of radius R, radial coordinate r, $Wo = 15$ and abdominal aortic flow conditions. The mean component of the analytical solution is a Poiseuille velocity profile and the oscillating component is calculated using Fourier coefficients obtained from the bulk flow rate data in Les *et al.*[20] The calculation of an oscillating velocity profile requires the bulk flow rate to be shifted to it's corresponding pressure gradient and this is done using correlations given by Womersley.[45] In Fig. 1b the analytical velocity profile is shown at various times during systole and early-diastole. As the blood flow decelerates, close to the wall it reverses in direction at $t/T = 0.29$. For all of diastole the velocity profile consists of a low negative component close to the wall and a low positive component in the core region. Blood flow that oscillates in direction while maintaining a net positive direction is referred to flow reversal without separation.[37] Where as, blood flow with a flow direction at the wall that is opposite to the dominate direction is referred to as a recirculation zone.

The extent of the flow reversal that occurs for a given pulse profile is govern by Wo and this parameter defines the ratio of pulsatile inertia forces to viscous forces. Since ν and T are fixed parameters within the cardiovascular system, Wo is dependent on the size of the artery. In small arteries and capillaries, where $Wo << 1$, the pressure gradient is aligned with the flow rate and the flow can be treated as quasi-steady. As Wo is increased, the bulk flow rate begins to lag behind the pressure gradient.[45] Close to the arterial wall, oscillations in the blood flow will be more aligned with the oscillations in the pressure gradient compared to the blood flow in the center region of an artery. As described by Hale *et al.*,[8] near wall velocity is low, therefore it will have less momentum and can be more easily reversed by the pressure gradient.

Figure 2 shows for case 1, mid-sagittal CTA, instantaneous and time-averaged contours of streamwise velocity plotted on the mid-sagittal section. During systole, the blood flow is predominately channeled within the AAA. By late-systole, a jet has formed that is directed towards the anterior wall and there is a small zone of recirculating blood along the posterior wall. During diastole, although the bulk flow rate in the abdominal aorta is effectively zero, the high momentum jet structures continue to flow downstream, shearing/impinging against the anterior wall and transition to turbulence. By $t/T = 0.56$ the structures have traversed to the mid-region of the AAA. In the upstream aorta, throughout the cardiac cycle, the blood flow behaves qualitatively similar to the analytical solution shown in Fig. 1b. The time-averaged streamwise velocity shows blood flow channeling along the anterior wall and a region of recirculating blood along the posterior wall. Referring to the mid-sagittal CTA, anterior wall is devoid of ILT and the posterior wall exposed to recirculation correlates with ILT deposition.

Figure 3 shows for cases 2–4, mid-sagittal CTA, instantaneous coherent structures visualized using the Q-criterion and time-averaged streamlines. During diastole for case 2 and 3, turbulent vortexes shearing along the anterior wall and recirculating blood occurs along the posterior wall. The wall is devoid of ILT at the impingement site and directly below this region ILT accumulates and the posterior wall has considerable ILT. White arrows shown on the CTA indicate

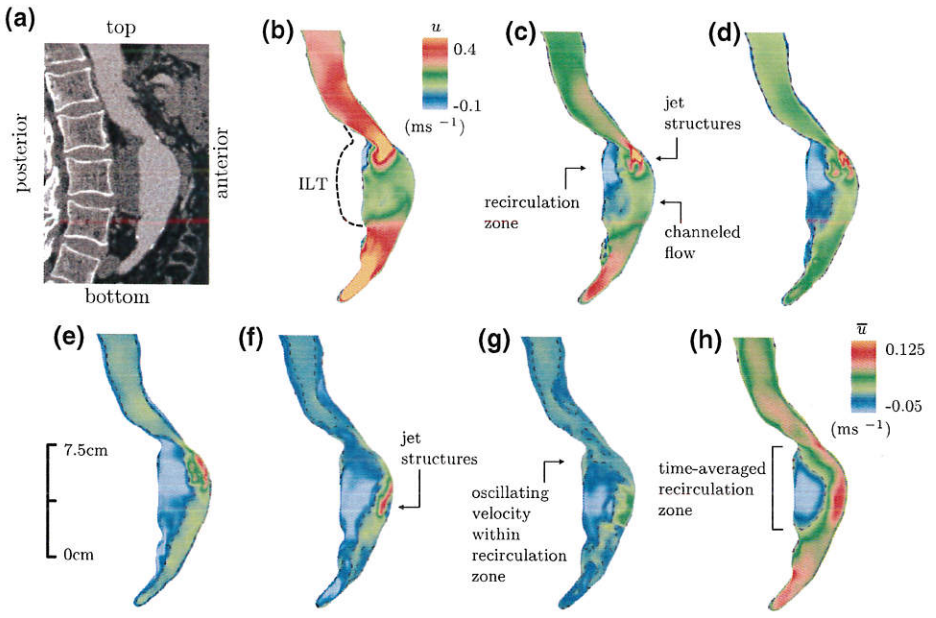

FIGURE 2. Case 1. (a) Mid-sagittal CTA. Instantaneous streamwise velocity at (b) $t/T = 0.24$, (c) $t/T = 0.32$, (d) $t/T = 0.36$, (e) $t/T = 0.4$, (f) $t/T = 0.56$ and (g) $t/T = 0.72$. (h) Time-averaged streamwise velocity. Dashed line in contours seperates regions of positive and negative velocity. Dashed line outside flow channel in (b) shows ILT deposition.

the location on the anterior wall ILT starts to accumulate. Case 4 is devoid of ILT and although a jet forms at the neck during systole, the vortexes stagnate at the neck region without propagating downstream into the AAA. The time-averaged streamlines indicate the blood flow is predominately channeled for this case.

Figure 4 and 5 shows for case 1 and 2, respectively, mid-axial CTA, instantaneous and time-averaged contours of streamwise velocity plotted on the mid-axial section. The jet is initially laminar and transitions to turbulence once it impacts against the wall. White arrows shown on the CTA indicate the location on the wall ILT starts to accumulate. The region of high velocity is devoid of ILT and the edge of this region correlates with the start of ILT accumulation. For case 1, the layer of posterior ILT results in the circular shaped AAA having an oval shaped lumen and the oval shape is tilted in the direction of impingement.

Wall Shear Stress

The peak WSS calculated from the analytical solution in Fig. 1b is 2.4 N m^{-2} and this value will be used as a reference. Figure 6 shows for case 1, anterior facing surface contours of $\tau_{w,x}$ at various times during diastole. From late-systole to early-systole of the next pulse the blood flow reverses in direction close to the wall and this results in the streamwise-component of WSS having low and negative values for a majority of the cardiac cycle. Regions of elevated $\tau_{w,x}$ correspond to the impact of vortexes against the wall. The peak WSS magnitude within the AAA occurs at $t/T = 0.52$ and is $\|\boldsymbol{\tau}_w\| = 3.4$ N m^{-2}. Although WSS caused by impingement is significantly higher then the surrounding regions in the AAA, it is comparable to the peak value obtained from the analytical solution. In the upstream aorta, peak WSS varies based on aortic diameter but is similar to the value predicted by the analytical solution.

Figure 7 shows for case 2, the streamwise-component of WSS plotted along the circumference of the axial slice shown in Fig. 5a. At peak-systole, $\tau_{w,x}$ is low and uniform along the circumference. During late-systole, $\tau_{w,x}$ continues to be low but has reversed in direction along the posterior-right side. During diastole, turbulent vortexes shear pass the anterior-left side causing high and fluctuating WSS.

Surface contours of OSI for cases 1–4, are shown in Figs. 8a–8d. Since a uniform velocity was imposed at the inlet, OSI is low directly downstream of the inlet. Once an oscillating boundary layer develops, OSI is high within the straight segments of the aorta. For cases 1–3, the continuous blood motion from impingement causes low OSI within this region. Case 2's recirculation zone has low OSI, indicating continuous upstream motion caused by the jet's downstream motion on the opposite side. The recirculating zone for cases 2 and 3 contain regions with both high and low OSI values. High OSI within a recirculation zone is the

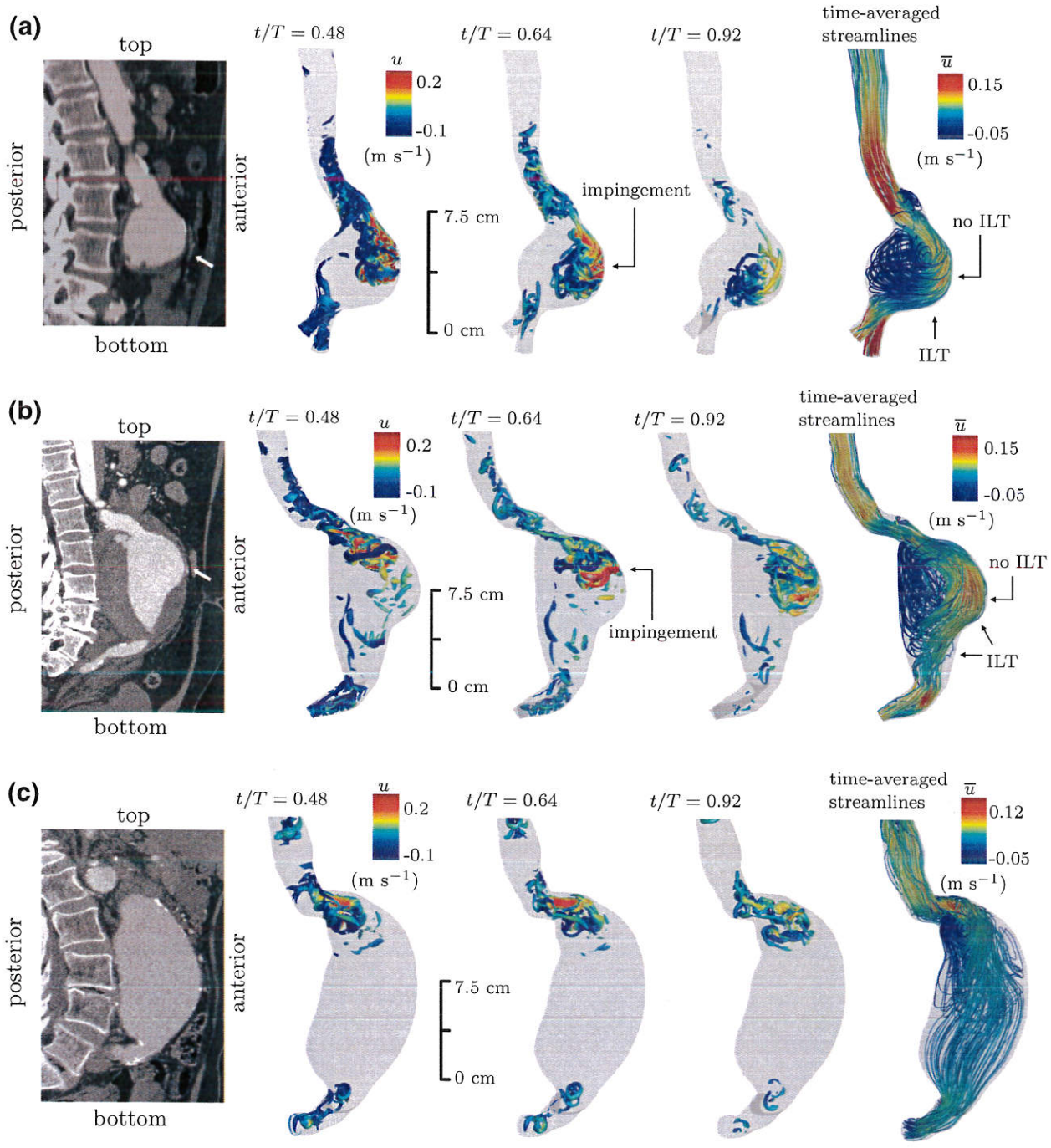

FIGURE 3. Mid-sagittal CTA with white arrow indicating the region on the anterior wall ILT starts to accumulate, instantaneous coherent structures visualized using the Q-criterion and time-averaged streamlines for (a) case 2, (b) case 3 and (c) case 4.

result of oscillating velocity similar to that shown in Fig. 2d. For cases 2 and 3, directly below the impingement region OSI remains low and the lower anterior wall for case 3 has high OSI. For case 4, aside from the neck region, OSI is predominately high within the AAA.

Surface contours of normalized transWSS are shown for cases 3–4 in Figs. 8e and 8f. Within the straight segments of the aorta transWSS is low and this indicates that although the blood flow is highly oscillatory, the oscillations occur along a single axis. Within the impingement region, transWSS is high combined with

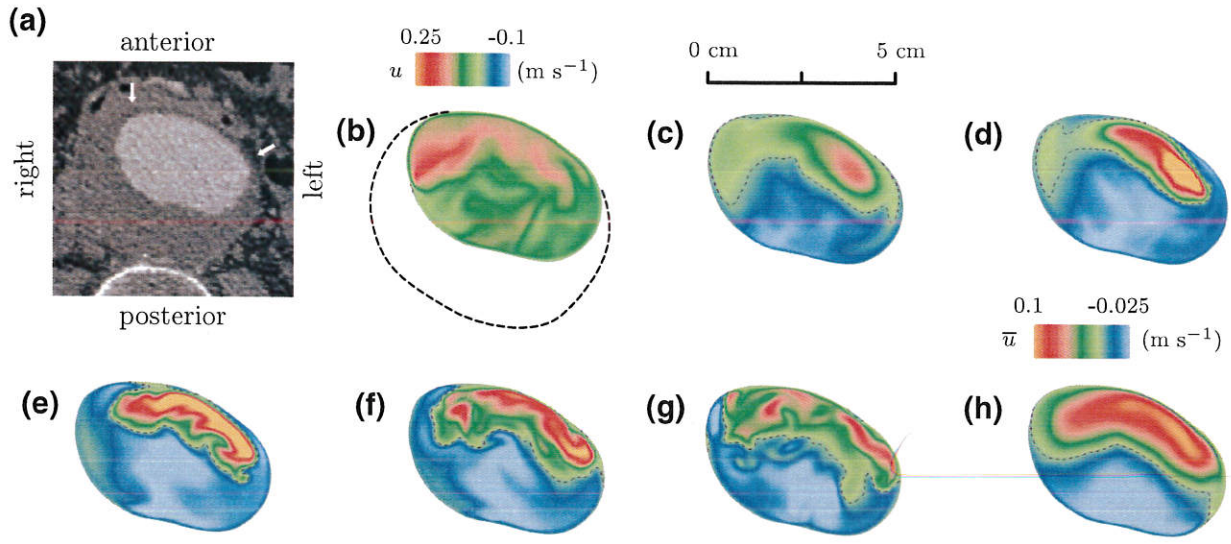

FIGURE 4. Case 1. (a) Mid-axial CTA with white arrows indicating the region on the aortic wall ILT starts to accumulate. Streamwise instantaneous velocity at (b) $t/T = 0.20$, (c) $t/T = 0.4$, (d) $t/T = 0.44$, (e) $t/T = 0.52$, (f) $t/T = 0.60$ and (g) $t/T = 0.72$. (h) Time-averaged streamwise velocity. Dashed line in contour separates regions of positive and negative velocity. Dashed line outside flow channel in (b) shows ILT deposition.

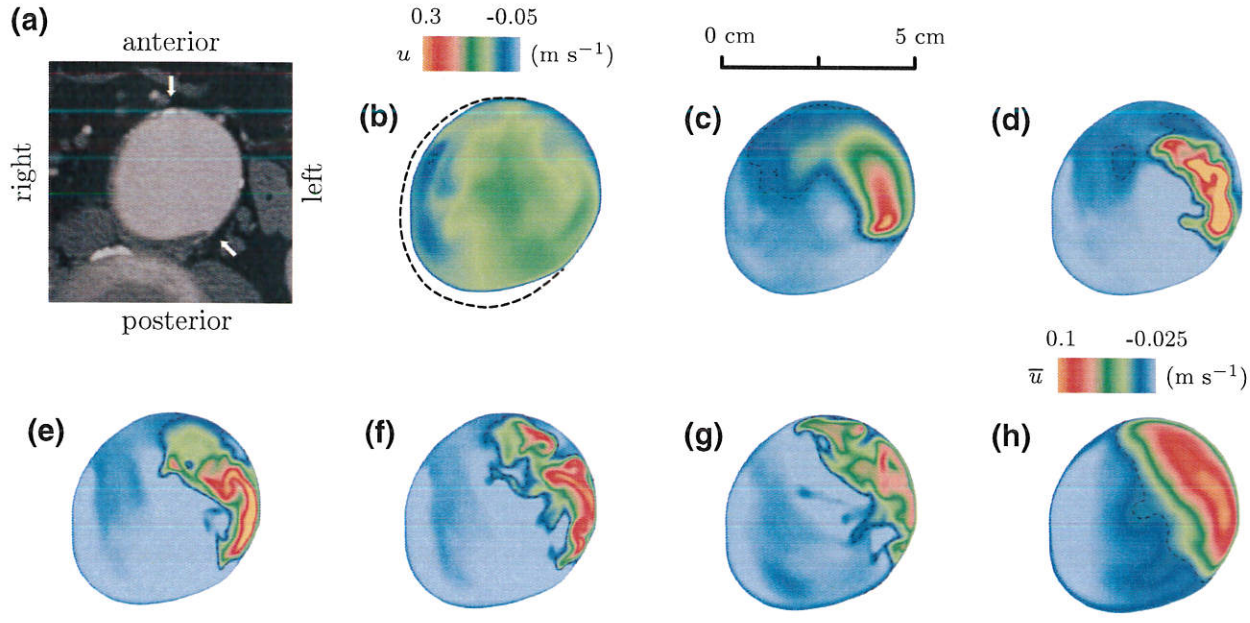

FIGURE 5. Case 2. (a) Mid-axial CTA with white arrows indicating the region on the arterial wall ILT starts to accumulates. Streamwise instantaneous velocity at (b) $t/T = 0.20$, (c) $t/T = 0.36$, (d) $t/T = 0.40$, (e) $t/T = 0.44$, (f) $t/T = 0.48$ and (g) $t/T = 0.56$. (h) Time-averaged streamwise velocity. Dashed line in contour separates regions of positive and negative velocity. Dashed line outside flow channel in (b) shows ILT deposition.

low OSI. This indicates the instantaneous WSS vector fluctuates about the dominate axis and the fluctuation remain directed along the dominate flow direction. Although case 4 has a large lumen, transWSS is predominately low, indicating laminar blood flow within the AAA. At most wall locations, an inverse relationship is found between OSI and transWSS.

DISCUSSION

Results are presented from simulations of pulsatile blood flow in four medium-to-large-sized AAA. It is found that a jet forms at the AAA neck during systole. For cases 1–3, during diastole turbulent vortexes from the jet continue to circulate within the AAA and im-

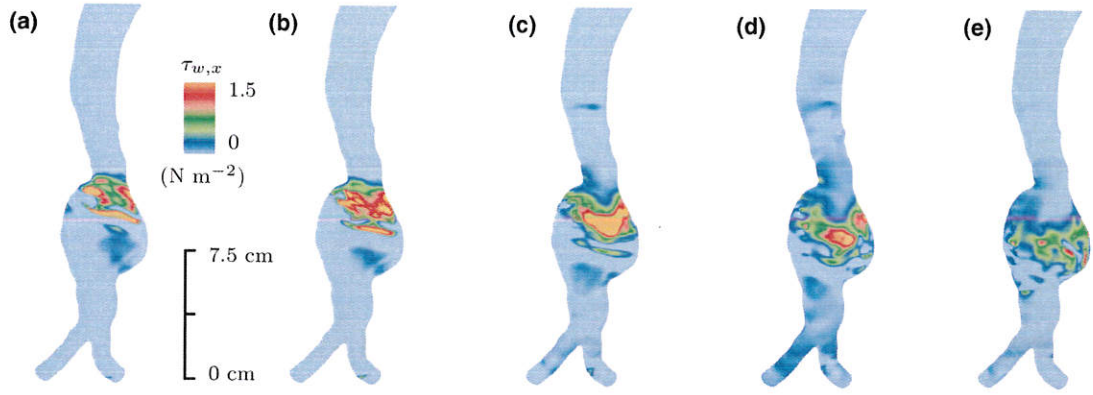

FIGURE 6. Case 1. Anterior facing surface contour of the instantaneous streamwise-component of WSS at (a) $t/T = 0.4$, (b) $t/T = 0.44$, (c) $t/T = 0.52$, (d) $t/T = 0.6$ and (e) $t/T = 0.72$. Light blue colour indicates $\tau_{w,x} \leq 0$.

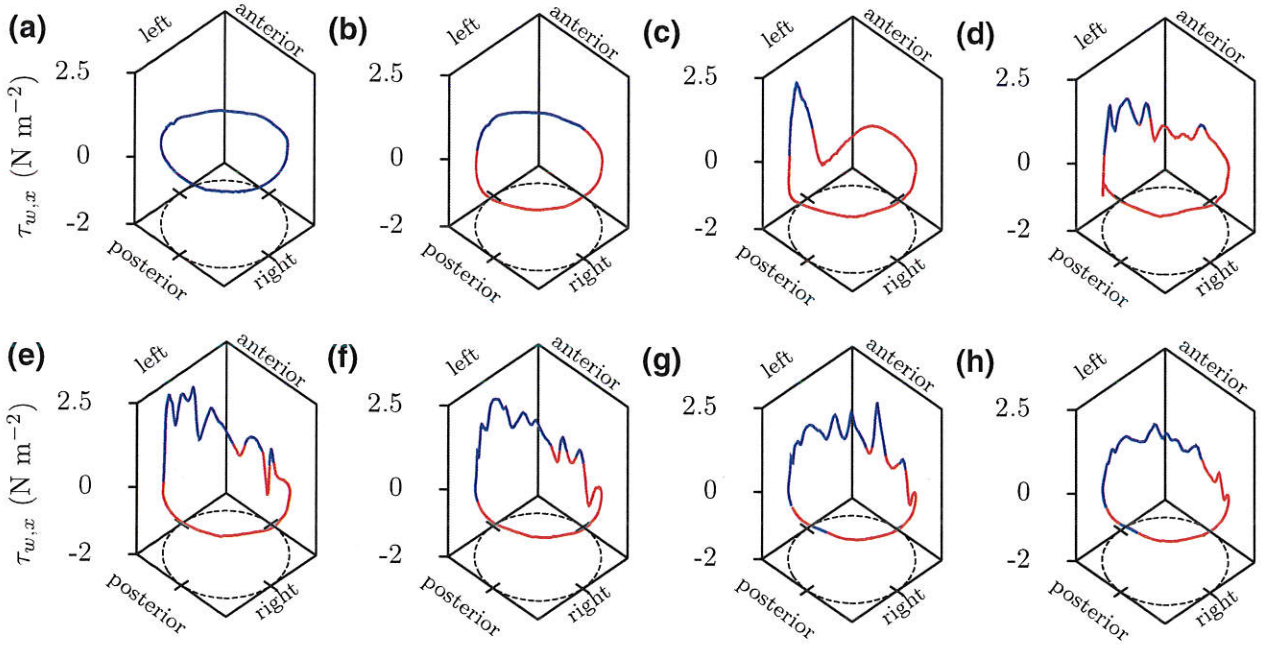

FIGURE 7. Case 2. Instantaneous streamwise-component of WSS plotted along the circumference of the mid-axial slice shown in Fig. 5a at (a) $t/T = 0.20$, (b) $t/T = 0.32$, (c) $t/T = 0.40$, (d) $t/T = 0.48$, (e) $t/T = 0.52$, (f) $t/T = 0.56$, (g) $t/T = 0.60$ and (h) $t/T = 0.64$. Blue and red color distinguishes positive and negative values, respectively.

pinge against the anterior wall with a zone of recirculating blood forming along the posterior wall. It can be seen in Figs. 3, 4, and 5 that the impingement site is devoid of ILT and there is a build-up in ILT remote from this region. Figure 7 shows that within the AAA, WSS caused by impingement is significantly higher than peak-systolic WSS. We present an argument that high WSS from the impact of a vortex prevents the attachment of ILT to the aortic wall.

It has been established by previous studies that recirculating blood correlates with vascular disease. Regions of recirculating blood have been shown to develop atherosclerosis in carotid bifurcation[49] and ILT in intracranical aneurysms.[30] Doyle *et al.*[7] investigated the growth and rupture in an AAA and it was shown that low WSS corresponded with the region with AAA growth, ILT deposition and rupture. Zambrano *et al.*[48] studied ILT growth in a group of 14 various sized AAA and observed ILT deposition occurred in regions with low WSS and ILT accumulation began in a localized region before spreading out to other regions. Since our present study uses a single static CTA for each case, it does not provided any new insight into the hemodynamic cause of ILT deposition. Rather it identifies a hemodynamic factor that may locally prevent the accumulation of ILT.

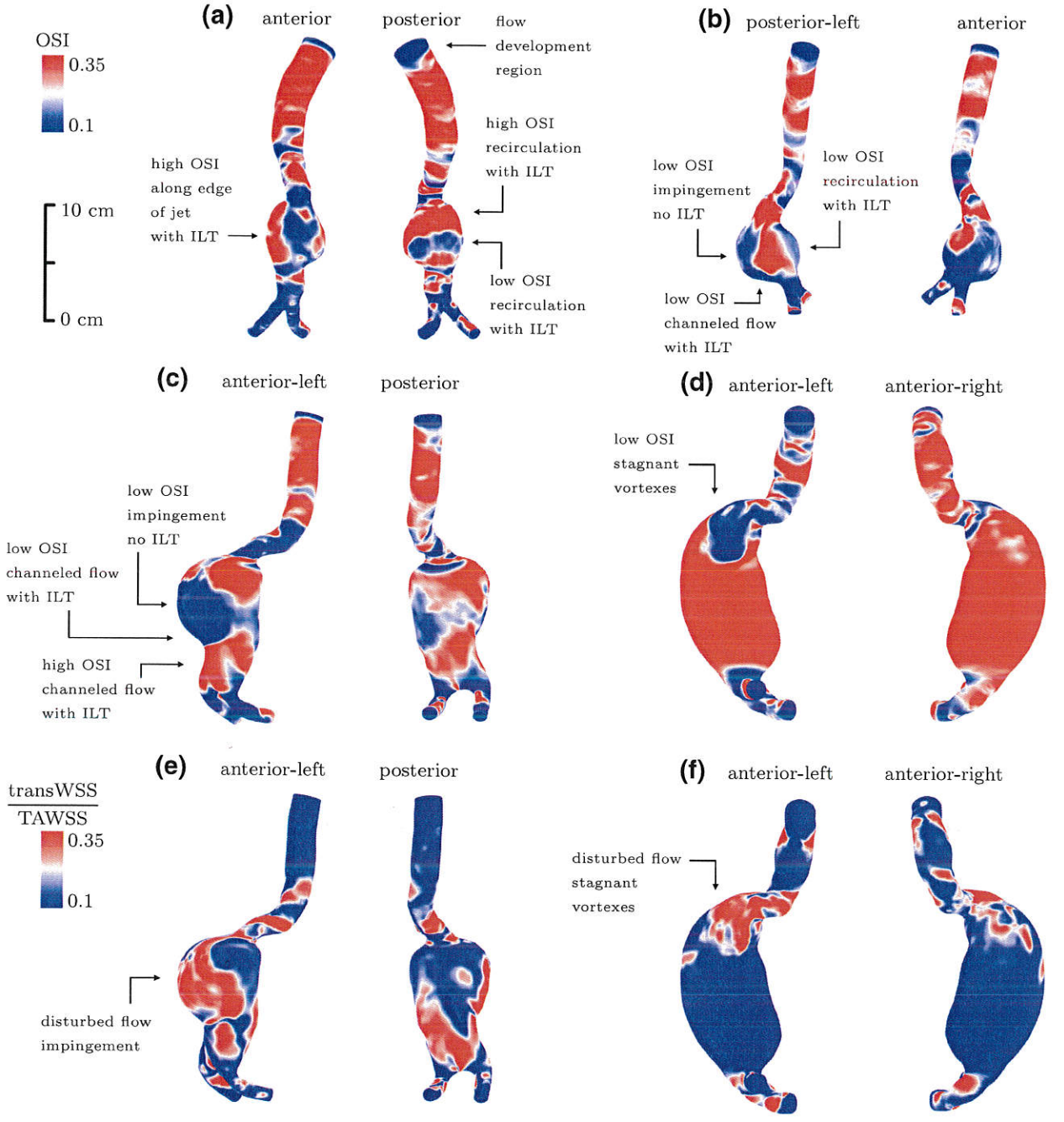

FIGURE 8. Surface contour of OSI for (a) case 1, (b) case 2, (c) case 3 and (d) case 4. Surface contour of normalized transWSS for (e) case 3 and (f) case 4.

It has been suggested high WSS from impingement in intracranial aneurysms contributes to growth and rupture[21] and Dolan *et al.*[6] defined high WSS as >3 N m^{-2}. Although our simulations showed WSS from impingement is relatively high, it is comparable to peak-systolic WSS in a straight normal-sized aorta. Therefore, vortexes shearing along the wall may not directly damage the aorta. Caro *et al.*[4] suggested increased cardiac output from exercise would raise WSS and have a protective effect against atherogenesis. It has been shown exercise conditions raised WSS and lowered OSI within the abdominal aorta.[35,38] Similar results were found to occur in AAA[19,34] with it being suggested this would reduce AAA growth[19] or the accumulation of ILT.[48] Exercise promoting aortic health by raising WSS is consistent with the concept of

high shear from impingement locally preventing ILT. An increased cardiac output is not considered a cardiovascular risk and this supports the hypothesis that impingement does not cause shearing damage.

It can be seen in Fig. 8 that cases 1–3 experience greater expansion on the side the flow structures impact. Although the continuous impact of these vortexes may have a positive effect by locally preventing ILT, the wall-normal force exerted by these impacts could contribute to expansion. This is consistent with a previous finding that AAA from patients with single above-knee leg amputations were more likely to expand on the side with the amputation due to asymmetric blood flow[40] and it was suggested by Lasheras[17] that tensional stresses, and not shear stresses, are the cause of AAA remodeling. Since impingement is found to occur primarily during diastole, the vortexes are relatively slow-moving compared to peak-systole flow velocity. It can be speculated that although their impact may gradually influence expansion, it has insufficient force to be the cause of mechanical failure (rupture) in the wall. In our previous work, we examined the location of rupture in a group of 7 RAAA,[3] and found that although high pressure and WSS occurred at the impingement site, rupture occurred in regions dominated by low WSS, recirculating blood and ILT deposition.

For this study a total of 23 AAA cases with diameter $\geq$ 5 cm were simulated. The AAA size, ILT location and impingement location if present, are summarized in Table 1. It is observed that blood flow impingement similar to cases 1–3 only occurs in AAA with medium-to-large-sized lumen and requires a sudden expansion in lumen cross-sectional area at the neck. For AAA geometries with small-sized lumen or gradual increases in lumen diameter at the neck, flow structures stagnant at the neck (similar to what was seen with case 4). Irrespective of the size or shape of an AAA, during peak-systole the blood flow is channeled and predominately laminar. The time-averaged velocity field gives an overall description of the hemodynamics, but does not fully capture the disturbed flow dynamics that can occur during late-systole and diastole. For example, Fig. 2 shows the size of the recirculation zone varies with time and Fig. 6 shows the region of high WSS moves along with the vortexes as they flow downstream.

Impingement is found to occur in 9 cases with the jet structures always flowing in the direction the neck angles the blood flow. For 8 of these cases, ILT of various thickness is present remote from the impingement site. Six cases have anterior-eccentric ILT and one case has circumferential-eccentric ILT. For these cases, a thick layer of ILT results in a small-sized lumen flow channel and the blood flow is stable without impingement or recirculation. From a single static CTA, it can not be identified what hemodynamic factors would cause ILT to deposit on the anterior wall. The remaining 7 cases experience flow dynamics similar to case 4, where there is no impingement and minimal ILT. Again this study does not identify why AAA similar to case 4 would develop.

TABLE 1. Patient information.

Case	Sex	Maximum AAA diameter (cm)	Neck angulation (°)	Maximum ILT thickness (cm)	ILT deposition location	Impingement location
1	M	6.8	45	1.8	Posterior	Anterior
2	M	6.0	45	0.4	Posterior-right	Anterior-left
3	M	11.0	60	4.4	Posterior	Anterior
4	M	7.4	80	0.0	–	–
5	F	5.0	45	0.5	Right	Anterior-left
6	M	5.3	25	1.0	Anterior	–
7	F	5.5	60	1.0	Circumferential-anterior	–
8	M	5.5	40	1.4	Posterior	Anterior
9	M	8.0	45	2.8	Circumferential-posterior	–
10	F	5.4	70	0.0	–	Left
11	M	6.5	30	4.0	Anterior	–
12	M	5.5	20	2.0	Right	Left
13	M	6.9	35	2.8	Anterior	–
14	M	5.7	45	0.4	Anterior-left	–
15	F	6.6	0	2.0	Circumferential-anterior	–
16	M	5.5	0	1.0	Posterior	–
17	M	5.7	50	1.0	Posterior	Anterior
18	M	5.5	20	0.4	Posterior-left-right	–
19	M	5.9	15	1.0	Circumferential	–
20	F	5.5	20	2.4	Anterior	–
21	M	9.2	75	0.8	Right	Left
22	M	8.0	80	0.0	–	–
23	M	5.5	20	2.8	Anterior	–

Previous studies have shown it to be more common for ILT to be anterior-eccentric in AAA.[9,22,28] Since our study showed impingement is primarily directed towards the anterior wall, this could indicate that the shape that leads to impingement is less common compared to other AAA shapes. In Metaxa *et al.*[22] it was found that AAA with posterior-eccentric ILT have lower growth rates compared to AAA with anterior-eccentric ILT. Although impingement may contribute to expansion, the possible removal of ILT deposition along the anterior wall may result in a overall slower rate of growth compared to AAA with a thick layer of anterior-eccentric ILT. Despite case 4 having a large lumen, its blood flow is predominately non-disturbed and no ILT deposition was present. As such, it may represent a type of AAA geometry that is at lower risk of further growth and rupture.

The question was raised in Peiffer *et al.*[26] whether high OSI and low WSS adequately describe relevant blood flow features. Since WSS is proportional to diameter, in general WSS will decrease as AAA size increases. Although OSI provides a useful description of the flow dynamics, we believe within AAA it is not the correct metric to use when identifying abnormal hemodynamics. It should be noted that a wide variety of pulse profiles and values for Re_b and Wo can occur within the cardiovascular system. Any observations made for AAA hemodynamics may not hold for different cardiovascular locations. For example, typical non-dimensional parameters in intracranical aneurysms are $Re_b = 436$, $Wo = 1.8$ and $\beta = 0.6$ (Valen-Sendstad *et al.*[39]). Although Re_b is similar between these cardiovascular locations the large differences in Wo and β will produce vastly different flow dynamics, i.e., in intracranical arteries high OSI may be an indication of disturbed flow behavior.[21] Below is a summary of the observed flow dynamics compared with OSI and ILT deposition.

- At the location the jet structures impinge OSI is low, WSS and transWSS are high and the wall is devoid of ILT. Simply from this observation it could be concluded that low OSI has an preventative affect on ILT deposition; however, we believe that the mechanism is the shearing caused by the impact of vortexes and low OSI is only a consequence of this flow.
- For cases 2 and 3 directly below the impingement region OSI remains low and ILT accumulates. The blood flow in this region can be described as channeled and unidirectional.
- For case 3 along the lower segment of the anterior wall there is a thick layer of ILT and OSI is high. While case 4 has predominately high OSI and there is no ILT. This flow can be described as a attached boundary layer that oscillates in direction. Figure 8a and 8b show that along the edge of the impingement region, blood flow exhibits this behavior and ILT is present.
- Zones of recirculating blood are characterized by low time-averaged velocity flowing opposite to the dominant flow direction. Figure 8a shows the recirculation zone can have distinct regions of both low and high OSI, and these variations do not appear to affect ILT thickness.

From this study a direct correlation can not be identified between OSI and ILT deposition or AAA shape. This is due to different flow dynamics having similar OSI values. Arzani *et al.*[2] performed a study on ILT growth in 10 small-sized AAA and regions with low OSI experienced the most ILT growth. Low OSI was thought to represent recirculating blood and this is consistent with what we observed in the recirculation zone of case 2. A similar observation was made by ORourke *et al.*[24] where, in three small-sized AAA, there was a correlation between regions with low OSI and ILT growth. Since both of these studies used small-sized AAA, they may have observed more normally channeled flow and not the greater disturbances in flow that can occur in larger AAA.

A limitation of this study is the model excluded arteries that branch off of the aorta and instead implemented the infrarenal flow rate at the supraceliac level in the aorta. Disturbances in the blood flow have been observed at the renal arteries.[15] Since the bulk flow rate is effectively zero during diastole, these flow disturbances would stagnant at the renal arteries and not propagate downstream pass the AAA neck. Therefore it is unlikely that the inclusion of visceral arteries would significantly alter our results.

In conclusion, this study shows that high WSS from the impingement of vortexes is associated with an absence of ILT deposition. It is unlikely that impingement is beneficial, as the continuous impact of vortexes could, over an extended period of time, be contributing to AAA expansion. The continuous downstream motion from the vortexes results in low-velocity recirculation on the opposite side and this flow dynamic increases the likelihood of a layer of posterior-eccentric ILT forming. Wall hypoxia is potentially caused by the layer of ILT preventing adequate oxygen diffusion and this results in the deterioration of the posterior aortic wall; the typical location of aortic rupture.[9] It would be beneficial to further investigate how the risk of rupture for an AAA with impingement and posterior-eccentric ILT compares to an AAA with stable blood flow and a layer of anterior-eccentric ILT.

ACKNOWLEDGMENTS

We acknowledge Grant support from the University Medical Group, Department of Surgery, University of Manitoba and computational resources provided by Western Canada Research Grid (WestGrid).

CONFLICT OF INTEREST

All authors declare that they have no conflict of interest.

STATEMENT OF HUMAN AND ANIMAL STUDIES

Ethics approval for this work was granted by the University of Manitoba Research Ethics Board, Research Protocol Number: REB B2013:130. No animal studies were carried out by the authors for this article.

REFERENCES

[1]Arzani, A., A. S. Les, R. L. Dalman, and S. C Shadden. Effect of exercise on patient specific abdominal aortic aneurysm flow topology and mixing. *Int. J. Numer. Methods Biomed. Eng.* 30(2):280–295, 2014.

[2]Arzani, A., G.-Y. Suh, R. L. Dalman, and S. C. Shadden. A longitudinal comparison of hemodynamics and intraluminal thrombus deposition in abdominal aortic aneurysms. *Am. J. Physiol.Heart Circ. Physiol.* 2014. DOI: 10.1152/ajpheart.00461.2014.

[3]Boyd A. J., Kuhn D. C., Lozowy R. J., and G. P. Kulbisky. Low wall shear stress predominates at sites of abdominal aortic aneurysm rupture. *J. Vasc. Surg.* 63(6):1613–1619, 2016.

[4]Caro, C. G., J. M. Fitz-Gerald, and R. C. Schroter. Atheroma and arterial wall shear observation, correlation and proposal of a shear dependent mass transfer mechanism for atherogenesis. *Proc. R. Soc. London. Ser. B Biol. Sci.* 177:109–133, 1971.

[5]Di Martino, E. S., S. Mantero, F. Inzoli, G. Melissano, D. Astore, R. Chiesa, and R. Fumero. Biomechanics of abdominal aortic aneurysm in the presence of endoluminal thrombus: experimental characterisation and structural static computational analysis. *Eur. J. Vasc. Endovasc. Surg.* 15:290–299, 1998.

[6]Dolan, J. M., J. Kolega, H. Meng. High wall shear stress and spatial gradients in vascular pathology: a review. *Ann. Biomed. Eng.* 41:1411–1427, 2012.

[7]Doyle, B. J., T. M. McGloughlin, E. G. Kavanagh, and P. R. Hoskins. From detection to rupture: a serial computational fluid dynamics case study of a rapidly expanding, patient-specific, ruptured abdominal aortic aneurysm. In: *Computational Biomechanics for Medicine*, edited by B. Doyle, K. Miller, A. Wittek, and P. M. F. Nielsen. New York: Springer, 2014, pp. 53–68.

[8]Hale, J. F., D. A. McDonald, and J. R. Womersley. Velocity profiles of oscillating arterial flow, with some calculations of viscous drag and the Reynolds number. *J. Physiol.* 128:629–640, 1955.

[9]Hans, S. S., O. Jareunpoon, M. Balasubramaniam, and G. B. Zelenock. Size and location of thrombus in intact and ruptured abdominal aortic aneurysms. *J. Vasc. Surg.* 41:584–588, 2005.

[10]He, X., and D. N. Ku. Pulsatile flow in the human left coronary artery bifurcation: average conditions. J. Biomech. Eng. 118:74-82, 1996.

[11]Hunt, J. C. R., Wray, A. and P. Moin. Eddies, stream, and convergence zones in turbulent flows Center for Turbulence Research Report CTR-S88, 1988.

[12]Hussain, A. K. M. F., and W. C. Reynolds. The mechanics of an organized wave in turbulent shear flow. J. Fluid Mech. 41:241–258, 1970.

[13]Issa, R., I. Solution of the implicitly discretized fluid flow equation by operator-splitting. *J. Comput. Phys.* 62(1):40–65, 1985.

[14]Kazi, M., J. Thyberg, P. Religa, J. Roy, P. Eriksson, U. Hedin, and J. Swedenborg. Influence of intraluminal thrombus on structural and cellular composition of abdominal aortic aneurysm wall. *J. Vasc. Surg.* 38:1283–1292, 2003.

[15]Ku, D. N., S. Galgov, J. E. Moore, and C. K. Zarins, Flow patterns in the abdominal aorta. *J. Vasc. Surg.* 9:309–316, 1989.

[16]Ku, D. N. Blood flow in arteries. *Annu. Rev. Fluid Mech.* 29(1):399–434, 1997.

[17]Lasheras, J. C. The biomechanics of arterial aneurysms. *Annu. Rev. Fluid Mech.* 39:293–319, 2007.

[18]Lederle, F. A., G. R. Johnson, S. E. Wilson, D. J. Ballard, W. D. Jordan, Jr., J. Blebea, F. N. Littooy, J. A. Freischlag, D. Bandyk, J. H. Rapp, A. A. Salam, and I. Veterans Affairs Cooperative Study Rupture rate of large abdominal aortic aneurysms in patients refusing or unfit for elective repair. *JAMA* 287:2968–2972, 2002.

[19]Les, A. S., S. C. Shadden, C. A. Figueroa, J. M. Park, M. M. Tedesco, R. J. Herfkens, R. L. Dalman, and C. A. Taylor. Quantification of hemodynamics in abdominal aortic aneurysms during rest and exercise using magnetic resonance imaging and computational fluid dynamics. *Ann. Biomed. Eng.* 38:1288–1313, 2010.

[20]Les, A. S., Yeung, J. J., Schultz, G. M., Herfkens, R. J., Dalman, R. L., and C. A. Taylor. Supraceliac and infrarenal aortic flow in patients with abdominal aortic aneurysms: mean flows, waveforms, and allometric scaling relationships.*Card. Eng. Tech.* 1:39–51, 2010.

[21]Meng, H., V. M. Tutino, J. Xiang, and A. Siddiqui. High WSS or Low WSS? Complex interactions of hemodynamics with intracranial aneurysm initiation, growth, and rupture: toward a unifying hypothesis. *Am. J. Neuroradiol.* 35:1254–1262, 2014.

[22]Metaxa, E., N. Kontopodis, K. Tzirakis, C. V. Ioannou, and Y. Papaharilaou. Effect of intraluminal thrombus asymmetrical deposition on abdominal aortic aneurysm growth rate. *J. Endovasc. Ther.* 22(3):406–412, 2013.

[23]Mower, W. R., W. J. Quiones, and S. S. Gambhir. Effect of intraluminal thrombus on abdominal aortic aneurysm wall stress. *J. Vasc. Surg.* 26:602–608, 1997.

[24]O'Rourke, M. J., J. P. McCullough, and S. Kelly. An investigation of the relationship between hemodynamics and thrombus deposition within patient-specific models of abdominal aortic aneurysm. *Proc. Inst. Mech. Eng.* 226:548–564, 2012.

[25]Parr, A., M. McCann, B. Bradshaw, A. Shahzad, P. Buttner, and J. Golledge. Thrombus volume is associated with cardiovascular events and aneurysm growth in patients who have abdominal aortic aneurysms. *J. Vasc. Surg.* 53:28–35, 2011.

[26]Peiffer, V., S. J. Sherwin, and P. D. Weinberg. Does low and oscillatory wall shear stress correlate spatially with early atherosclerosis? A systematic review. *Cardiovasc. Res.* 99:242–250, 2013.

[27]Peiffer, V., S. J. Sherwin, and P. D. Weinberg. Computation in the rabbit aorta of a new metric the transverse wall shear stress to quantify the multidirectional character of disturbed blood flow. *J. Biomech.* 46:2651–2658, 2013.

[28]Pillari, G., J.B. Chang, J. Zito, J.R. Cohen, K. Gersten, A. Rizzo, et al. Computed tomography of abdominal aortic aneurysm. An in vivo pathological report with a note on dynamic predictors. *Arch. Surg.* 123:727–732, 1988.

[29]Pope, S. B. *Turbulent Flows*. Cambridge: Cambridge University Press, 2000.

[30]Rayz, V. L., L. Boussel, M. T. Lawton, G. Acevedo-Bolton, L. Ge, W. L. Young, R. T. Higashida, and D. Saloner. Numerical modeling of the flow in intracranial aneurysms: prediction of regions prone to thrombus formation. *Ann. Biomed. Eng.* 36:1793–1804, 2008.

[31]Satta, J., E. Laara, and T. Juvonen. Intraluminal thrombus predicts rupture of an abdominal aortic aneurysm. *J. Vasc. Surg.* 23:737–739, 1996.

[32]Speelman, L., G. W. H. Schurink, E. M. H. Bosboom, J. Buth, M. Breeuwer, F. N. van de Vosse et al. The mechanical role of thrombus on the growth rate of an abdominal aortic aneurysm. *J. Vasc. Surg.* 51:19–26, 2010.

[33]Stenbaek, J., B. Kalin, and J. Swedenborg. Growth of thrombus may be a better predictor of rupture than diameter in patients with abdominal aortic aneurysms. *Eur. J. Vasc. Endovasc. Surg.* 20:466–499, 2000.

[34]Suh, G. Y., A. S. Tenforde, S. C. Shadden, R. L. Spilker, C. P. Cheng, R. J. Herfkens, R. L. Dalman, and C. A. Taylor. Hemodynamic changes in abdominal aortic aneurysms with increasing exercise intensity using MR exercise imaging and image-based computational fluid dynamics. *Ann. Biomed. Eng.* 39:2186–2202, 2011.

[35]Tang, B. T., C. P. Cheng, M. T. Draney, N. M. Wilson, P. S. Tsao, R. J. Herfkens, and C. A. Taylor. Abdominal aortic hemodynamics in young healthy adults at rest and during lower limb exercise: quantification using image-based computer modeling. *Am. J. Physiol. Heart Circ. Physiol.* 291:H668–H676, 2006.

[36]Tarbell, J. M., Z. Shi, J. Dunn, H. Jo. Fluid mechanics, arterial disease, and gene expression. *Annu. Rev. Fluid Mech.* 46:591–614, 2014.

[37]Tardu, S. F., G. Binder, R. F. Blackwelder. Turbulent channel flow with large-amplitude velocity oscillations. *J. Fluid Mech.* 267:109–151, 1994.

[38]Taylor, C. A., C. P. Cheng, L. A. Espinosa, B. T. Tang, D. Parker, and R. J. Herfkens. In vivo quantification of blood flow and wall shear stress in the human abdominal aorta during lower limb exercise. *Ann. Biomed. Eng.* 30:402–408, 2002.

[39]Valen-Sendstad, K., K. Mardal, M. Mortensen, B. A. P. Reif, and H. P. Langtangen. Direct numerical simulation of transitional flow in a patient-specific intracranial aneurysm. *J. Biomech.* 44:2826–2832, 2011.

[40]Vollmar, J. F., E. Paes, P. Pauschinger, E. Henze, and A. Friesch. Aortic aneurysms as late sequelae of above-knee amputation. *Lancet* 2:834-835, 1989.

[41]Vorp, D. A., P. C. Lee, D. H. Wang, M. S. Makaroun, E. M. Nemoto, S. Ogawa, and M. W. Webster.r Association of intraluminal thrombus in abdominal aortic aneurysm with local hypoxia and wall weakening. *J. Vasc. Surg.* 34:291–299, 2001.

[42]Vorp, D. A., W. J. Federspiel, and M. W. Webster. Does laminated intraluminal thrombus within abdominal aortic aneurysm cause anoxia of the aortic wall? *J. Vasc. Surg.* 23:540-541, 1996.

[43]Wang, D. H., M. S. Makaroun, M. W. Webster, and D. A. Vorp. Effect of intraluminal thrombus on wall stress in patient-specific models of abdominal aortic aneurysm. *J. Vasc. Surg.* 36:598–604, 2002.

[44]Wolf, Y.G., W. S. Thomas, F. J. Brennan, W. G. Goff, M. J. Sise, and E. F. Bernstein. Computed tomography scanning findings associated with rapid expansion of abdominal aortic aneurysms. *J. Vasc. Surg.* 20:529–535, 1994.

[45]Womersley, J. R. Method for the calculation of velocity, rate of flow and viscous drag in arteries when the pressure gradient is known. J. Physiol. 127:553-563, 1955.

[46]Wood, N.B. Aspects of fluid dynamics applied to the larger arteries. *J. Theor. Biol.* 199:137–161, 1999.

[47]Xenos, M., N. Labropoulos, S. Rambhia, Y. Alemu, A. Tassiopoulos, N. Sakalihasan, and D. Bluestein. Progression of abdominal aortic aneurysm towards rupture: refining clinical risk assessment using a fully coupled fluid structure interaction method. *Ann. Biomed. Eng.* 43:139–153, 2014.

[48]Zambrano, B. A., H. Gharahi, C. Lim, F. A. Jaberi, J. Choi, W. Lee and S. Baek. Association of intraluminal thrombus, hemodynamic forces, and abdominal aortic aneurysm expansion using longitudinal CT images. *Ann. Biomed. Eng.* 44:1502–1514, 2016.

[49]Zarins, C. K., D. P. Giddens, B. K. Bharadvaj, V. S. Sottiurai, R. F. Mabon, and S. Glagov. Carotid bifurcation atherosclerosis. Quantitative correlation of plaque localization with flow velocity profiles and wall shear stress. *Circ. Res.* 53:502–514, 1983.